INVESTIGATION OF THE PROPERTIES OF NICKEL TITANIUM SHAPE MEMORY ALLOYS FOR APPLICATIONS IN SELF-HEALING MATERIALS

by

Muhammad Istiaque Haider

A Dissertation Submitted in

Partial Fulfillment of the

Requirements for the Degree of

Doctor of Philosophy

in Engineering

at

The University of Wisconsin-Milwaukee

August 2023

ABSTRACT

INVESTIGATION OF THE PROPERTIES OF NICKEL TITANIUM SHAPE MEMORY ALLOYS FOR APPLICATIONS IN SELF-HEALING MATERIALS
by

Muhammad Istiaque Haider

The University of Wisconsin-Milwaukee, 2023
Under the Supervision of Professor Nathan P. Salowitz

This research explores the design and properties of self-healing metal-metal composites, with a specific focus on incorporating shape memory alloys (SMAs) and investigating the characteristics of post-constrained recovery residual stresses (PCRRS). The objective is to enhance the functionality, durability, and longevity of mechanical structures through the realization and optimization of self-healing materials.

The research delves into the experimental and analytical studies to gain a comprehensive understanding of the underlying mechanisms of PCRRS and SMA-reinforced self-healing metal matrix composites, specifically examining the interface strength between nickel-titanium (NiTi) wire and bismuth-tin (BiSn) solder. NiTi SMAs manifest a distinctive property, termed as PCRRS, observed when they undergo a path of constrained recovery and are subsequently brought back to a low-temperature state while being constrained. This research pursued an array of mechanical experiments to delve deeper into the nature of the PCRRS state. Principal tasks encompassed evaluating the stability of PCRRS across various cycles involving different strain applications, discerning the impact of pre-working or training on PCRRS, studying the mechanical properties while loading from the PCRRS state, analyzing the material phase in the PCRRS state, and assessing the regeneration capabilities of the PCRRS in NiTi SMAs. This research showcases the stability and repeatability of PCRRS, thereby offering

invaluable insights into its prospective application in self-healing mechanisms, underscored by its ability to actuate without the continuous provision of energy. Moreover, this thesis elucidates the interfacial attributes between NiTi and BiSn, considering the complications posed by the development of an inert titanium dioxide (TiO_2) layer on NiTi. As interfacial bonding is crucial for composite behavior, experimental and theoretical approaches were employed to understand the interfacial bonding, by studying the pull-out behavior of NiTi wires embedded in the BiSn matrix. In this investigation, two different states of NiTi wire were examined in a comparative study – one state maintained the presence of the TiO_2 layer as a control, while the other state represented an experimental condition where the TiO_2 layer was removed through a chemical etching procedure carried out in an inert environment. Subsequent to testing, the specimens undergo a microscopic assessment to identify the failure modes at the interface. The study reveals the influence of interfacial strength on the pull-out process and highlights the presence of an alternative failure mechanism involving mechanical interlocking. This study's results will quantify the enhanced NiTi and BiSn interfacial strength from the applied process, providing vital data for optimizing composite design and performance.

The findings of this research contribute to the understanding of self-healing materials and their potential in engineering applications. Characterization of PCRRS of NiTi SMAs and the interfacial characteristics of NiTi and BiSn, broadly metal-metal self-healing composite offer new possibilities for designing structures with enhanced durability, reduced maintenance requirements, and the ability to restore functionality after damage. These insights provide a foundation for further advancements in the field of self-healing materials and their practical implementation in real-world engineering scenarios.

To my family

TABLE OF CONTENTS

LIST OF FIGURES

LIST OF TABLES

ACKNOWLEDGEMENTS

Foremost, I would like to express my deepest appreciation and heartfelt gratitude to my esteemed supervisor, Professor Nathan Salowitz, whose unwavering support, guidance, and inspiration have been instrumental in the completion of my PhD research. Over the past several years, his encouragement has been invaluable, and his mentorship has taught me to approach problems from the perspective of a researcher rather than a student. I am immensely grateful for his patience and understanding throughout this challenging journey.

I would also like to extend my profound gratitude to Professor Benjamin Church, who has been an indispensable source of guidance and support in every aspect of this research. His enthusiasm, keen insights, and steadfast encouragement have truly inspired me. Additionally, I would like to express my appreciation to my committee members, Dr. Rahman, Dr. Avdeev, and Dr. Yahiaoui, for their insightful evaluations and constructive feedback on my work.

I am particularly grateful to my colleagues at the Advanced Structures Lab, especially Maysam Rezaee, whose invaluable suggestions and camaraderie have greatly enriched my experience. I would also like to express my gratitude to John Condon from the CEAS Machine Shop for his indispensable assistance in the fabrication of experimental setups and specimens. Furthermore, I am indebted to Dr. Steven E Hardcastle from the Advanced Analysis Facility of UWM for his expert instruction and support in operating various sophisticated instruments such as the Dynamic Mechanical Analyzer (DMA), Differential Scanning Calorimeters (DSC), X-ray Diffractometers (XRD), and Confocal Microscope.

My utmost appreciation is reserved for my loving parents and my wonderful wife, Mahmuda, whose unwavering love, support, and encouragement have been the bedrock of my achievements. This dissertation would have been impossible without their incredible patience, sacrifices, and continuous support. Finally, I would like to dedicate my heartfelt love to my precious son, Taseen, whose presence and affection have provided me with the strength and motivation to persevere each day.

Introduction

Functionality, durability, and longevity are crucial factors in the design of mechanical structures. Conventional engineering practices involve selecting materials for the structure that minimize the risk of critical damage throughout its service lifetime. Recently, there has been a surge of interest in self-healing materials, as these materials possess the potential to extend a material's lifespan, reduce replacement costs, and enhance product safety and reliability [1]. The design philosophy underlying self-healing materials focuses on enabling them to not only tolerate damage but also possess an inherent capacity to repair (heal) the damage and restore the product's functionality to acceptable levels (above 70% of the initial functionality) [2], [3].

Self-healing materials often feature a sophisticated internal structure comprising constituent materials with distinct functionalities. One of the primary strategies for reinforcing self-healing materials involves incorporating shape memory alloys (SMAs) that can be activated to restore geometry and close a fracture. This study provides an in-depth analysis of material properties and interfacial interactions within metal-metal composites, paving the way for the design and development of optimized SMA-reinforced self-healing metal composites that balance both strength and self-repairing capacity. This is achieved by conducting experimental explorations of post-constrained recovery residual stresses (PCRRS), a recently discovered property observed in NiTi SMAs that may be harnessed to develop a novel self-healing mechanism and characterizing the interface strength between nickel-titanium (NiTi) wire and bismuth-tin (BiSn) solder to ensure proper stress transfer capabilities.

Recent experimental findings reveal that NiTi SMAs can generate residual stresses following constrained recovery and returning to a low-temperature, martensitic state while

remaining constrained. This capability has the potential to be advantageous in applications such as self-healing materials where loads are desirable without the continuous application of heat or energy. This research represents experimental and analytical studies aimed at understanding the underlying mechanisms of PCRRS and discussing its potential application scope and benefits in the design of self-healing materials.

Furthermore, this research presents a comprehensive experimental analysis of the interface strength and microscopic evaluation of the failure mechanism at the interface between nickel-titanium (NiTi) wire and bismuth-tin (BiSn) solder. The insights gained from the PCRRS studies and the interface evaluation will be applied to optimize the self-healing metal-metal composite using established composite theories and will contribute to the development of a novel self-healing mechanism.

Motivation

Inspired by biological systems, self-healing materials strive to emulate a unique characteristic - the autonomous restoration of function, harnessing the resources intrinsically within their reach for self-repair. [4]. This remarkable characteristic offers the potential to alleviate the necessity for frequent inspections in damage monitoring, decrease the expenses associated with product maintenance and replacement, and reduce the likelihood of service interruptions due to product failure [5]. The innate ability of self-healing materials to repair damage and restore structural strength paves the way for a paradigm shift in the design and analysis of structures, redefining the concept of 'failure' and resulting in lighter, more efficient, and longer-lasting structures. Given the broad applicability of self-healing materials in spacecraft and aerospace structures, automotive structures, and defense industries [6], the

development of these materials has garnered significant attention, with researchers dedicating several decades to the topic.

Although replicating the biological process of healing in inorganic systems poses a considerable challenge, the majority of research efforts have been focused on non-metallic materials, owing to their ease of implementation. Metallic self-healing composites are of considerable practical interest due to their structural properties, which are superior to those of polymer and ceramic-based self-healing materials [7]. This advantage can be attributed to the prevalent practice of encapsulating liquid resin or adhesives within polymer and ceramic self-healing materials. Upon sustaining damage, the encapsulated liquid is released, flowing into the affected area and re-adhering the structure. However, this approach presents several challenges, including the added weight of the encapsulated liquid, which does not contribute to the structure's strength until released, and the formation of voids upon release. Moreover, polymers and liquid adhesives are generally ill-suited for the wide range of extreme temperatures encountered during space flight. In contrast, metal-metal self-healing composites exhibit greater temperature tolerance and the advantage of being entirely solid, thus providing load-bearing capabilities.

The study of PCRRS) in NiTi SMAs offers significant potential for innovation and advancement within the realm of smart materials and self-healing metallic structures. This research is spurred by the novel phenomenon of PCRRS, which introduces a pioneering approach for employing NiTi as an actuator. This approach could revolutionize existing applications such as self-healing materials, and stimulate novel applications, like using a dispersion of NiTi particles to prevent fatigue cracking in material structures. The motivation for

investigating PCRRS stems from its inherent ability to generate residual crack-closing loads, which are essential for maintaining structural integrity under fatigue loads. Importantly, these loads can be generated without the continuous application of energy. Hence, this property potentially heralds a paradigm shift in the design of self-healing materials, enabling structures that can endure external forces without constant energy input. Furthermore, the exploration of PCRRS in the development of self-healing metallic materials, particularly for generating consistent crack-closing loads, has profound implications for the future of material development. The research into PCRRS, therefore, represents an exciting frontier in the quest to develop more efficient, resilient, and intelligent materials and structures.

The motivation behind the research of interfacial bonding lies in the transformative potential of self-healing materials - especially metal-metal composites - and the specific challenges that have arisen in harnessing this potential. Such materials, with their inherent ability to recover from damage, could fundamentally redefine structural integrity and design paradigms, resulting in lighter, more resilient structures that require significantly less maintenance. However, a major stumbling block to the effective realization and widespread adoption of these materials, particularly the NiTi and BiSn composite, is the problematic interface bonding. This is primarily due to the formation of an inert titanium dioxide (TiO_2) layer on the surface of NiTi, which significantly weakens the interface strength between the NiTi fibers and BiSn matrix. Inspired to address this crucial barrier, the central aim of this research has been to delve into the properties and failure mechanisms of the NiTi-BiSn interface. By developing a comprehensive understanding of the interfacial behavior, especially in the presence and absence of the TiO_2 layer, the research has sought to offer quantitative insights

into the enhancements possible through specific chemical etching processes. This in-depth analysis provides critical data that could inform the design of optimized composites, influencing decisions around fiber sizing and potentially paving the way for the development of better-performing self-healing composites. This research contributes to the broader field of materials engineering, bringing us closer to a future where structures can autonomously recover and maintain their functionality. This significant stride towards self-healing structures holds immense potential benefits, from economic savings through reduced maintenance to improved sustainability through extended material lifespan. As such, the motivation behind this research extends far beyond the realms of academic curiosity, potentially offering tangible solutions to some of the most pressing challenges in contemporary materials engineering.

Background

Self-healing materials aim to decrease structural weight, downtime, maintenance expenses, and failure by incorporating the ability to repair damage during service, thus preventing the accumulation of damage that could result in structural failure. In this section, we provide a detailed introduction to self-healing materials, focusing specifically on shape memory alloy (SMA)-reinforced self-healing metallic materials and the SMA properties investigated for developing metal-metal composite designs using SMA.

Overview of Self-Healing Materials

Over the past two decades, substantial research has been conducted on self-healing materials with an innate capacity to repair damage. These investigations have led to the development of various self-healing materials utilizing diverse healing mechanisms. Self-healing

materials can be classified as autonomous or non-autonomous and homogeneous or heterogeneous [8]:

1. Autonomous self-healing materials typically contain an encapsulated healing agent or a stored energy potential that is released upon damage occurrence.
    a. The automatic initiation of the healing process eliminates the need for damage detection but results in a repaired structure with any deformations caused by the damage, which could constitute a form of failure.
    b. Healing agents or stored energy are consumables that eventually deplete, limiting the frequency of self-healing events.
    c. Encapsulated liquid healing agents add weight to a material but cannot bear tensile or shear loads in their liquid state, reducing strength-to-weight ratios. This limitation is evident when the strength of healed structures is often reported to be greater than that of the pristine structure (healing efficiency > 100%).
    d. Encapsulated healing agents create stress concentrations and fatigue initiation points within the structure.
2. Non-autonomous self-healing materials typically possess more organized internal structures, akin to composite materials.
    a. Awareness of damage presence is required to activate healing processes, usually via the application of energy in the form of heat, electricity, or light.
    b. Structures enable geometric recovery and multi-step healing processes, emulating the more complex healing observed in biological organisms.

c. Non-autonomous composite structures have demonstrated the potential to achieve the most advanced and complex self-healing capabilities.

Although significant research has been conducted on self-healing materials, the majority has focused on polymeric or ceramic materials due to their relatively simpler synthesis. Metal alloys and metal-metal composites (MMCs) possess numerous properties that are advantageous for the development of self-healing materials. However, there has been limited research in the field of self-healing MMCs due to challenges associated with high-temperature processing and precision in metallurgy.

Metallic Self-healing Materials

The widespread use of metals in our society necessitates designs that minimize failures to avoid severe consequences and costly repairs. Proper design and utilization are essential for preventing fatigue, creep, and fracture failures, but even well-designed materials can contain defects, leading to degradation and failure. Developing self-healing metals that adapt to unpredictable service environments and material properties is a significant challenge. Although self-healing structural metals offer potential advantages and commercial importance, research in this area remains scarce. Recent studies, however, have started exploring new possibilities in self-healing metals.

Presently, metallic self-healing materials are categorized according to their healing mechanisms, emphasizing material structure or autonomy as shown in Figure 1. These bulk metallic self-healing concepts can be divided into two groups based on the characteristic length of the healed damage:

1. Healing of micro scale voids (concepts involving precipitation and nano-scale shape memory alloy (SMA) dispersoids).
2. Healing of macro scale cracks (concepts including SMA-clamp and melt, solder tubes/capsules, coating agent, and electro-healing).

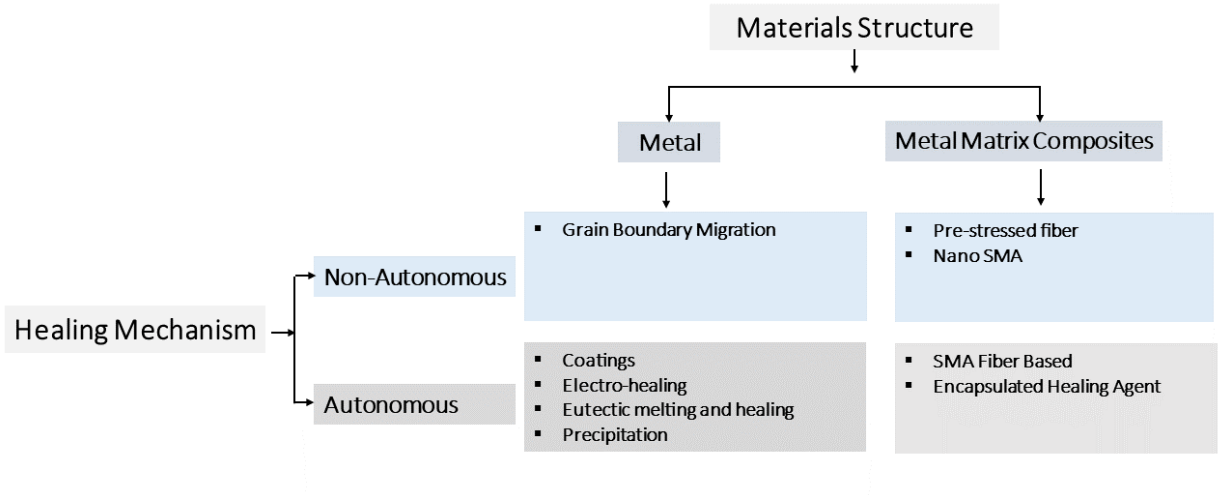

Figure 1: Classification of the investigated metallic self-healing materials [8].

Non-autonomous self-healing materials need external actuation, while autonomous ones do not, although most autonomous metallic self-healing structures are predominantly theoretical with limited experimental validation. Self-healing metal-metal composites (MMCs) feature a macroscopic inhomogeneous structure, often incorporating SMA fibers or encapsulated healing agents in a matrix. Long or short SMA wires have been embedded as reinforcements in metal matrixes (Al, Zn, Sn, or Sn-Bi alloy) to synthesize SMA-based self-healing materials [9]–[14]. Encapsulated healing agent-based self-healing materials are synthesized by including capsules or tubes with healing agents like solder [15], [16]. In contrast, self-healing metals employ more homogeneous healing mechanisms, such as coating-based [17], electro-healing [18], eutectic-based [10], and precipitation-based healing [19]–[23].

The development of autonomous self-healing metals focuses on nano-scale mechanisms, including nano-SMA-dispersoid-based self-healing and grain boundary migration [24], [25]. Precipitation healing has been investigated at high temperatures (575–750˚C) primarily in stainless steel and Cr-Mo-V alloys [25], [26], and at low temperatures (120–185˚C) in Al alloys [20], [23], [27], [28]. Precipitation-based healing, however, is limited to small-scale damage and primarily useful in early damage stages. Nano-SMA-dispersoids-based healing, proposed by Grabowski and Tasan [25], aims to close nanovoids through SMA nanoparticle phase transformation. Although still in the modeling stage, this approach has potential to alter fatigue properties of material structures. Nevertheless, the lack of bonding capabilities might limit its effectiveness.

White et al. pioneered the development of autonomous self-healing polymers by incorporating microcapsules filled healing agent, within a polymeric epoxy matrix containing a catalyst [4], where upon crack propagation, which ruptures the capsules of the monomer agent, and subsequently, the agent flows into the crack and bonds in place upon polymerization due to contact with the catalyst dispersed in the matrix [29]. Self-healing MMCs were devised utilizing encapsulated healing agents, similar to the approach employed in polymers. Rohatgi et al. proposed encapsulated solders for self-healing, to create novel self-healing MMCs [30], [31].

In these techniques, encapsulated low-melting-temperature materials within ceramic shells are dispersed in a high-melting-temperature matrix. Upon crack formation, ceramic carriers break, releasing the melted solder to fill and bond the crack, with strength recovery dependent on wettability and alloy properties [32]. Strength restorations of up to 60% of the original, pre-damaged strength have been achieved. Martinez-Lucci et al. investigated

embedding $Sn_{60}Pb_{40}$ solder-filled Al_2O_3 microtubes in an Al-206 alloy matrix [30]. Ruzek similarly incorporated low-melting healing agents within Al_2O_3 microballoons in metallic matrices, creating self-healing composites [10]. Designing matrix microstructure with capsules filled with solders poses challenges due to pressure infiltration requirements. Additionally, the solder tubes/capsules concept faces challenges during damage and healing phases. Cracks must break the ceramic shell to release solder into the crack, and proper wetting and bonding must occur for effective healing [25]. Unlike self-healing polymers, capsule-based healing in metals requires heat and may introduce residual stress concentrations or affect structural function when bonding in damaged geometry.

Leser et al. developed a self-healing coating for titanium alloys using a 60% Indium and 40% Tin (wt.%) composition, which can be activated multiple times in inert environments, showing potential for multi-cycle heating [33]. Zheng et al. investigated electro-healing in pure nickel sheets, successfully healing cracks and recovering nearly 96% tensile strength [18]. However, the need for immersion in a bath and the small healing scale may be limiting. Ruzek and Rohatgi explored eutectic-based healing, using eutectic liquid as a healing phase while solid dendrites maintain structural integrity [10]. The method involves a matrix alloy composition that forms primary phase dendrites first, pushing interdendritic liquid to the eutectic composition. Upon heating, the eutectic melts, flows into cracks, and solidifies when cooled, enabling self-healing.

SMA-Based Self-healing Metallic Materials

Shape memory alloys (SMAs) integrated into self-healing materials offer a unique capability for restoring bulk geometry after fractures, a crucial attribute for re-establishing a

structure's original functionality following significant damage. SMAs exhibit two distinct properties: shape memory effect and pseudoelasticity [34], which facilitates the necessary actuation upon heating and cooling. However, SMA-reinforced self-healing materials necessitate external actuation, typically heating, to initiate the healing process, rendering them inherently non-autonomous.

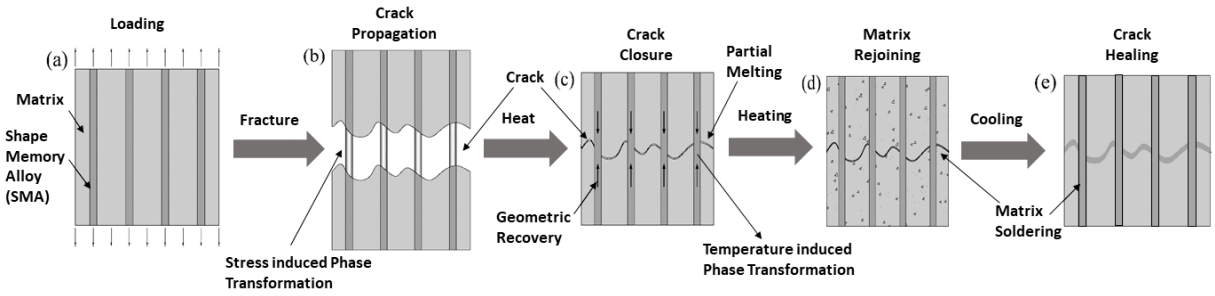

Figure 2: Self-healing process in NiTi reinforced metal-metal composite. a) Initial structure b) fracture c) geometric recovery d) soldering e) healed [9], [11].

The SMA based self-healing concept, schematically represented in Figure 2, involves a composite microstructure comprising SMA reinforcement wires embedded in a solder matrix material, possessing a significantly lower melting point than that of the SMA wires (Figure 2a). When stress exceeding the solder material's ultimate tensile strength is applied to the SMA-solder composite, a crack forms in the solder material, while the SMA wires undergo transformation into the martensite phase (Figure 2b). To accomplish self-healing, the composite sample must be externally heated (Figure 2c) above the austenite transition temperature, inducing a phase transformation of the SMA wires from martensite to austenite. This transition generates compressive stress, contracting the composite sample and bringing the fractured surfaces together (Figure 2d). The temperature must be further increased to melt

the solder, facilitating the rejoining of the fractured surfaces and healing the structure upon cooling (Figure 2e).

The self-healing concept utilizing shape memory alloy (SMA) reinforcement in metal-metal composites has been investigated by numerous researchers [9], [35], [36]. Manuel and Olson have successfully demonstrated the implementation of this self-healing concept in their work, where they optimized a Sn-13at%Bi alloy matrix embedded with continuous uniaxially oriented equiatomic NiTi SMA wires [9]. The schematic representation of the SMA-based self-healing process, as seen in Figure 2, consists of a composite microstructure with SMA reinforcement wires embedded in a solder matrix material. This solder material exhibits a significantly lower melting point compared to the SMA wires. When stress surpassing the solder material's ultimate tensile strength is applied to the composite, a crack forms in the solder material, while the SMA wires transform into the martensite phase. In order to achieve self-healing, the composite sample must be externally heated above the austenite transition temperature, triggering a phase transformation of the SMA wires from martensite to austenite. This transition generates compressive stress, contracts the composite sample, and brings the fractured surfaces together. The temperature must then be increased further to melt the solder, enabling the rejoining of the fractured surfaces and healing the structure upon cooling. It was observed that the crack was closed and the healed specimens demonstrated a recovery of 95% of its original tensile strength. The heating process served a dual purpose, activating the SMA to restore geometry and softening the matrix solders to bond the fracture back together. As the NiTi wires heated, they exerted forces on the matrix while attempting to return to their original geometry (shorter lengths), corresponding to the trained shape of the SMA. Despite the

potential for repeated self-healing under ideal conditions, this approach presents disadvantages such as a strong anisotropic response and the necessity for an externally applied trigger to activate the self-healing process.

Alternative alloys have been explored as matrix materials for self-healing components [9], [13], [14], [36], [37]. Manuel's research on magnesium-based matrices revealed partial healing at specific temperatures [35]. Rohatgi investigated incorporating NiTi SMA wires in an Al-A380 matrix [21]. Due to poor bonding between the wire and matrix, SMA wires were wrapped around a threaded stainless steel rod and cast with Al-A380. The rod functioned as a mechanical anchor, allowing the SMA to pull even if disbonded from the matrix. The reinforced component exhibited nearly double the strength and ductility compared to the unreinforced sample, with a substantial reduction in crack width, but no significant recovered strength [38], [39].

Recent investigations have concentrated on more industrially pertinent host matrix materials, such as the research by Ferguson et al. [14] on a commercial ZnAlCu alloy enforced with NiTi SMA wires, which retained 30% ultimate tensile strength after self-healing. Misra recently developed a self-healing metal matrix composite (MMC) using a Sn-20Bi (wt.%) matrix and 20% NiTi wire reinforcement. Improved bonding was achieved by removing the titanium oxide layer from NiTi and encasing it in flux before casting. Healing assessment involved measuring plastic strain recovery from a three-point bending test. Furthermore, NASA explored Al-based alloys to enhance damage tolerance in aeronautical structures [36], revealing that an AlSi matrix reinforced with 2vol% SMA wires retained more than 90% ultimate tensile strength after self-healing.

Critical challenges for SMA-reinforced self-healing materials encompass securing bonding between the SMA and the matrix, ensuring compatibility between SMA and the metal matrix during synthesis, comprehending the mechanics of the SMA-reinforced matrix and the kinetics of recovery, providing continuous heat supply to activate SMA actuation, and identifying damage location to activate the healing mechanism.

Limitations of SMA-Based Self-healing Metallic Materials

Self-healing materials have garnered significant interest in scientific and industrial applications due to their potential to increase the longevity and reliability of various systems. However, to realize the full potential of these materials, several limitations and concerns must be addressed, particularly for SMA-reinforced self-healing materials. The critical challenges facing the development and implementation of these materials include:

1. Ensuring effective bonding between the SMA and the matrix is of paramount importance for the healing process to occur. Inadequate bonding can lead to reduced mechanical strength, compromising the material's performance, especially in stress-bearing applications. Investigating innovative methods to improve bonding and understanding the interface's physical and chemical properties are essential steps towards overcoming this challenge.
2. Compatibility between the SMA and the metal matrix during synthesis is another crucial aspect to be considered. Achieving compatibility is necessary for creating a successful self-healing material, as not all metallic alloys possess the required phase and composition characteristics to achieve self-healing. Identifying suitable alloy combinations and developing tailored fabrication techniques will help address this issue.

3. A comprehensive understanding of the mechanics of the SMA-reinforced matrix and the kinetics of recovery is essential for optimizing the material's self-healing capabilities and overall performance. Further research into the microstructural, mechanical, and thermodynamic properties of SMA-reinforced composites will enable a more accurate prediction of their behavior and facilitate the development of improved self-healing materials.
4. Providing a continuous heat supply to activate the actuation of SMA remains a challenge, as current self-healing processes necessitate the application of external thermal energy to facilitate healing. Achieving autonomy in the healing process is challenging, and as such, the term "assisted self-healing process" may be more appropriate. Developing novel methods for in-situ heat generation or harnessing environmental energy could help overcome this limitation.
5. Knowledge of damage location is critical for activating the healing mechanism effectively. This requirement implies the need for damage monitoring systems that can detect and initiate the healing process in a timely manner. Integrating advanced sensing and monitoring technologies, such as embedded sensors or non-destructive evaluation techniques, will play a vital role in addressing this challenge.

Furthermore, additional concerns that warrant attention include the number of healing cycles a material can undergo during its service life, ensuring an even distribution of the healing agent within the metal matrix, and the process technology and cost implications of fabricating micro-sized cavities for healing agents. While SMA-reinforced self-healing materials hold

immense potential for various applications, addressing these critical challenges and limitations is essential for their successful development and implementation.

Research Objectives

The main objectives of this research are twofold: firstly, to investigate the potential of utilizing post constrained recovery residual stresses (PCRRS) developed in the Nickel Titanium (NiTi) Shape Memory Alloy (SMA) towards development of self-healing metallic materials; and secondly, to characterize the interfacial bonding between nickel titanium (NiTi) shape memory alloy (SMA) wires and bismuth-tin (BiSn) solder to enable the optimization and design of self-healing metal-metal composites.

Key Research Activities and Thesis Outline

The key research activities of this thesis will concentrate on investigating the post constrained recovery residual stresses (PCRRS) in NiTi shape memory alloys (SMAs) and characterizing the interfacial bonding between NiTi wire and bismuth-tin (BiSn) solder. These two aspects are critical for the successful development of self-healing metal-metal composites. Hence, this thesis will divide into two parts. Part I will focus mainly into details of PCRRS and Part II will concentrate on the interfacial debonding of NiTi and Metal Matrix.

The research activities will encompass the following:

1. Investigation of the Post Constrained Recovery Residual Stress (PCRRS)
    a) Characterization of NiTi SMA mechanical properties to understand the factors influencing PCRRS.

b) Examination of the phase transformation processes in NiTi SMAs, including austenite-martensite transformations and the effect of temperature and different constrained condition on PCRRS performance.

c) Study of the PCRRS regeneration and to evaluate its compatibility for self-healing composite fabrication.

d) Study of the materials phase to evaluate PCRRS stability

2. Interfacial Debonding between NiTi and Metal Matrix:

a) Evaluation of different fabrication techniques to improve the mechanical and chemical properties of the NiTi wire-BiSn solder interface.

b) Investigation of surface treatment methods, such as etching, to enhance interfacial adhesion and overall self-healing performance.

c) Conducting pull testing to evaluate the effectiveness of the interfacial bonding strategies on the composite's performance.

d) Conducting analytical modelling to evaluate the interfacial shear strength and failure phenomena.

Part I:

Insights into the Nature and Characteristics of Post Constrained Recovery Residual Stress in Nickel-Titanium Shape Memory Alloys: A Comprehensive Investigation

This part of the thesis delves into the characteristics of the post constrained recovery residual stress (PCRRS), which is observed in nickel titanium (NiTi) shape memory alloys (SMAs) when they undergo a process of constrained recovery and are returned to a low-temperature condition while maintaining their constraint. A thermomechanical cycling procedure was implemented to instigate the state of PCRRS, following which a series of experiments were carried out. These experiments introduced various deflection profiles from the PCRRS state and subsequently monitored the alterations in the residual stress.

The outcomes from all experiments demonstrated a consistent reduction in stress after each loading cycle, demonstrating a pattern akin to cyclic softening. Intriguingly, the method that was initially employed to generate PCRRS, when repeated, reinstated the original magnitude of the PCRRS. This suggests that the observed reduction in residual stress represents a stable, reproducible, and reversible event, rather than representing actual material degradation.

In order to gain a deeper understanding of PCRRS, a comparative analysis was conducted that examined the modulus correlating stress and strain at different stages of the thermomechanical loading process. This examination revealed that NiTi, in its PCRRS state, exhibits a mix of twinned and detwinned martensite.

The comprehensive understanding of PCRRS, its properties, and its stability could unlock new potentials for advanced engineering applications. This could pave the way for creating materials that exhibit self-healing and fatigue-resistant characteristics by generating stress without requiring continuous actuation over extended periods.

SMA properties and PCRRS

Shape Memory Alloys (SMAs) are at the cutting edge of active material research, primarily attributed to their extraordinary energy density [40]. They are utilized across a broad spectrum of applications as actuators, a role in which they excel due to their unique property of being able to recover their original form through a reversible phase transition. This transformation can be triggered either by thermal actuation or by stress reduction, thereby initiating the Shape Memory Effect (SME) and Pseudoleastic Effect (PE), respectively [41]–[45].

Nickel Titanium (NiTi) alloys, which are approximately equiatomic, are predominantly used in engineering applications. Their popularity can be attributed to their robust characteristics, high recovery potential, and excellent mechanical performance across a range of loading conditions and environments [34]. During the process of constrained recovery, NiTi has been observed to generate significant blocking stresses [41]. This marked stress is produced when continuous thermal actuation prevents NiTi wires from reverting to their original shape.

The Shape Memory Effect (SME) is a unique feature of NiTi, giving it the ability to regain its original shape following deformation. This effect becomes evident when NiTi experiences a solid-state thermo-elastic phase transition. As shown in Figure 3, this transition involves a shift from a high-temperature body-centered cubic austenitic '*parent*' phase (*B2*) to a low-temperature monoclinic martensitic '*product*' phase (*B19´*) [46], [47]. The martensitic phase can present in several variants, primarily twinned and detwinned, based on the applied load. These variants correspond to the same crystal structure but with different spatial orientations in relation to the parent phase [48], [49]. In scenarios where the material is not subjected to mechanical loading or deformation, the NiTi will assume its parent geometry in the high-

temperature austenite state. When the material is cooled through its martensite transition start (M_s) and martensite transition finish (M_f) temperatures without any load or constraints, it undergoes a phase transformation. This transformation leads from austenite to self-accommodated twinned martensite, a process known as the *forward transformation* [50]. The atomic displacements involved in this transformation result in what is termed a *transformation strain*.

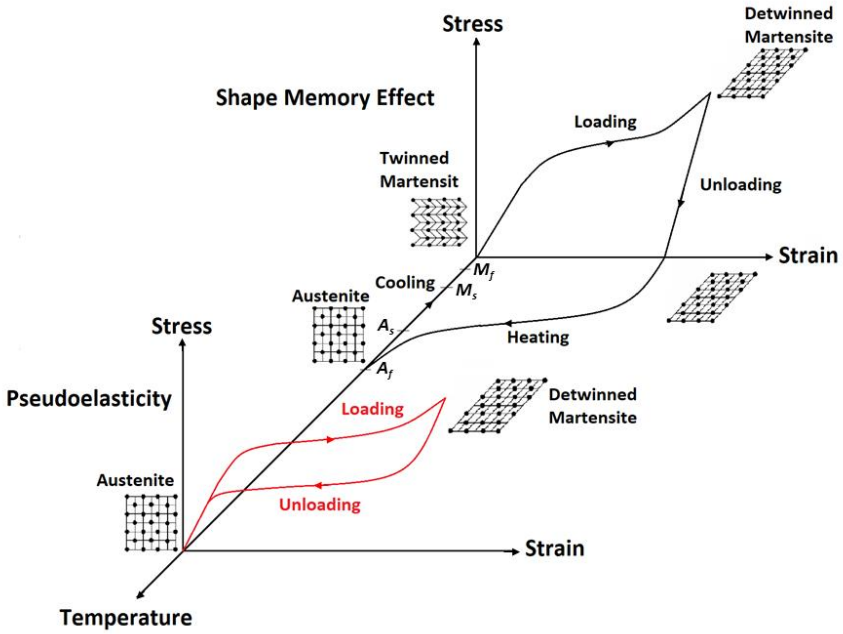

Figure 3: Various thermomechanical responses of a generic shape memory alloy. The two major attributes that the SMAs typically demonstrate as actuators are: shape memory effects (SME) and superelasticity (or pseudoelasticity). Underlying all these behaviors are complex microstructure changes involving reversible martensitic phase transformations and twinning/detwinning processes [51].

When the martensite variants are equally present, the macroscopic strain is near zero, indicating the state of self-accommodated twinned martensite. This balance of variants is crucial in understanding the behavior of NiTi under different conditions and can lead to the development of more efficient and resilient materials in future engineering applications. In the martensitic state at lower temperatures, SMAs can be deformed, appearing to undergo

'apparent' plastic (recoverable) deformations due to the detwinning of martensite. The reorientation of domains result in *recoverable strain* that remains after the load is removed. The detwinning process in SMAs is capable of producing significant strains, exceeding 5% in martensite states and 12% in the austenite state, which is noteworthy considering most metals fail around a strain of 3% [52], [53].

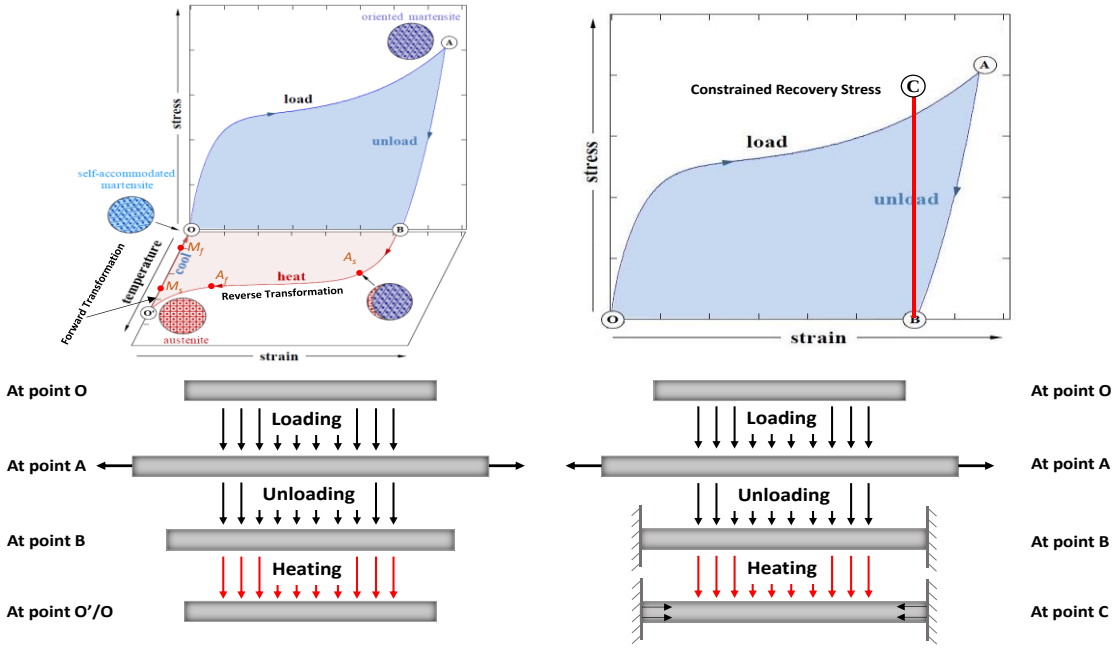

Figure 4: Stress-strain behavior upon thermomechanical loading on SMA: (a) shape memory effect (SME); (b) recovery stress.

The deformation of Shape Memory Alloys (SMAs) in the low-temperature martensite state, when sufficient, can trigger a transformation within martensitic crystalline domains. This transformation shifts the structure from a self-accommodated twinned configuration to a detwinned one. As a result of this reorientation, the material displays a *recoverable strain* that persists even after the applied load has been removed [52], [53]. Upon heating the material through its austenite start (A_s) and finish (A_f) temperatures, the alloy undergoes a *reverse transformation*. This change prompts the re-emergence of the austenitic structure and the

material's inclination to revert to its original, *parent geometry*, thus recouping the recoverable strain [54].

In scenarios where the material is free from physical constraints, this process is termed *stress-free recovery*. During this process, strains as significant as 8% can be recovered [41]. On the other hand, when the NiTi alloy is heated above its A_f temperature while being constrained from resuming its parent geometry, the process is referred to as *constrained recovery* [55], [56]. This procedure can yield a *blocking stress* of over 800 MPa [57]. Two properties - geometric recovery and blocking stress generation via the Shape Memory Effect (SME) - have been harnessed extensively in various industrial applications. These properties find usage in the creation of fasteners, seals, connectors, clamps [41], and even medical devices [58], demonstrating the versatility and practicality of SMAs.

There is a well-established understanding that when the shape memory effect is activated, the thermoelastic martensitic transformation is co-dependent on both stress and temperature, forming a nonlinear relationship [59]. However, predicting the state of phase transformation of Shape Memory Alloys (SMAs) during constrained actuation poses a significant challenge. The generation of blocking stress takes place in a heated mixed state of austenite and stress-induced detwinned martensite during reverse transformation. Typically, these stresses have been found to exhibit a linear relationship with the applied temperature for reverse transformation. This behavior can be illustrated by the Clausius-Clapeyron equation, which is well-known in the field [41], [60]. Although this equation is most fitting for a single crystal of SMA, in polycrystalline situations, linear fits are often obtained by measuring the slopes.

In his seminal work, Duerig et al. delved into the intricate details of the constrained recovery mechanism and its engineering applications [41]. Subsequently, numerous experimental studies have been conducted to probe the nature of recovery stress, its mechanical attributes, the characteristics of its phase transformation, and the influence of different thermomechanical loading scenarios or previous mechanical treatments. For example, Šittner et al. studied the generation of recovery stress in $Ti_{50}Ni_{45}Cu_5$ wires through thermomechanical experiments, employing electric resistance measurements and algorithms to predict the behavior of SMA polycrystals [60]. Li et al. concentrated on understanding the phase transformation behaviors of NiTi during the generation of constrained recovery stress [61]. Vokoun et al. conducted experiments to examine the impact of different constraint conditions on recovery stress [62].

In parallel to experimental investigations, numerous attempts to model the constrained recovery processes theoretically have been made, with the aim of predicting the evolution of constrained shape recovery stresses. Phenomenological models of SMA behavior in a one-dimensional context were proposed by Tanaka [63] and later modified by Liang and Rogers [64] and Brinson [65]. These models aimed to analytically predict the behavior of SMAs in a constrained state. Specifically, Kato et al. developed a one-dimensional model to predict the constrained recovery stress of NiTi SMA based on temperature state and the maximum strain applied. This model utilized the elastic strain energy and the Helmholtz free energy of the two phases [66]. Videnic et al. presented multiple studies on constrained recovery in SMA wires using generalized plasticity, as developed by Lubliner and Auricchio [67], [68]. This work

assumed a non-constant value of Young's Modulus, and the predicted SMA behaviors were corroborated with experimental results [69]–[71].

Recent Studies on PCRRS

Shape memory alloys (SMAs) comprising Nickel Titanium (NiTi) have garnered considerable attention and application due to their extraordinary resilience against large deformations and their capacity to generate substantial forces over extended distances. Recent empirical studies have unveiled a novel phenomenon in which these alloys can generate sustained stress without the need for ongoing thermal actuation [38], [72]–[75]. In scenarios where the SMA undergoes constrained recovery and subsequently has its temperature lowered to ambient conditions while retaining its constrained geometry, it is found to produce what is termed as 'post constrained recovery residual stresses' (PCRRS). This unique feature potentially revolutionizes the use of the material as an actuator, offering advantages in areas such as self-healing materials, while also paving the way for innovative applications. For instance, employing a dispersion of NiTi particles could potentially mitigate fatigue cracking in material structures.

Subsequent experiments examining PCRRS have confirmed the ability of the alloy to produce residual stresses independent of continuous energy input, offering promising prospects for the development of smart materials and structural designs. However, the understanding of the macro-scale stability and origins of this characteristic remains a topic of ongoing research. The present study aims to augment our understanding of PCRRS properties through experimental analysis, focusing on the different loading conditions impacting the residual stress state.

Prior research primarily emphasized the mechanics of the blocking stress generated in the high temperature constrained state. Only a handful of researchers have highlighted the generation of PCRRS, and even fewer have conducted comprehensive studies to unravel the mechanisms underlying its generation. Despite these initial efforts, a detailed exploration into the state, stability, and nature of PCRRS, including the mechanisms beyond its generation, remains a critical area to uncover. Daghia et al. proposed a low-temperature stress generation model following constrained recovery, a modification of the existing Brinson model [76]. Yet, a thorough understanding of the transformational behavior at low temperatures and low stress is required to accurately characterize this phenomenon. Tran et al. performed a parametric study on the generation of low-temperature stress in NiTi wires using a modified analytical model. They demonstrated that PCRRS is influenced by the amount of recoverable strain generated during the loading and unloading from the martensite state prior to constrained recovery [77].

The Swiss Federal Laboratories for Materials Science and Technology, Empa, spearheaded a series of comprehensive investigations into the characteristics of iron-based shape memory alloy (SMA) materials, with an emphasis on applications within the realm of civil engineering. The researchers presented experimental findings on the generation of stress at low temperatures following a state of constrained recovery [78]–[81]. It is important to distinguish between the mechanisms underpinning the shape memory effect (SME) in Nickel Titanium (NiTi) and iron-based SMAs. For NiTi, SME is predicated on the motion of various martensite variants. On the other hand, in iron-based SMAs, SME arises from the stress-induced transformation from the parent austenite γ-phase (face-centered cubic- fcc) to the martensite ε-phase (hexagonal close packed- hcp), followed by heat-induced reversion from ε-phase back

to γ phase [82]. A key distinction between these materials lies in their stress behavior during cooling to ambient temperature under constrained conditions. In the case of iron-based SMAs, stress increases during this process, whereas NiTi experiences stress reduction. This pattern of stress generation was also observed by Choi et al. in their study of NiTi-Nb materials, indicating a similar trend to NiTi [83], [84].

Nonetheless, these investigations did not delve into the comprehensive analysis of post constrained recovery residual stresses (PCRRS), its mechanisms, or its potential applications. A notable gap in these studies is the absence of insight into the behavior of these materials under varying loading conditions following the formation of PCRRS. Additionally, the long-term stability of these materials remains unexplored in the aforementioned studies. While the residual loads produced during the constrained recovery process have been utilized in various actuation applications, these methods typically demand a continuous application of energy to maintain the SMA at an elevated temperature. Yet, achieving actuation without the need for constant energy application could lead to greater efficiency in several applications, particularly in the realm of self-healing materials or pre-stressed structures.

Recent studies have demonstrated that the residual loads generated post constrained recovery and thermal actuation have potential advantages, as they can be repeatedly generated without the need for continuous heat energy application [38], [72]–[75]. After the process of constrained recovery, where stress is generated through reverse martensitic transformation, subjecting the SMA elements to forward transformation (by cooling them below the martensite transition finish temperatures, M_f, in a constrained geometry) results in

the formation of stable stress within the martensitic phase. This is known as Post Constrained Recovery Residual Stress (PCRRS).

Challenges

Previous studies have primarily focused on the capacity to produce Post Constrained Recovery Residual Stress (PCRRS) in singular formulations of equiatomic Nickel Titanium (NiTi) wires, with emphasis on the mechanical creation of this residual stress. The potential of this unique phenomenon to generate enduring residual stress without the necessity for continuous thermal energy could open new avenues in existing applications, such as self-healing materials. Additionally, it could pave the way for the innovative usage of NiTi Shape Memory Alloys (SMAs) in novel applications, for instance, employing a dispersion of NiTi particles to curtail fatigue cracking in various material structures [38]. Nevertheless, our comprehension of the characteristics, origins, and extent of this phenomenon remains rather limited.

There remains a substantial amount of work to thoroughly decode the underlying mechanisms that give rise to PCRRS and to understand the evolution of PCRRS under persistent thermo-mechanical loading. A profound exploration of the effects of training or pre-working, along with a detailed microstructural analysis, is essential to formulate theoretical explanations, gain insights, and develop models that adequately represent the PCRRS phenomenon.

The research presented here embarks on a detailed examination of the mechanical properties beyond the generation of PCRRS, with the ultimate aim of fostering a more comprehensive understanding of the mechanisms instigating this phenomenon. This work strives to delve into the potential properties existing beyond the PCRRS state, coupled with a

phenomenological analysis of the origins of PCRRS. The objective here is to uncover attributes pertinent to structural design and foster a deeper understanding of the PCRRS phenomenon.

Approach

The research presented in this work undertakes rigorous experimental testing, applying various strains from the Post Constrained Recovery Residual Stress (PCRRS) state. The main objective of this is to delve into the inherent nature and stability of the PCRRS state. Critical material properties, such as the local modulus of elasticity correlating to stress and strain at distinct stages in the thermo-mechanical cycling, were assessed. The data garnered from these tests were then analyzed to predict the material phases in the PCRRS states.

A series of mechanical experiments were carried out to gain insight into the mechanical and material properties encapsulating the PCRRS state. The experiments aimed to: 1) assess the stability of the observed PCRRS through several cycles involving both high strain and low strain applications, 2) determine the effects of pre-working or training the samples on PCRRSs, and 3) examine the mechanical properties when loading from the PCRRS state. To ensure the generality of our observations, these experiments were replicated on samples with varying formulations and transformation temperatures, thereby confirming that the observed properties were not specific to a single formulation.

This research endeavor aims to bolster the understanding of NiTi by broadening experimental explorations around PCRRS region. Consequently, this study presents both experimental results and analysis on the following: (i) the impact of releasing PCRRS (negative strain and associated tension reduction from the PCRRS state), (ii) investigation of material behavior while applying successive increasing strains from the PCRRS states, and (iii)

comparison and alignment of predictable states to unknown states based on the local elastic modulus relating stress and strain while applying small strain within the elastic range at different stages of the PCRRS loading path.

Methods

A series of thermomechanical tests were conducted on samples, all originating from the Post Constrained Recovery Residual Stress (PCRRS) state. To ensure uniformity and consistency, all samples underwent a preparation phase to confirm they were in their initial configuration, residing in a self-accommodated twinned martensite state as elucidated in the following section.

Following this, the samples were subjected to an initial cycle and were returned to their low-temperature martensitic state in order to engender the PCRRS. From the PCRRS state, a variety of different experiments were then carried out to investigate the stability and inherent nature of the PCRRS. It is crucial to note that, for maintaining the integrity of the study, all the strain rates applied and the rates of thermal cycling were kept consistent across the different experiments conducted in this research.

Sample Preparation

All experiments were performed on commercially available samples of NiTi with different formulations, diameters and properties supplied by Dynalloy Inc. (CA, USA) and SAES Getters S.p.A. (Lainate, Italy). Matching experiments were performed, and similar results were produced with Dynalloy's Flexinol 70 NiTi and SAES Group's SmartFlex NiTi 70, SmartFlex NiTi 95, and SmartFlex NiTiCu 75 with properties summarized in Table 1.

Table 1: SMA materials tested and their phase transformation temperatures

Material	A_s (˚C)	A_f (˚C)	M_s (˚C)	M_f (˚C)
Flexinol NiTi 90 (Ni-50%)	90	110	75	65
Flexinol NiTi 70 (Ni-50%)	70	80	60	50
SmartFlex NiTi 70 (Ni-55%)	70	90	60	40
SmartFlex NiTi 95 (Ni-54.8%)	95	115	85	65
SmartFlex NiTiCu 75 (Ni-54.8%, Cu-6%)	75	90	65	50

The experimental work carried out for this study utilized a DMA Q800 Dynamic Mechanical Analyzer (DMA) from TA Instruments, New Castle, DE. This device, equipped with integrated capabilities, was employed to apply and gauge mechanical loads, physical displacements, and thermal cycles. Except where otherwise indicated, the specific results discussed in this dissertation were mainly derived from tests conducted on Flexinol 90 NiTi wire from Dynalloy, possessing a diameter of 0.004 inches (0.10 mm). All imposed strain rates were kept at 0.5% strain/min, and rates for the application and removal of heat were maintained at 5 °C/min. Despite the fact that the magnitude of the results varied with different materials, the observed trends aligned consistently with those presented for Flexinol 90. The initial preparation procedures of the samples for the DMA experiments have been outlined in detail in previous works on PCRRS by Haider et al [72], [74].

In order to ensure a consistent starting point for all testing and same phase at the onset of the experiment, samples were thermally actuated in same manner to obtain the self-accommodated twinned martensite stat. The initial loading steps are followings:

- Step-1: obtain a purely austenite parent phase by increasing the temperature above A_f in a free and unconstrained condition.

- Step-2: obtain a purely self-accommodated martensite specimen by decreasing the temperature under M_f in a free and unconstrained condition.

No changes in the geometry were observed during the forward transformation, therefore the samples at this point were considered to be in their parent geometry in the martensitic state or in their 'initial configuration'.

Initial Cycle to Generate PCRRS

Samples, in it's the low temperature self-accommodated twinned martensite state in the parent geometry, were mounted into the DMA and loading cycle began to generate PCRRS. As shown in the Figure 5, following loading steps were applied to obtain PCRRS:

- Step-1: Apply a tensile strain while maintaining the temperature represented by 'path 1' from point O to point A, a predesignated maximum strain, ε_A with corresponding stress, σ_A.
- Step-2: Unload to zero stress, following the 'path 2' between points A and B and a recoverable strain, ε_R is observed at the zero-stress state at point B. This process is well understood and attributable to the detwinning of martensite, due to fact that, compared to the initial length of the wire at Point O, the final length at point B is higher.
- Step-3: Keeping the sample constrained at point B, the temperature was increased beyond A_f to return to austenite state, following 'path 3' through the reverse transformation to an austenite state. A 'blocking stress, σ_C' develops in the wire, as it would like to recover its initial length undergoing constrained recovery.

- Step-4: While continuing to maintain constrained conditions, the temperature was reduced back lower than M_f following 'path 4' through the forward transformation leading to martensite production and stress decrease because the material optimizes the proportions of martensite variants to relax the stresses in the specimen. After these phase transitions, while maintaining the length, a residual load called post constrained recovery residual stress, σ_{CS} was observed in the low temperature state at point D in the schematic diagram. The (recoverable) strain, (constrained) length, and temperature (20° C) at point 'D' are cumulatively referred to as the PCRRS State and served as a base point for the continued experimentation.

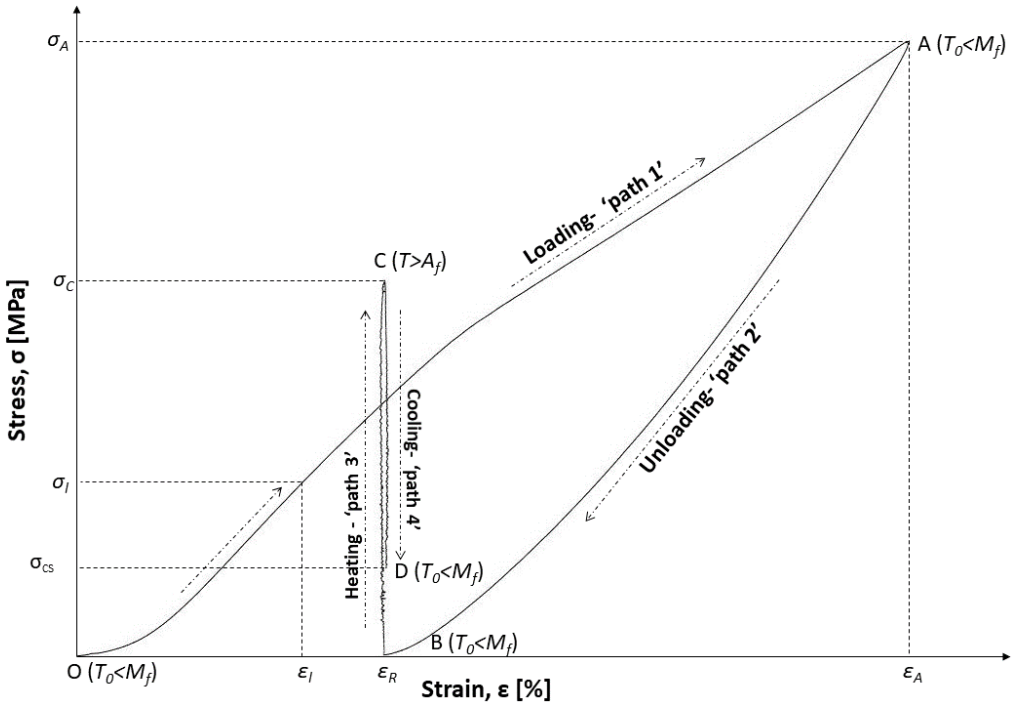

Figure 5: A representation of the corresponding stress-strain response upon thermomechanical loading to generate PCRRS.

In the third phase of the experimentation, some variations in this experimental process were imposed with maximum temperatures up to 150° C to ensure that A_f was reached independent of the constraint/applied strain. No differences were observed between the 120°

C and 150° C cycles, so 120° C was used as the standard for the experiments. It is well understood that stress can shift the transition temperatures governing the SME. Similarly, at a given temperature above A_f, the application of stress can induce the reverse transformation, leading to stress induced martensite and the PE. As a result, simply raising the temperature beyond A_f would not guarantee full Austenite transformation, however, the stress induced shift in transition temperatures didn't change the experimentally observed results.

Subsequent tests were conducted with various predetermined maximum strain levels set at 3.4%, 3.9%, 4.4%, and 5.0%. These tests adhered to the same thermo-mechanical loading parameters as previously stated. The response to these varying levels of strain is illustrated in Figure 6, which presents a three-dimensional Stress-Temperature-Strain plot. To establish a relationship between the recoverable strain and the magnitude of the PCRRS generated in relation to the maximum strain to which the samples were subjected, linear regression analyses were performed. The data used for these analyses is compiled in Table-2.

In the course of testing the ternary alloy, specifically SmartFlex NiTiCu 75 (comprising Ni-54.8% and Cu-6%), a peculiar oscillation in stress was observed. This occurred as the material was heated through the reverse transformation and underwent constrained recovery. Notwithstanding this irregularity, the material continued to generate the Post Constrained Recovery Residual Stress (PCRRS) under investigation, subsequent to cooling through the forward transformation to room temperature martensite. These tests were replicated on several distinct samples of the material, and the outcomes remained consistent. It is conceivable that this unexpected phenomenon could be the result of an R-phase transformation, potentially linked to the additional Cu alloying element [44]. However, as this

irregularity did not influence the production of PCRRSs, and subsequent results aligned with the findings from other tested formulations, the anomaly was deemed to be of minor significance to this research. As a result, it was not subject to further scrutiny within the confines of this study.

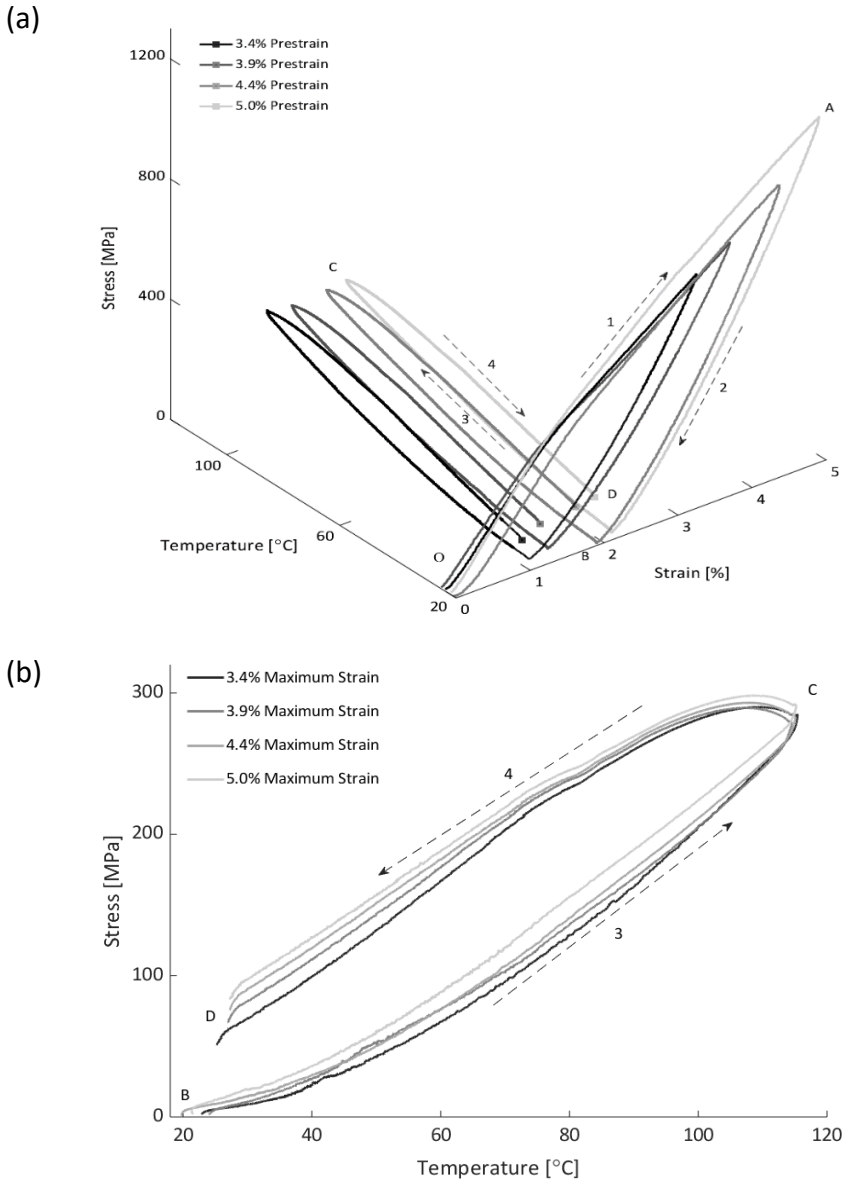

Figure 6: (a) Experimentally measured Stress-Strain-Temperature relationships for NiTi initial cycles of PCRRS loading path for predetermined prestrain (point A) of 3.4%, 3.9%, 4.4% and 5% and resulting in PCRRS (point D) following the constrained recovery. For the ease of interpretation, paths and points are labeled for the 5% strain case (dashed line) and (b) Stress Temperature 2D plane showing the thermal loading path from the constrained state.

Table 2: Recoverable Strain and PCRRS values corresponding to different maximum strain applied to NiTi SMA

Maximum Strain (ε_A), %	Recoverable Strain (ε_R), %	PCRRS (σ_{CS}), MPa
3.4	1.13	51.28
3.9	1.44	67.16
4.4	1.93	75.86
5.0	2.20	83.19

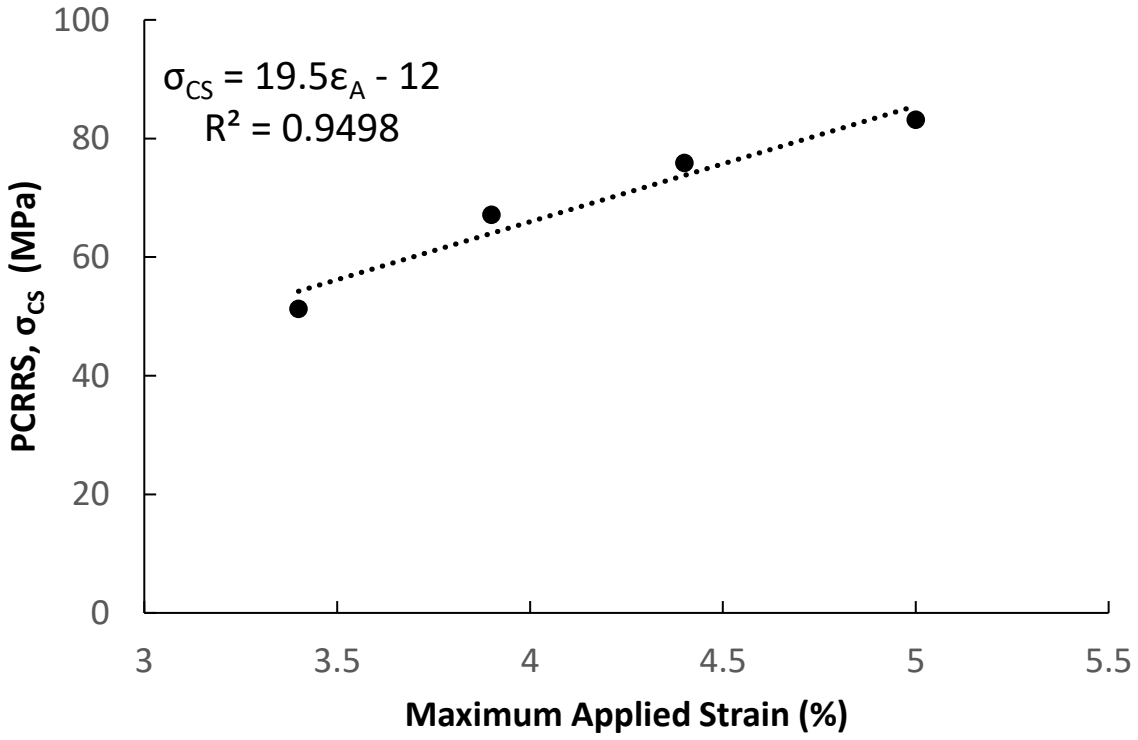

Figure 7: Magnitude of PCRRS generated as a function of maximum strain applied to the sample.

A series of linear regressions were conducted to establish the relationship between the recoverable strain and the magnitude of the PCRRS produced, with respect to the maximum strain the samples were subjected to. This was performed using the data depicted in Figure 6 and collated in Table 2. The recoverable strains (ε_R) were assessed at point B and were maintained at a constant rate throughout the thermal cycle, which encompasses paths 3 and 4,

including points C and D. The magnitudes of the recoverable strains, expressed as a percentage, were correlated with the magnitudes of the maximum strain (ε_A) at point A, also represented in percentage terms. The derived equation, $\varepsilon_R = 0.7\varepsilon_A - 1.22$, was found to be a good fit for the data, as evidenced by a high coefficient of determination (R^2) of 0.978. Similarly, the constrained stress or PCRRS (σ_{CS}), measured in MPa at point(s) D, was correlated with the maximum strain (ε_A) at point A (expressed as a percentage). This relationship was captured in the equation, $\sigma_{CS} = 19.5\varepsilon_A - 12$, which exhibited a strong fit with the data, indicated by an R^2 value of 0.95 (see Figure 7).

Figure 7 presents evidence of a fairly linear relationship between the maximum strains imposed and the consequent constrained stresses (σ_{CS}), revealing an intrinsic link between these two parameters. This relationship is further supported by the analogous trends observed in the thermomechanical loading paths across all experiments applying these maximum strain values, as depicted in Figure 6.

To ensure continuity and comparability in the interpretation of results, the subsequent results and accompanying analysis in this thesis are primarily based on the experiment implementing a maximum strain of 3.4%, unless explicitly mentioned otherwise. This decision was made to facilitate the examination of the PCRRS phenomenon under consistent conditions, thereby enabling a more cohesive and robust understanding of the material behavior under study. This approach will ensure that the findings presented are reliable and that the conclusions drawn are grounded in rigorous experimental data.

Property Explorations from PCRRS

This research involved four distinct experimental protocols, all conducted on analogous samples of NiTi wire. Each experimental sequence commenced with the generation of the PCRRS within the sample, employing the method detailed in previous section. Subsequently, the samples in the PCRRS state were subjected to various mechanical conditions designed to examine the evolution of residual stress under different loading scenarios:

In the first set of experiments, the sample was strained back to the maximum strain initially used to induce the PCRRS state (3.4%, 3.9%, 4.4%, or 5%). This was followed by relaxing the sample back to its original constrained length, thus observing how the sample responds to a full strain cycle.

The second experimental protocol involved the repeated application and removal of a tensile strain of 0.5% relative to the constrained length. This allowed to evaluate the sample's resilience and adaptability to cyclic tensile loading conditions.

In the third set of experiments, the sample was subjected to an increasing sequence of tensile strains, followed by their subsequent removal. This incremental approach provided insights into the sample's response to a progressively escalating mechanical stimulus.

Lastly, the fourth experiment centered on the repeated application and removal of negative strain, implying a reduction in length from the constrained state. This served to investigate how the sample coped with compressive strain cycles and the subsequent impacts on the PCRRS state.

These experiments, designed meticulously, allowed to explore a wide range of mechanical conditions that NiTi wires could face in practical applications, thereby providing a comprehensive understanding of the behavior and potential of NiTi wires in the PCRRS state.

Repeated Large Strains Applications with Thermal Cycling

The experimental process commenced from the Post Constrained Recovery Residual Stress (PCRRS) state, represented by point D. Here, the samples were subjected to a total strain that was congruent with the maximum strain utilized during the creation of the PCRRS (e.g., a total of 3.4% from the initial length). This was carried out through 'path 5', which mirrored 'path 1', and subsequently unloaded in accordance with 'path 2', as illustrated in Figure 8.

Upon reaching this stage, the PCRRS was observed to have diminished to almost zero. This reduction to a zero-stress state at the same recoverable strain as in the initial cycle suggests an equivalent detwinning of the martensite phase at ambient temperature. Following this, the thermal cycle and constrained recovery were repeated, passing through the reverse and forward transformations, thereby leading to the reformation of the PCRRS at point D.

This procedure was repeated on multiple occasions, each time successfully eliminating and then reinstating the PCRRS, with the magnitude remaining largely consistent. This consistent pattern suggests that the PCRRS generation and removal process is not only stable but also reversible. Over multiple cycles, there was a marginal reduction in the magnitude of the PCRRS during the initial few cycles. However, this value eventually stabilized, as depicted in Table 3 and Figure 9. This pattern is in line with the known 'training' behavior of NiTi shape memory alloys, where repeated cycling leads to a stabilization of the material's properties.

(a)

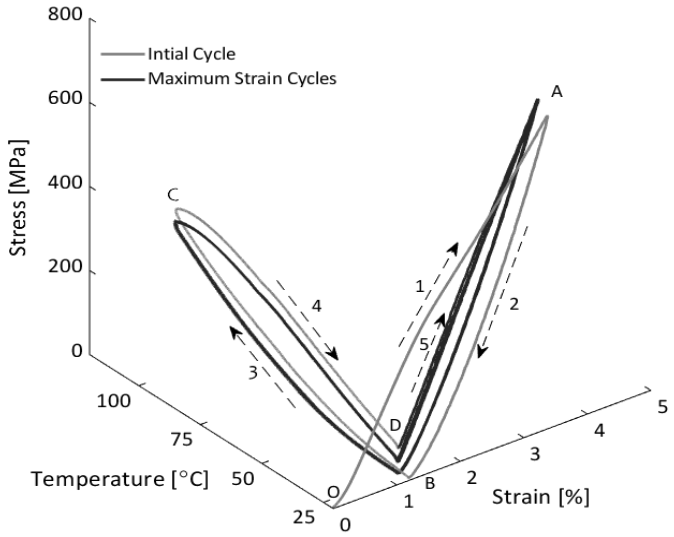

(b)

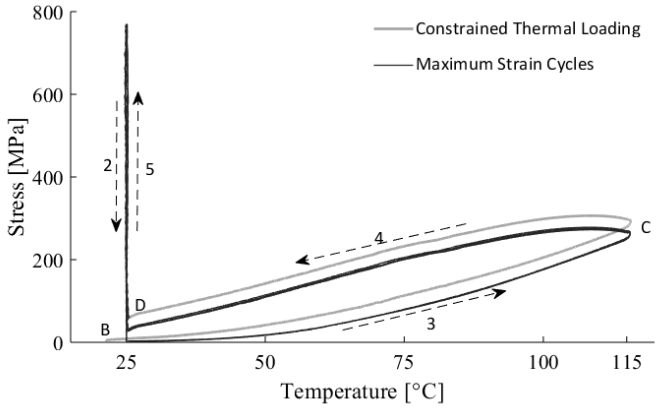

Figure 8: (a) Stress-Temperature-Strain relationship for NiTi for samples subjected to repetition of the maximum strain starting from the PCRRS state and (b) Stress- Temperature 2D plane showing PCRRS regeneration upon the thermal loading and unloading while in constrained state.

Table 3: PCRRS values corresponding to repeated maximum strain cycles applied from the PCRRS state

Repeated Maximum Strain	Constrained Stress (σ_{CS}), MPa
Initial PCRRS Cycle	58.77
Maximum Strain Cycle 1	31.18
Maximum Strain Cycle 2	27.91
Maximum Strain Cycle 3	27.42
Maximum Strain Cycle 4	26.65

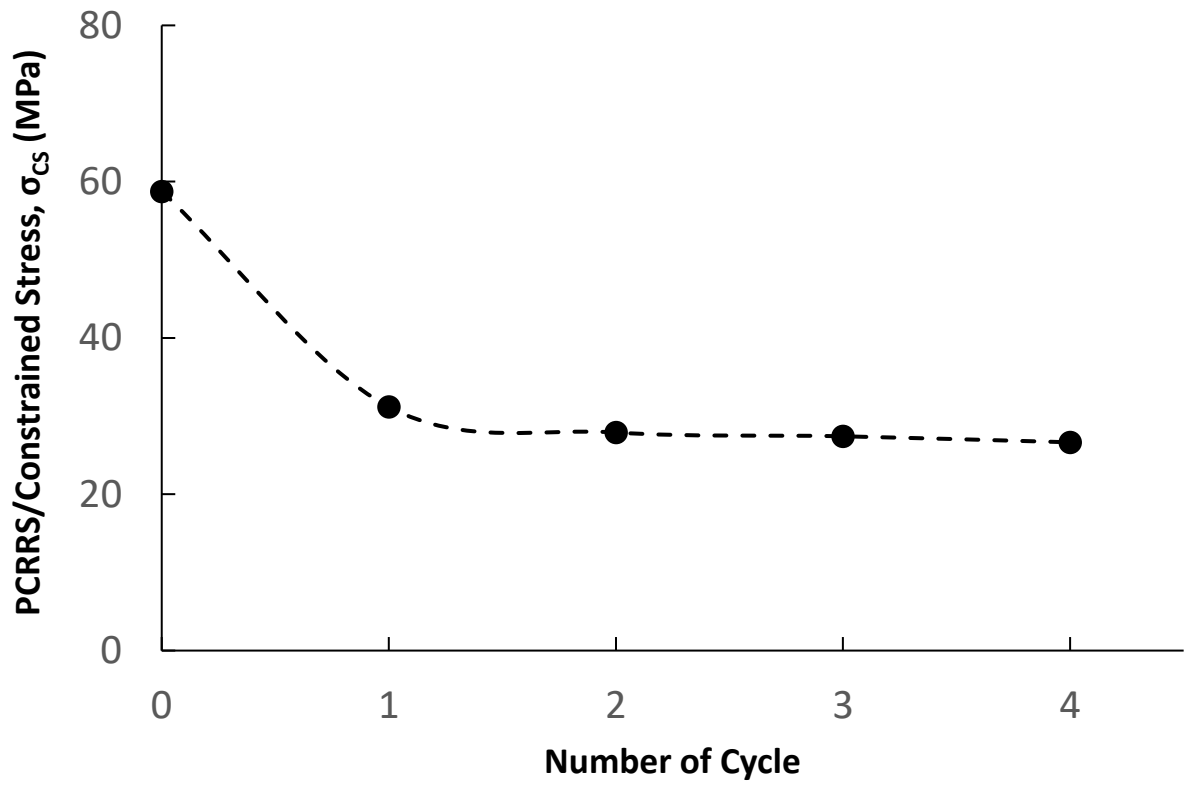

Figure 9: PCRRS measured as initially generated (0) and after multiple cycle s of exposing specimens to maximum strain and a repeated thermal mechanical cycle to regenerate the PCRRS.

Repeated Application and Removal of 0.5% Tensile Strain

Commencing from the PCRRS state at point D, and under ambient temperature conditions, the samples were subjected to repeated cycles of applying and then removing an extra 0.5% tensile strain relative to the PCRRS. This process is represented by 'path 5' and 'path 6' in Figure 10. After each strain cycle, a slight reduction in the PCRRS was observed, as evidenced in Table 4 and Figure 11. Remarkably, the PCRRS could be reestablished via thermally cycling in the constrained state, reinforcing the reversible nature of this phenomenon. Despite generating a marginally smaller initial PCRRS in the first cycle (58.77 MPa versus 53.37 MPa), there was an intriguing similarity between the trained and untrained specimens. Both exhibited nearly identical slopes when observing the reduction of PCRRS upon the cyclical process of loading and unloading.

(a)

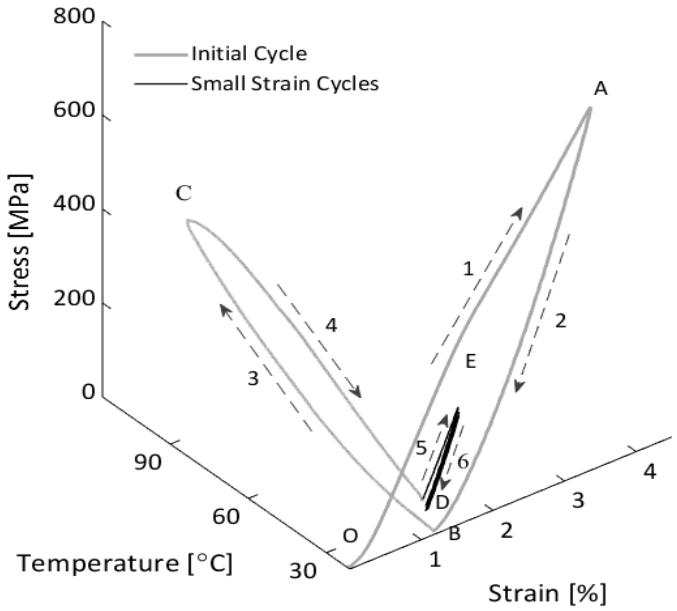

(b)

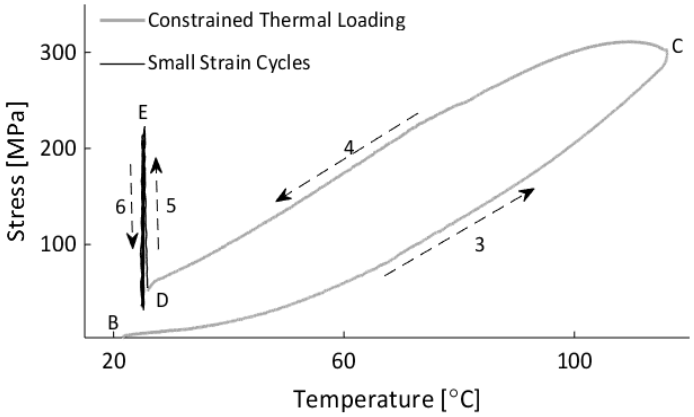

Figure 10: (a) Stress-Temperature-Strain relationship for NiTi for samples exposed to smaller strain from the PCRRS state and (b) Stress- Temperature 2D plot showing PCRRS regeneration upon small strain application from the constrained state.

The measured stress and temperature were plotted on an approximate phase diagram. This highlights that the phenomena of interest, cycling between points D and E, occurred well in the martensite region, far from the austenite and martensite transition regions. Because application of the 0.5% strains occurred well below M_f, martensite should be the only stable phase possible, however the twinned vs. detwinned state was unknown.

Table 4: Stress-Temperature-Strain relationship for NiTi for samples exposed to repeated 0.5% strain cycles from the PCRRS state

Repetitive 0.5% Strain from PCRRS State	Constrained Stress (σ_{CS}), MPa
Initial PCRRS Cycle	53.37
0.5% Strain Cycle 1	42.48
0.5% Strain Cycle 2	35.90
0.5% Strain Cycle 3	31.62
0.5% Strain Cycle 4	30.30

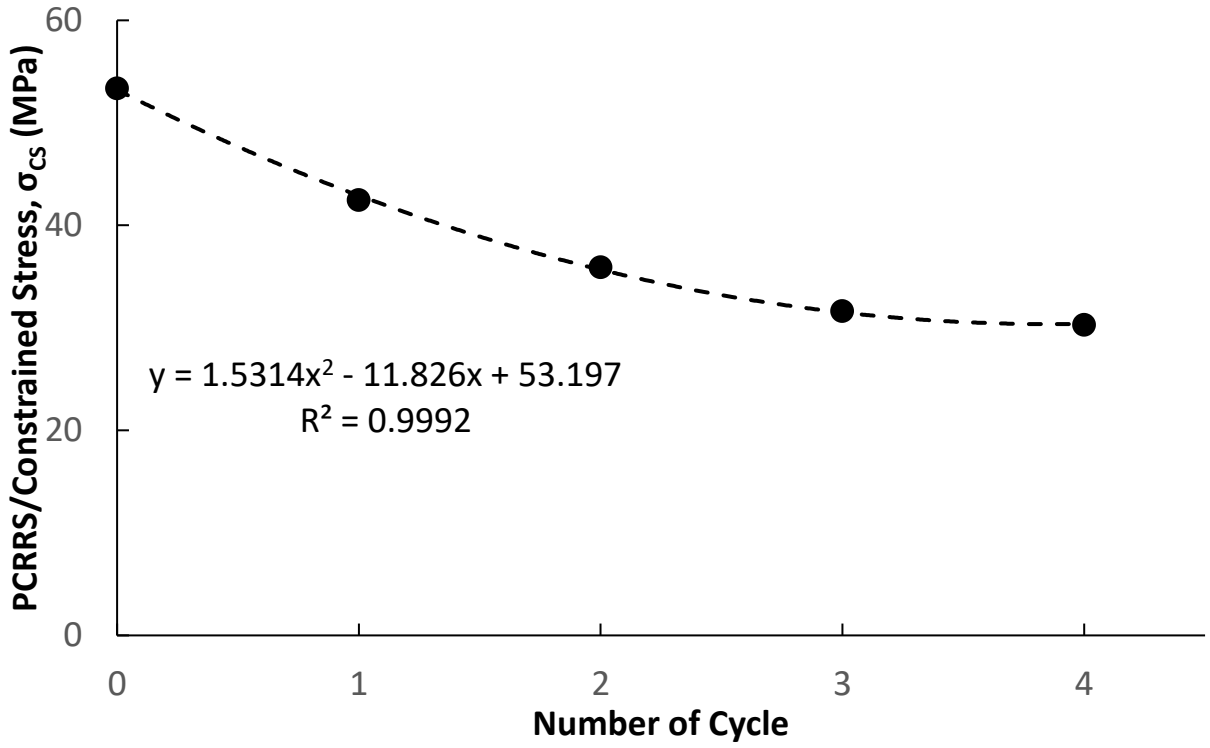

Figure 11: Residual stress measured after initial generation of PCRRS (0) and cycles of application and removal of 0.5% strain.

Repeated Application and Removal of Incrementally Increasing Tensile Strain (0.1%-0.5%)

In the quest for a more comprehensive understanding of the Post Constrained Recovery Residual Stress (PCRRS) phenomenon, an additional experiment was designed that focused on variational loading starting from the PCRRS state. This experimental strategy was distinct in that it wasn't limited to monotonic small strain applications. The samples, beginning from the PCRRS state at point D and under ambient temperature conditions, were exposed to five cycles of

incrementally increasing tensile strain. This was initiated from a modest strain of 0.1%, progressively increasing in increments to reach 0.5%, relative to the PCRRS state at point D shown in Figure 12.

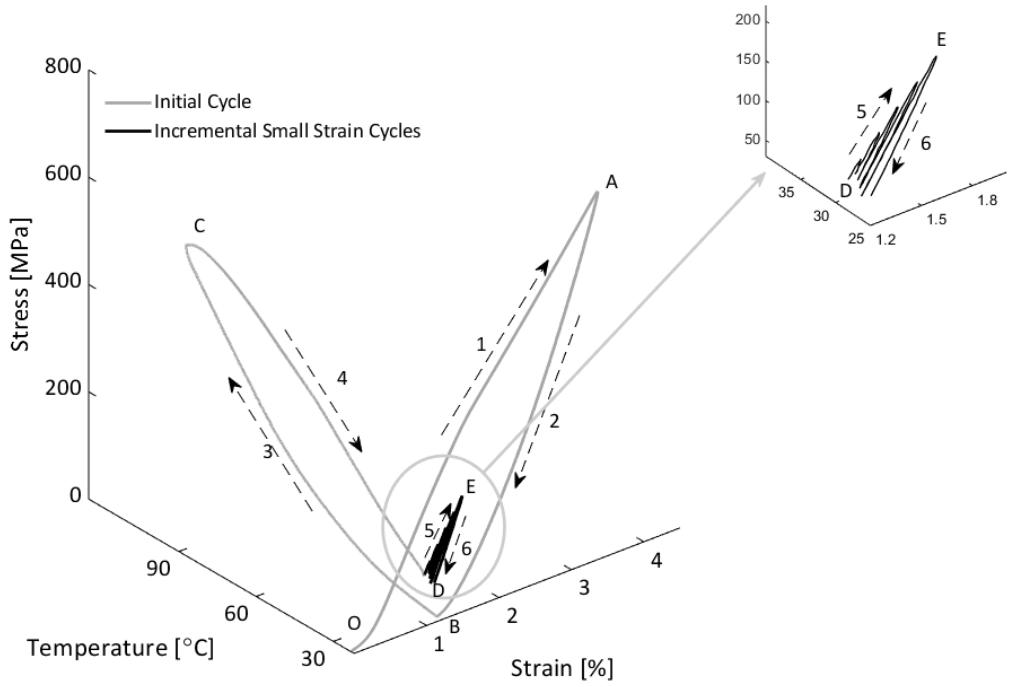

Figure 12: Stress-Temperature-Strain relationship for NiTi for samples exposed to increasing strain from the PCRRS state.

Insightful results emerged as shown in Figure 13, where the NiTi wires exhibited similar behavior across each strain cycle, characterized by comparable slopes. This consistent pattern suggests a predictable response of the material to these variational loading cycles. Notably, a gradual reduction in PCRRS values was observed upon each strain application shown in Table 5, indicating a possible relationship between the applied strain and the evolution of PCRRS. This result contributes to a more nuanced understanding of the stability and adaptability of PCRRS under varying strain conditions.

Table 5: PCRRS values corresponding to consecutive increasing strain cycles applied from the PCRRS state

Incrementally Increasing Strain from PCRRS State	Constrained Stress (σ_{CS}), MPa
Initial PCRRS Cycle	65.23
0.1% Strain Cycle	62.92
0.2% Strain Cycle	56.18
0.3% Strain Cycle	47.55
0.4% Strain Cycle	39.19
0.5% Strain Cycle	36.35

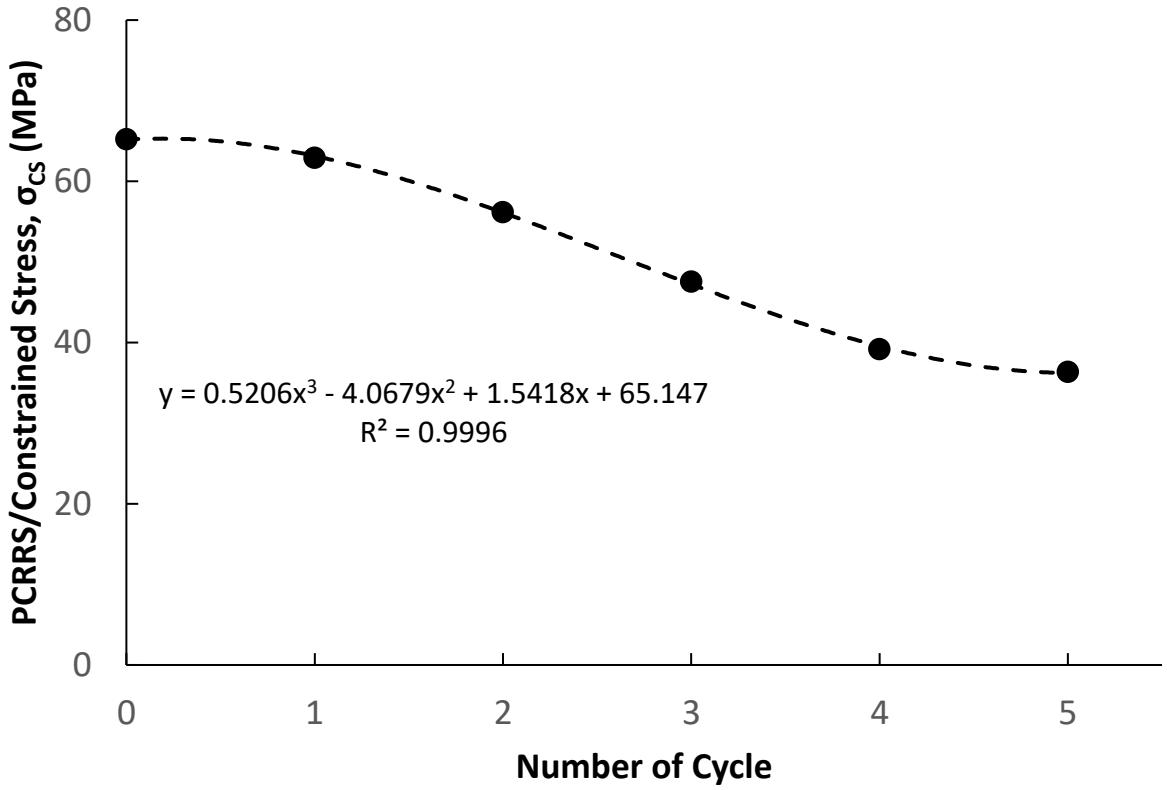

Figure 13: Plot of regression analysis of Post Constrained Recovery Residual Stress, PCRRS (σ_{CS}) with respect to repeated application and removal of incrementally increasing strain cycle from 0.1% to 0.5%.

Repeated Release and Restoration of Small Strain

In the pursuit of a comprehensive understanding of the PCRRS phenomenon, an experiment was conducted that began with samples in the PCRRS state at point D and ambient temperature. The samples were then subjected to a cycle of stress and strain reduction,

followed by a restoration of the material to its constrained length. This experimental procedure was carried out with meticulous care to prevent any compression, given the likelihood of buckling due to the slim profile of the wire samples, which were only 0.10 mm in diameter.

The procedure involved reducing the strain by 0.1% from the constrained length, as illustrated by 'path 5' in Figure 14. Subsequently, the samples were returned to the constrained length characteristic of the PCRRS state. This iterative process resulted in a consistent decrease in constrained stress with each cycle, as evidenced by the data in Table 6 and the graphical representation in Figure 15.

Interestingly, despite the reduced constrained stress, the complete PCRRS could be regenerated through a process of thermal cycling while constrained. This finding underscores the resilience and adaptability of the PCRRS phenomenon under varying conditions, contributing to our expanding knowledge base on this intricate material behavior.

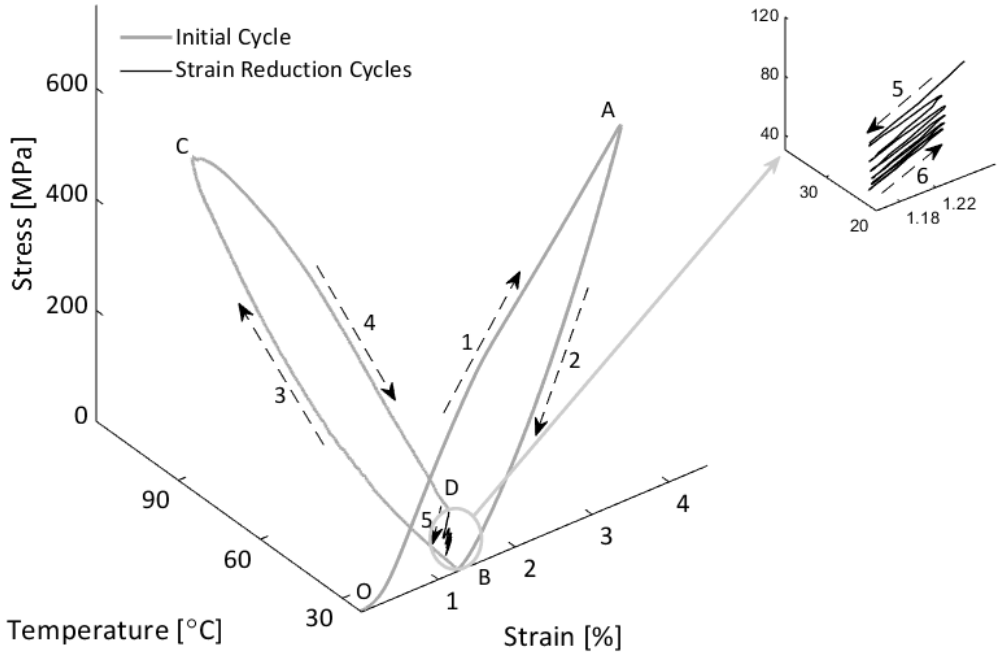

Figure 14: Stress-Temperature-Strain relationship for NiTi for samples exposed to residual load reduction cycle after initial cycle from the PCRRS state.

Table 6: PCRRS values corresponding to repeated relaxation and restoration of -0.1 strain cycles applied from the PCRRS state

Repetitive Strain Release from PCRRS State	Constrained Stress (σ_{CS}), MPa
Initial PCRRS Cycle	62.36
-0.1% Strain Release Cycle 1	52.74
-0.1% Strain Release Cycle 2	45.92
-0.1% Strain Release Cycle 3	40.72
-0.1% Strain Release Cycle 4	36.50
-0.1% Strain Release Cycle 5	32.82

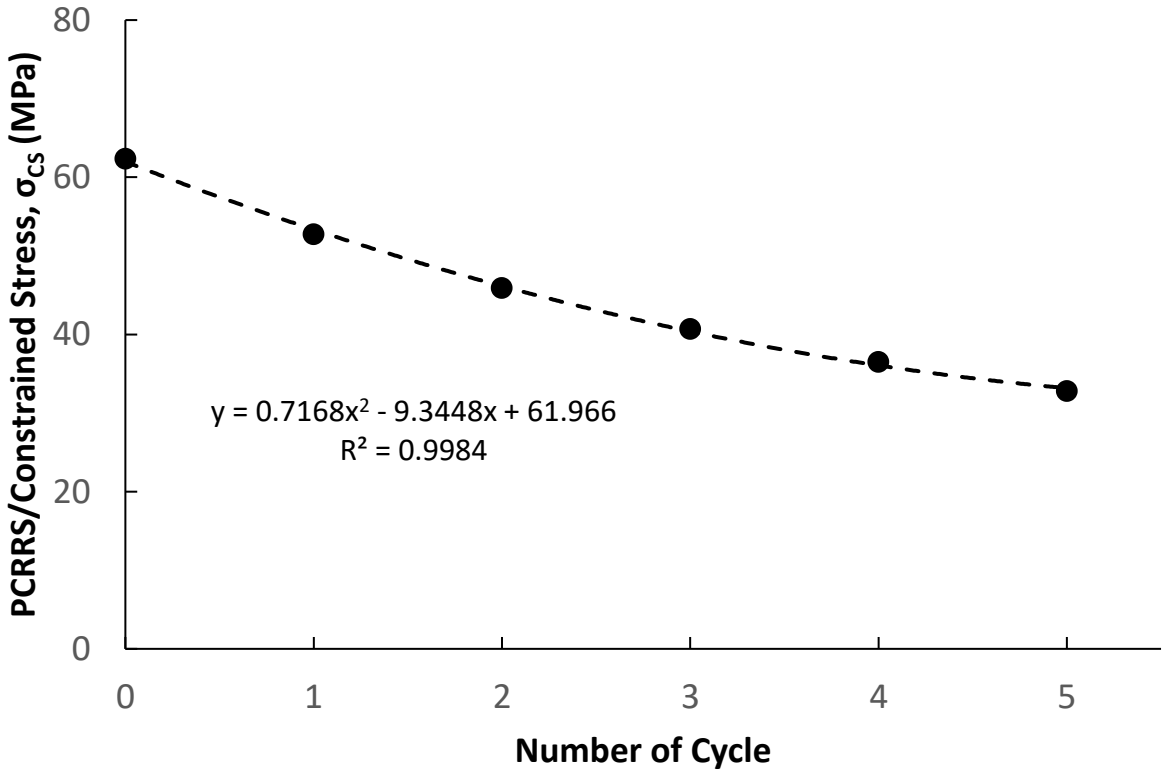

Figure 15: Plot of regression analysis of Post Constrained Recovery Residual Stress, PCRRS (σ_{CS}) corresponding to repeated relaxation and restoration of -0.1 strain cycles applied from the PCRRS state.

Further investigations on reduction of PCRRS exposed to different loading cycles

The preceding series of experiments elucidated that the magnitude of PCRRS experienced a decrement with each loading cycle. A plausible assumption to explain this

observation is the potential role played by grain boundary stabilization, which could possibly be negated by training the samples. To further investigate this phenomenon and discern the reasons behind the reduction in PCRRS upon exposure to cyclic strains, two additional experiments were undertaken.

The first experiment aimed to mitigate the potential discrepancies that might be brought about by grain boundary stabilization from one cycle to another. This was accomplished by subjecting the specimens to a repetitive thermomechanical cycle, thereby training them. This training process was designed to equalize the conditions across different cycles, reducing variability and providing a more controlled environment to understand the influences of grain boundary stabilization on PCRRS.

The second experiment was centered on the exploration of the material's response when subjected to a specific pattern of strain cycles. This involved a sequence of sets of 0.5% strain cycles, followed by another thermal cycle, and then additional sequences of 0.5% strain cycles. The purpose of this experimental design was to discern the specific impacts of alternating thermal and mechanical cycles on PCRRS, facilitating the understanding of its behavior under varying conditions. These experiments were meticulously crafted to shed more light on the intricate nature of PCRRS and its dependencies on thermal and mechanical influences.

Training and its effect on PCRRS

The phenomenon of repeated cycling or training of Shape Memory Alloys (SMAs) is widely acknowledged to diminish discrepancies in the stress-strain relationship across consecutive thermal cycles. The mechanism of training in SMAs incites modifications within the

internal microstructure of the materials, leading to observable changes in their macroscopic material behaviors.

This transformative process is attributed to the effect of grain boundary stabilization, a key feature in the microstructural evolution of these alloys during the training process [85]. Essentially, the grain boundaries in the alloy reach a more stable state due to the cyclic loading, which, in turn, impacts the macroscopic performance of the material. This change is manifested in a more consistent stress-strain relationship across varying thermal cycles, enhancing the predictability and repeatability of the material's response. The microstructural adaptation of the material due to training, and its subsequent impact on macroscopic behavior, underscores the intricate relationship between microscopic processes and macroscopic properties. This interplay between the micro- and macro-scale phenomena is a crucial aspect of the study and application of SMAs, providing valuable insights into their behavior under varying conditions.

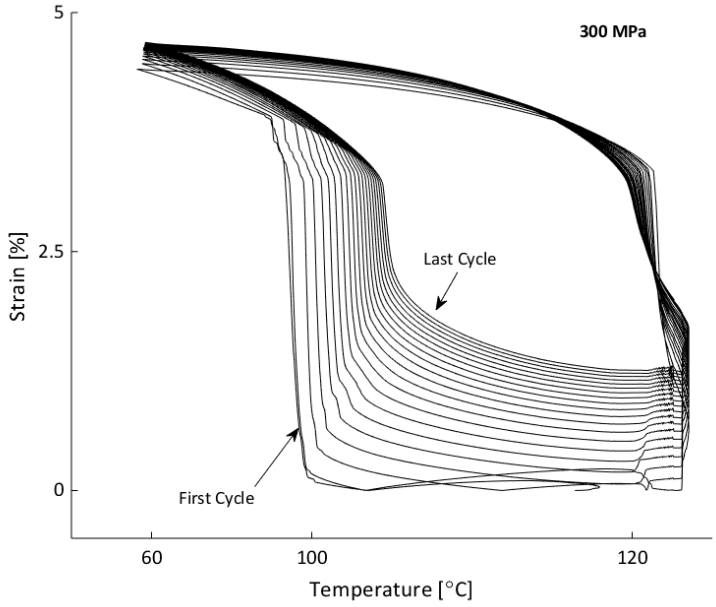

Figure 16: Plot for Cyclic loading at 300 MPa for training of sample NiTi samples.

Investigations were conducted to ascertain whether training had an impact on the generation of PCRRS, or if this was instrumental in the observed reduction of PCRRS when exposed to numerous small strain cycles. To this end, NiTi samples were maintained under a constant stress of 300 MPa. They were then subjected to a heating process which triggered a reverse transformation, taking temperatures beyond the austenite finish temperature, A_f. This was followed by a cooling process, inducing the forward transformation to a temperature below the martensite finish temperature, M_f.

These training cycles were repeated 20 times to stabilize the hysteresis response, which can be seen in Figure 16. The figure also illustrates the progression of cycles, represented by an arrow, and the subsequent stabilization indicated by the converging cycle paths. The varied response to training was evident across different NiTi formulations. Some demonstrated a notable degree of variation, while others exhibited minimal changes in the strain-temperature profile. The training cycles did not necessarily result in full stabilization, but provided sufficient conditioning to explore the impact of training and partial stabilization on PCRRS trends.

Following training, the samples were subjected to the same testing protocol detailed in section “Repeated Application and Removal of 0.5% Tensile Strain" akin to the procedure depicted in Figure 10. One discernible difference between trained and untrained specimens was in the initial PCRRS generated. For instance, while an untrained sample yielded an initial PCRRS of 53.37 MPa, the trained samples produced a slightly lower initial PCRRS of 50.42 MPa. When the trained sample was subjected to five cycles of 0.5% strains, a reduction in the residual stress was still observed after each cycle. Interestingly, the reduction pattern, or slope,

of stress from one cycle to another, remained consistent in both trained and untrained samples as demonstrated in Figure 17.

This suggested that while training could modulate the magnitude of the PCRRS, it did not significantly alter the cyclical stress changes in the low-temperature, martensitic state. A crucial observation was that the training process did not inhibit the generation of PCRRS, thereby affirming the robustness of this feature across different conditioning processes.

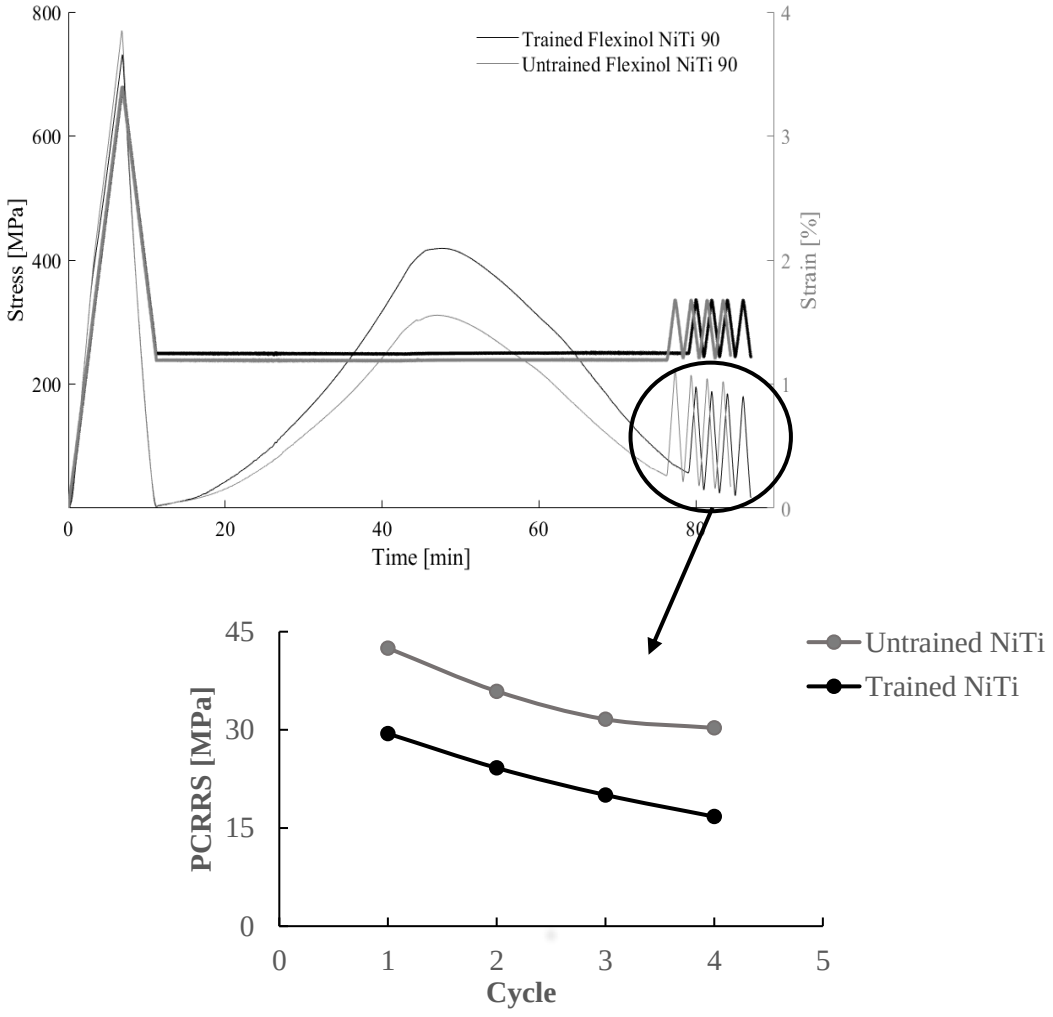

Figure 17: Comparison of the trend of PCRRS formed in the low temperature state across cycles of small strain application and removal for both trained and untrained NiTi samples.

Sequential Thermal cycling after exposure to cyclic strain

As noted earlier, samples subjected to an initial procedure to induce a PCRRS, followed by repeated application of a 0.5% strain, exhibited a reduction in residual stress with each subsequent strain cycle. To examine if the original PCRRS magnitude could be revived, an experiment was performed. This experiment involved subjecting the sample to an additional sequence of thermal actuation and constrained recovery, as visualized in Figure 18.

Interestingly, executing a thermal cycle through the reverse and forward transformations revitalized the PCRRS. The restored PCRRS exhibited only minor variations in magnitude when compared to the original residual stress. When these samples underwent an additional sequence of five cycles of 0.5% minor strain, the characteristic reduction in residual stress across the cycles was observed again. This pattern was consistent when the thermo-mechanical sequence was repeated multiple times, with each iteration successfully reproducing the PCRRS and the associated decline in residual stress across cycles.

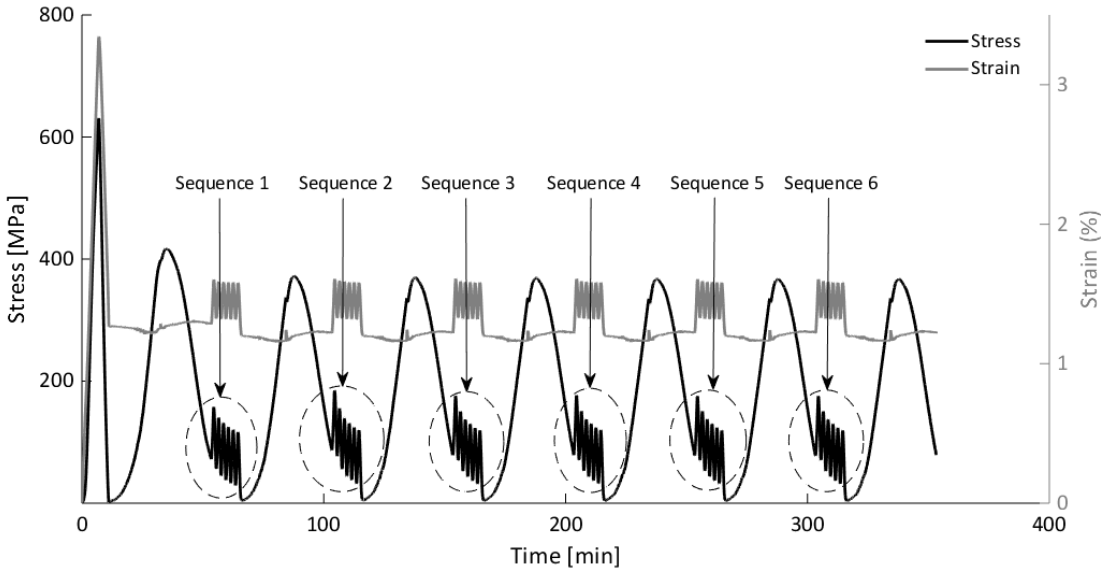

Figure 18: Regeneration of residual stress magnitudes after reapplication of thermal cycles after each sequence. Sequences are the cycles of small strain applications from the PCRRS state.

The most significant variation between sequences was observed in the initial PCRRS generated during the first and second sequences, deviating by less than 10% of the original PCRRS. Additional sequences resulted in a stabilization of the response, to the extent that, starting from the third sequence, the variations across cycles became negligible, as depicted in Figure 21. This comprehensive thermo-mechanical training process resulted in stabilized performance. Importantly, it did not prohibit the generation of a PCRRS, further confirming the resilience and replicability of this phenomenon across varying experimental conditions.

Strain in the austenite phase and PE

As discussed earlier, various recoverable strains (ε_R) were achieved by subjecting samples to different maximum strains (ε_A) and subsequently returning them to a zero-stress state. Following this, the samples were constrained and heated beyond their austenite finish temperature (A_f), which for this material is identified to be 110˚C. However, it is well established that phase transition temperatures are sensitive to stress. To further explore the possibility of generating stress-induced martensite beyond A_f during the formation of PCRRS, an experiment was conducted. In this experiment, NiTi wires were held at 115˚C and stressed to the (formerly) recoverable strains (ε_R) as listed in Table 2. These samples were then unloaded to zero stress while simultaneously measuring the force, resulting in the data represented in Figure 19. Subsequently, samples were strained to fracture at 115˚C in order to analyze the full stress-strain curve up to the point of failure for comparison purposes.

From Figure 19, it can be observed that the stress plateaued around a strain of ε_{M_s} = 1.75%, signifying the onset of detwinned martensitic transformation. The stress maintained a near-constant value until the end of the plateau at ε_{M_f} = 7.8%, at which point the material

would have fully transformed into detwinned martensite. This experiment, along with the results presented earlier, suggests that PCRRS formation occurs regardless of the completion of the austenite transition during constrained recovery. Nevertheless, the magnitudes of PCRRS appear to correlate with the fraction of the austenite transformation.

In this study, four different constrained strains (recoverable strain, ε_R) from Table 2 were used. Constrained thermal loading beyond A_f for the first two constrained strains of 1.13% and 1.43% resulted in a full transition to austenite. This is because these strains fall below the onset of the martensitic transformation strain, ε_{M_s} = 1.75%. However, for the remaining two cases, which had constrained strains of 1.92% and 2.19%, the transformation into the austenite phase was only partial. Despite the temperature being beyond A_f, a fraction of detwinned martensite would form upon loading, given that these strains extend beyond ε_{M_s}.

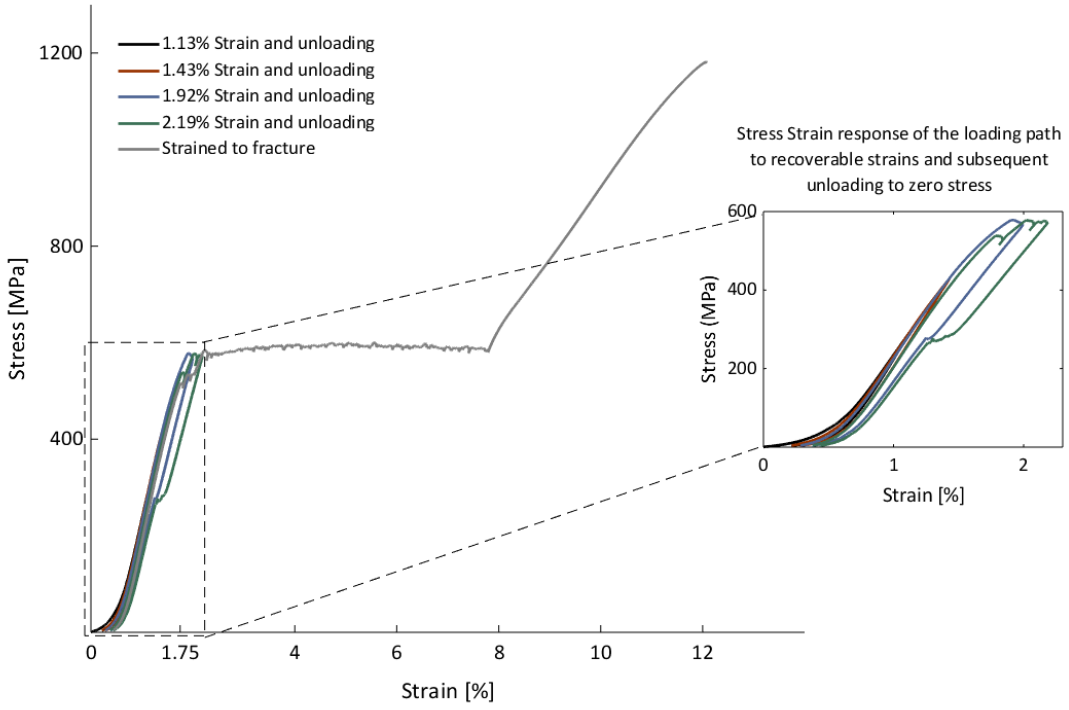

Figure 19: Stress-Strain response of for NiTi for samples in austenite phase strained equivalent to recoverable/constrained stresses listed in Table 1 and subsequent unloading and finally strained to fracture.

Discussions

The ability to produce repeatable PCRRS and stress-strain relations from that point has the potential to support self-healing using NiTi in new and unique ways. Because all final measurements of interest were taken at the same temperature, the coefficient of thermal expansion was of minimal concern.

Apparent materials state by comparing local modulus

To gain deeper insights into the microstructural composition of the material in the PCRRS state, a detailed analysis on NiTi samples was conducted. The objective was to quantify the material properties, with a particular focus on the local stress-strain modulus across various states. Properties were measured in the states that displayed unique phenomena, such as PCRRS, and juxtaposed these with states that exhibited well-understood or predictable crystalline phases.

A tension test, conducted in the martensitic phase, revealed that the specific NiTi wires under study fractured at a strain of 7.05%, as elaborated further in the following section and depicted in Figure 22. The stress-strain responses allowed for the identification of distinct regions representing twinned and detwinned martensite phases upon loading. Analysis of the stress-strain plots indicated that, upon exposure to a 5% strain, NiTi samples would predominantly transform into detwinned martensite. However, a maximum strain of 3.4% would lead to a mix of twinned and detwinned martensite phases. For the purposes of this experiment, the loading path and analysis were shown for the PCRRS state with a 5% maximum strain. This allowed to examine the scenario involving complete transformation into the

detwinned form, as illustrated in Figure 20. The local stress-strain moduli were measured and compared using the rule of mixtures to infer the material state at PCRRS.

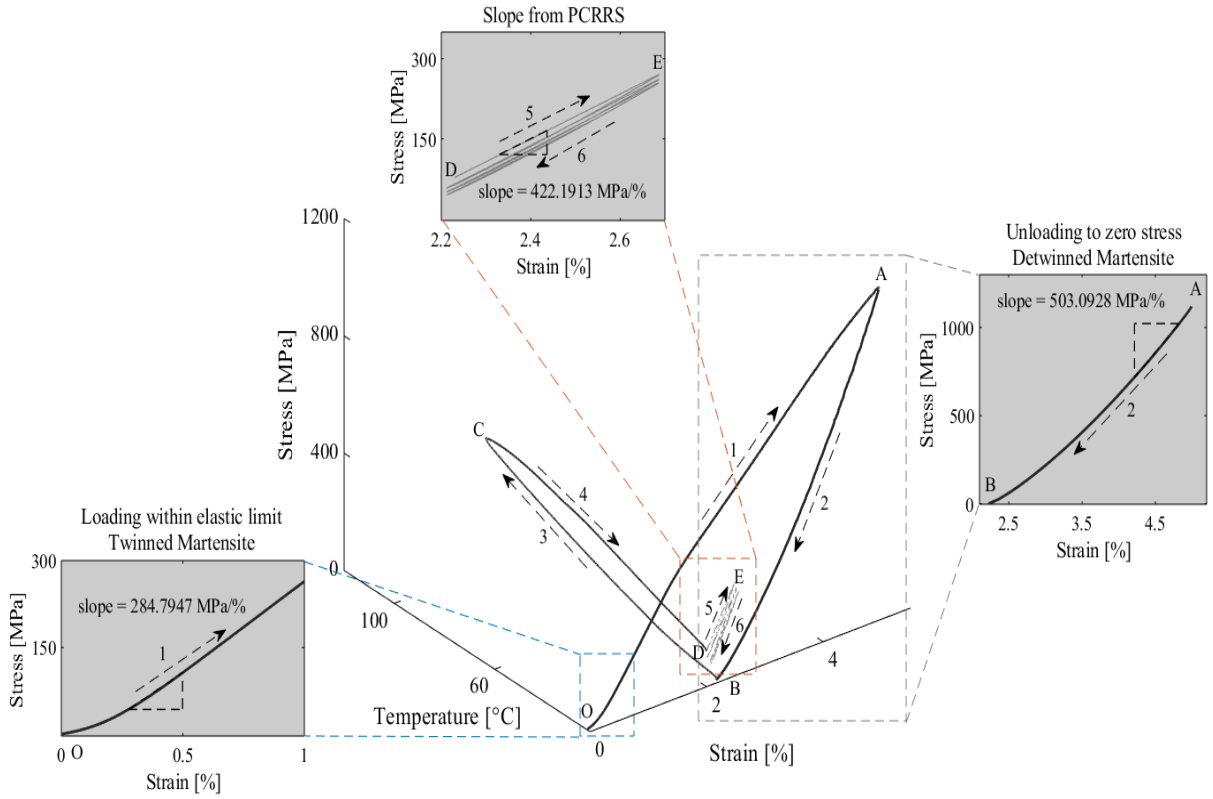

Figure 20: Thermo-mechanical load profile to generate and analyze PCRRS.

Table 7: Local modulus for different state of the thermomechanical loading response

Loading Paths	Local Modulus (MPa/%)
Loading within Elastic Limit- Twinned Martensite Modulus	284.7947
Unloading to zero stress- Detwinned Martensite Modulus	503.0928
Loading from PCRRS- PCRRS modulus	422.1913

The local elastic modulus was determined at various key points. Initially, local elastic modulus was evaluated at point O, where the sample maintained its parent geometry and was in a self-accommodated twinned martensite state. Subsequently, the sample was subjected to a 5% strain following 'path 1' to reach point A, and stress was then released, generating a

recoverable strain of 2.2% at point B. Post the loading and unloading process, the NiTi wires underwent a constrained recovery at point C, and a subsequent transfer to room temperature led to the generation of PCRRS at point D. In the final state, the elastic modulus was measured by subjecting the sample to a 0.5% tensile strain from the constrained length, similar to the procedure outlined in section – "Repeated Application and Removal of 0.5% Tensile Strain".

Analysis of the initial cycles and different loading

The observation that the original PCRRS can be regenerated in any of the non-destructive experiments performed by repeating the initial constrained recovery is consistent with the theory that the stress relief is due to added detwinning of the martensite from the PCRRS state, not a true material degradation. This is exemplified by the experiments and data produced by repeating the maximum strain used to generate the initial PCRRS (Section- "Initial Cycle to Generate PCRRS") but was repeated in all the other experiments. A comprehensive regression analysis was conducted on the residual stress that persisted after the recurrent application of varying strains from the PCRRS state, as delineated in section "Property Explorations from PCRRS". Intriguingly, a consistent reduction in residual stress was discernible after each cycle, irrespective of the magnitude and axial direction (whether it was an increase in 'tension' or 'relaxation').

The data emanating from the repeated application and withdrawal of an additional 0.5% strain from the PCRRS state was found to correspond with a 2nd order polynomial fit, $\sigma_{CS} = 1.53N^2 + 11.83N + 53.20$. This fit exhibited a coefficient of determination (R^2) exceeding 0.999. Here, σ_{CS} signifies the constrained stress measured after each cycle of straining from and returning to the constrained length, while N denotes the cycle number.

It is worth highlighting that the 2nd order polynomial fit had a superior R^2 value compared to a logarithmic fit to the same dataset (with an offset in cycle count to nullify the zero value). The appropriateness of the polynomial fit was further corroborated by the findings from the experiment involving incrementally escalating applied strains, as showed in Figure 12. The outcomes of this experiment were projected to exhibit an increasing rate of stress reduction. Given the linearly escalating magnitude of applied strain (as opposed to a constant one), the data was expected to align with an integral of the fit for the repeated 0.5% strain (i.e., transitioning from a 2nd order polynomial to a third order, or from logarithmic to logarithmic). Upon examining the data, it was evident that a third-order fit would be more suitable, yielding the equation $\sigma_{CS} = 0.52N^3 - 4.07N^2 + 1.54N + 65.15$ with an R^2 value exceeding 0.999. A logarithmic fit of this data resulted in a considerably lower R^2 value of 0.876, further reinforcing the appropriateness of polynomial fits for these results. The results from the experiment involving repeated 0.1% relaxation and also demonstrated an excellent 2nd order fit with the equation $\sigma_{CS} = 0.72N^2 - 9.34N + 61.97$ and an R^2 value exceeding 0.998, as showed in Figure 15.

It is interesting to note that the recurrent application of strain, both 0.5% in tension and 0.1% in compression (as detailed in Figure 11 and Figure 15), produced remarkably similar trends in terms of both shape and slope. Linear fits to these datasets resulted in slopes of -6.78 and -6.52, respectively, with R^2 values of 0.859 and 0.942. Furthermore, a linear fit to the incrementally increasing tensile load displayed a somewhat similar slope of -5.86 with an R^2 value of 0.964.

In light of the empirical evidence gathered, two pivotal observations have emerged:

1. There is a discernible reduction in stress even when very small strains are applied. Notably, these strains are significantly smaller than those required to trigger detwinning from a free, self-accommodated twinned state.
2. This decrease in stress takes place regardless of the orientation of the strain, be it tensile or relaxation.

These findings strongly suggest that, in the context of the PCRRS state, residual stresses and strains are maintaining the material at the precipice of detwinning. Furthermore, these observations underscore the fact that the formation of martensite in a constrained state does not fully and freely conform to the constraints of the geometry. This leads to the implication that the mechanisms underlying the generation of PCRRS warrant further examination and comprehension. Despite the advancements made thus far, the intricate phenomena that culminate in the production of PCRRS are still shrouded in a degree of uncertainty and remain an active area of scientific inquiry. These observations highlight the complexity of the material's behavior and underscore the need for further exploration to fully understand the nuanced and multifaceted nature of PCRRS generation.

Analysis on the PCRRS regeneration

The results of this study indicate that the post-strain reduction in residual stress, regardless of whether this stress reduction was due to repeated exposure to minor strains or a single exposure to a substantial strain, can be restored. This restoration was achieved by repeating the sequence of thermal actuation, followed by constrained recovery, and finally a return to the low-temperature state. The impacts of training and recurrent cycling on the generation of PCRRS were largely confined to influencing the initial magnitude of the residual

stress. Remarkably, after the third complete thermomechanical sequence, the material's response was found to stabilize.

The fact that the PCRRS can be restored suggests that the decrease in residual stress as a result of the application of strain is attributable to a reversible process, such as the detwinning of martensite. The modest yet consistent reduction in residual stress following each 0.5% loading sequence, as demonstrated in Figure 21, implies that incremental detwinning occurs with each cycle. This incremental detwinning further suggests that the material in the PCRRS state is likely a hybrid of twinned and detwinned martensite, poised at the precipice of further detwinning. It is important to note that the coefficient of thermal expansion was not a significant factor in this study since all relevant measurements were made at the same temperature.

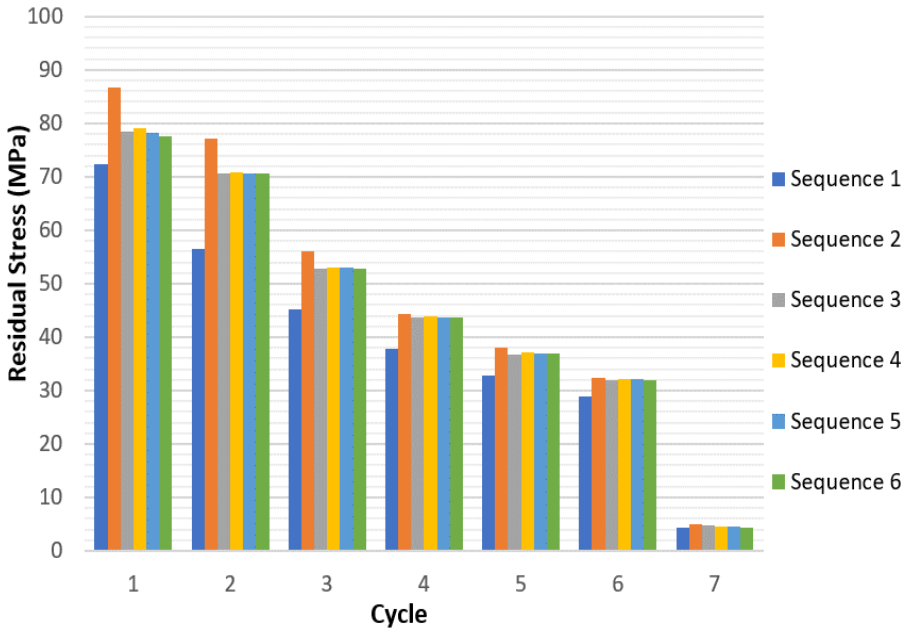

Figure 21: Trend of the PCRRS magnitudes over each Cycles of 0.5% small strain application for every sequence of loading to reproduce PCRRS.

The findings presented in this research are specifically for Flexinol 90 subjected to a maximum strain of 3.4% unless otherwise stated. However, comparable results were observed in several other formulations of NiTi. These included samples with different transition temperatures, provided by various manufacturers, and even those subjected to different maximum strains. The fact that the magnitude and repeatability precision were influenced by training or full cycle repetition suggests that these properties were, in fact, modulated by the stabilization of the material's microstructure. Nevertheless, the impact of training and stabilization was primarily observed in the form of enhanced consistency in the material's responses and did not compromise the PCRRS.

Material phase in PCRRS state

The experimental findings, analyses, and reasoned interpretations aimed at deepening the understanding of SMA behavior upon thermomechanical loading for PCRRS and its subsequent response have been synthesized to produce a schematic representation of the material's phases at different stages of the process. This illustrative depiction, presented in Figure 22, operates at the bulk scale.

As shown in Figure 22a, the entire loading path region is partitioned into three distinct sections. Section I denotes the region where both stress and strain remain within the elastic boundaries of the self-accommodated twinned martensite. However, when these elastic limits are surpassed, leading into Section II, the material commences the detwinning process (M_d), reorienting itself and accumulating a recoverable strain. It should be noted that this detwinning process doesn't necessarily alter the material's phase but rather enables it to align more favorably with the applied deformation.

Throughout the entirety of Section II, the material's structure comprises a mixture of both twinned and detwinned martensite variants. As the strain increases, a greater proportion of twinned martensite undergoes transition to its detwinned variants, generating recoverable strain. Given that the structure is bearing an increasing load, the escalating deformation in region II signifies a combination of elastic strain in existing twinned martensite, elastic strain in existing detwinned martensite, and recoverable strain resulting from the reorientation and detwinning of the martensite.

Upon complete detwinning of the martensite, the material advances into region III, where the detwinned martensite undergoes elastic deformation. As the load increases beyond Section III, the material deforms in a permanent and plastic manner, culminating in eventual fracture. Figure 22b showcases the overall material phases, a representation derived by amalgamating the experimental data from Figures 19, 20, and 22a, along with the pertinent material states during loading that contributed to the generation cycle of PCRRS. This illustration effectively conveys the combinations, quantities, and transitions among the material states at each point. At the commencement of the loading cycle, the NiTi wires were in a self-accommodated twinned martensitic state (M_t), depicted as point O in Figure 22b, mirroring the experimental representations in the preceding sections.

In the initial tensile loading phase, before reaching the elastic limit (Section I), the materials exhibit elastic behavior, retaining their original twinned structure. As per the experimental results outlined in section ‘Strain in the austenite phase and PE’, a strain of 3.4% transcends the elastic limit. Consequently, samples exposed to this strain would be located in Section II, where a blend of twinned martensite (M_t) and detwinned martensite (M_d) variants

coexist, as illustrated in Figure 22b. Unloaded samples would persist in this state, displaying a recoverable strain, which was observed to be 1.13%.

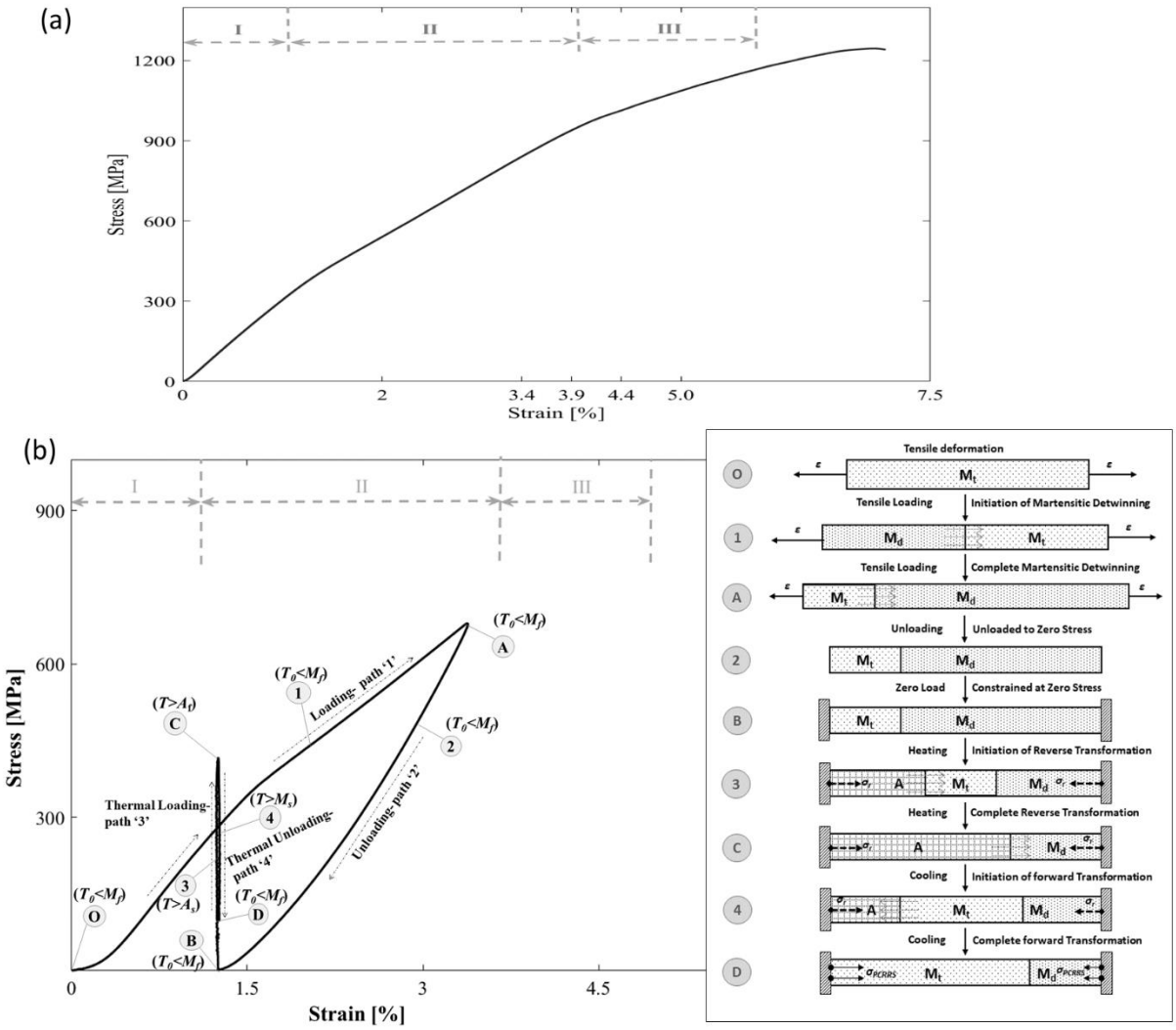

Figure 22: (a) Stress-strain response measured for NiTi wires in tension to fracture at 20°C, and (b) Stress-Strain loading path of PCRRS generation and schematic illustration of the phase transformation of NiTi wires undergoing thermomechanical loading to generate PCRRS for 3.4% maximum strain (phases volume shown are not exact rather conceptual and the horizontal light arrows represent the phase volume flow direction).

Given that the 1.13% strain is beneath the austenitic elastic limit at an elevated temperature (recoverable strain, ε_R = 1.75%), as observed in Figure 19, it can be inferred that heating the sample through the reverse transformation would result in a complete transformation of all martensite variants to austenite (*A*). Microscale heterogeneities in the

chemical composition could lead to minor variations in transition temperatures, thereby accounting for the observed range in the start and finish temperatures of the austenite and martensite transformations.

It is noteworthy that the blocking stress (σ_R), generated during the constrained recovery along path 3, exceeds the stress level associated with martensitic reorientation. Thus, it is plausible to posit that detwinned martensite remains present following constrained recovery. In instances where maximum strains of 4.4% and 5.0% were applied, the samples were constrained beyond the austenitic elastic limit (recoverable strain, ε_R = 1.75%, for reference, see section 'Strain in the austenite phase and PE'). Consequently, a hybrid combination of austenite and stress-induced detwinned martensite was formed upon constrained recovery in the high-temperature state, denoted by point C. As part of the final step in generating PCRRS, during the cooling process down to point D, the stress-induced martensite is likely to persist as detwinned martensite, while the austenite would transition to self-accommodated twinned martensite. It is anticipated that the stress-induced martensite variants would remain in their detwinned state as the cooling process continues. This is due to the lack of a mechanism to re-twin it once it has undergone the forward transformation from austenite to martensite. However, some regions would likely transition directly from austenite to twinned martensite due to the cooling process.

According to the stress/strain moduli observed and detailed in Table 7, the local modulus from point D was found to be lower than that from point B. This suggests the presence of marginally less detwinned martensite at point D, indicating a higher amount of twinned martensite at this point compared to point B.

The rule of mixtures was employed, applying the elasticity moduli measured at known states (as shown in Figure 20) to other states, in order to assess the relative amounts of twinned and detwinned martensite present. Utilizing the rule of mixtures and considering a state of 100% detwinned martensite variants near point A, it was discerned that around point D, 67% constituted detwinned martensite and the remaining 33% comprised twinned martensite variants. Collectively, these observations propose that when the material undergoes the forward transformation in a constrained state, it does not entirely form a self-accommodated twinned structure within the constrained geometry. This could potentially elucidate the existence of PCRRS.

Summary

Multiple was conducted to scrutinize the mechanical characteristics of NiTi Shape Memory Alloys (SMAs) and Post Constrained Recovery Residual Stress (PCRRS), with the objective to decode the responses of the material under various conditions. These investigations encompassed cyclically imposing and relieving strain from the PCRRS state, such as the repeated administration of 0.5% tensile strain, steadily escalating strain from cycle to cycle within the range of 0.1% to 0.5%, and iterative relaxation by 0.1%.

The outcomes demonstrated that residual stress diminished regardless of the magnitude of the additional strain tested or its orientation. The experimental finding that the initial magnitude of PCRRS (post-training) could be consistently regenerated by reapplying the thermo-mechanical cycle suggests that the process phenomena are stable, and the reduction of residual stresses is not a consequence of material degradation.

The decrease in residual stresses was ascribed to further detwinning of the NiTi from the PCRRS state. The deduction that the reduction resulted from both increase and relaxation of strain implies that it is associated with the strain deformation itself, rather than load transfer, providing substantial evidence for the detwinning of more martensite from the PCRRS state. This was observed even with a 0.1% strain, a level substantially below the strain required to trigger detwinning in a freely formed self-accommodated twinned martensite state. This outcome suggests that NiTi in the PCRRS state is on the brink of further detwinning.

Regression analyses of the residual stresses remaining after the repeated application of strains from the PCRRS state consistently concluded in a reduction in residual stress after each cycle, regardless of its magnitude and direction. Moreover, the data obtained from the repeated application and removal of an additional 0.5% strain and the repeated 0.1% relaxation from the PCRRS state were observed to fit a 2nd order polynomial equation, while the data derived from the experiment with progressively increasing applied strains demonstrated exceptional 3rd order fits. The application of polynomial fits was justified by superior coefficients of determination (R^2), and that increasing applied strain from a repeated constant to linearly increasing magnitudes unmistakably followed the pattern of integrating from a 2nd order polynomial to a 3rd order polynomial, as opposed to from a logarithmic fit integrated to another logarithmic fit. The consistency in the trends observed for different strains and directions lends additional credibility to the detwinning theory.

Furthermore, a rule of mixtures analysis was carried out employing the local moduli of elasticity measured at various phases of the thermo-mechanical cycle. This analysis disclosed that the PCRRS state is comprised of 67% detwinned martensite and 33% twinned martensite

variants. The existence of PCRRS in SMAs can be rationalized since twinned martensite variants constitute the majority of the material at the PCRRS state, thus facilitating additional detwinning when exposed to subsequent loading.

The capacity of NiTi SMAs to consistently produce the PCRRS phenomenon and regenerate it following thermal cycling paves the way for the conception of energy-efficient actuation methodologies. This consistent performance, free from the necessity for constant energy input, holds the potential to transform the advancement of smart materials. Therefore, the continuation of research is essential to understand the behavior of these newly discovered SMA properties. All in all, the ability of NiTi SMAs to create and regenerate PCRRS is a promising breakthrough for the evolution of smart materials, and its potential warrants further exploration.

Part II:

Detailed Analysis of Interface Strength and Etching Influences: Engineering Self-Healing Metal-Metal Composites from Nickel-Titanium and Bismuth-Tin

The potential of self-healing materials to revolutionize the engineering design of structures is immense. They offer the prospects of designing structures with reduced weight, enhanced efficiency, lower maintenance requirements, and a redefined concept of failure. Among self-healing materials, metal-metal composites are particularly noteworthy due to their exceptional capabilities. These composites exhibit entirely structural healing without the need for consumable healing agents, setting a new benchmark in the field of materials engineering.

However, the synthesis of these metal-metal self-healing composites poses considerable challenges, resulting in a majority of the existing research being centered around polymeric or ceramic self-healing materials. Nickel titanium (NiTi) fiber reinforced off-eutectic bismuth tin (BiSn) matrix composites have been observed to demonstrate some of the most advanced self-healing abilities. On incurring damage, these non-autonomic self-healing structures can be rejuvenated through the application of heat, which triggers the shape memory effect in NiTi, sealing the fractures. Further heating induces melting of the eutectic regions of the BiSn matrix, effectively soldering the matrix back together. This impressive sequence of processes allows for the restoration of macro-scale geometry and nearly complete strength recovery without utilizing any consumable reagents, implying a potentially infinite repetition of this healing process.

A main challenge in designing these composite structures is understanding the intricacies of the NiTi-BiSn interface. The properties and failure mechanisms of this interface significantly influence the composite design (for instance, determining fiber sizing) and affect the composite's strength. In this light, this research embarks on a comprehensive experimental and theoretical exploration of the interface properties between NiTi and BiSn. The

experimental specimens were meticulously synthesized, mechanically tested, and microscopically examined. Complementing the experimental findings, modeling was conducted to comprehend the internal states of the structure, and a theoretical framework was developed to rationalize the observed results.

The outcomes of this study will quantify the improvement in interface strength between NiTi and BiSn achieved through the employed etching process. This quantification will furnish critical data for the optimization of composite design and the determination of wire sizing. However, in contrast to inactive composites, these endeavors will have to accommodate for the internal loads generated by the healing process and potential reformation of TiO_2 upon damage occurrence. The insights gained through this research hold significant promise in propelling the progress of self-healing materials and, by extension, the broader field of materials engineering.

Literature Review on the Interfacial Debonding of Shape Memory Alloy

The promise of self-healing materials is rapidly gaining interest within scientific and engineering circles. Its potential to revolutionize multiple industries is reflected in the escalating research aimed at reducing structural weight, maintenance costs, operational downtime, and system failures. The underlying capability of these materials to autonomously repair in-service damage prevents further deterioration which could otherwise escalate into catastrophic failure [6]. This capability is particularly appealing within aerospace applications where repairs can be difficult, costly, or simply impossible to undertake.

Despite the enormous potential, a majority of research in the field of self-healing materials has primarily focused on polymeric and cementitious based composites [32]. This is because the incorporation of self-healing properties is typically more feasible within non-

metallic materials than their metallic counterparts. Yet, a specific category of self-healing metallic materials, the Shape Memory Alloys (SMAs), specifically the NiTi reinforced metal-metal composites, have been recognized for their immense potential to revolutionize self-healing material science [86].

Crucially, the performance of these composites is contingent upon efficient stress transfer across the interface between the wire and the matrix [87], [88]. Hence, interfacial bonding plays an instrumental role in the performance of these fiber-reinforced composite materials. Interfacial debonding, a common failure mode in composites, often results from severe interfacial stresses. Therefore, understanding this phenomenon is of prime importance for the development of reliable composites, and this is reflected in the numerous theoretical, numerical, and experimental studies dedicated to analyzing the interface between fibers and the matrix.

For example, Jia et al. utilized a cohesive zone model to conduct numerical simulations of a single carbon fiber pulling out from an epoxy matrix, which highlighted the influence of parameters such as fiber mechanical properties, interfacial cohesive properties, and fiber geometry on the debonding load [89]. Similarly, Wang et al. analyzed the fiber axial stress and interfacial stress distribution in SMA fiber-reinforced composites under thermomechanical loading, shedding light on the susceptibility of fiber embedded ends to failure [88], [90]. Other investigations have studied the impact of NiTi wire transformation and reorientation on interfacial debonding in single NiTi shape memory wire composites [91] and explored the influence of thermomechanical properties of NiTi wires on debonding behavior [92].

While these studies have made considerable progress, a gap remains in the understanding of bonding between SMA and metal matrices. Although several studies have been conducted in the domain of polymer matrix cases, a detailed mechanical analysis on the interfacial strength and evaluation of the interfacial failures between SMA wires and metal matrix remains elusive. Notwithstanding, achieving strong interfacial adhesion between SMA wire and metal matrix is essential to ensure efficient stress transfer. In the case of NiTi-reinforced metal-metal composites, the non-wettability of NiTi SMA caused by the formation of a stable titanium oxide (TiO_2) layer on the NiTi surface is a significant concern.

Various studies have sought to address this issue, for instance, Coughlin et al. proposed a NiTi curing process that shed light on the interfacial reactions that occur during the solder's (liquid Sn) melting process with NiTi [93], [94]. Furthermore, Misra leveraged this curing process to fabricate a metal matrix composite and carried out microstructural investigations on the interfacial bonding between NiTi and solder-like Sn alloys [11]. However, neither study quantified the interfacial strength between NiTi and BiSn. It was found that a comprehensive mechanical analysis on interfacial strength and a meticulous evaluation of the interfacial failures between SMA wires and metal matrix were missing in these researches.

Recognizing the importance of the interfacial region and its direct implications on the structural properties of self-healing MMCs, this research undertaking delves into a comprehensive evaluation of the interface between NiTi SMA wires and BiSn matrix. Through a combination of rigorous mechanical testing and modeling, this study seeks to quantify the interfacial strength and evaluate potential failure modes. By advancing the understanding of the complex interfacial phenomena, this research will contribute to the optimization of self-

healing MMC design and the realization of their potential in practical applications. A standout among the forefront of self-healing metallic materials presently under rigorous investigation is a metal-metal composite (MMC) constructed from nickel titanium (NiTi) shape memory alloy (SMA) fibers embedded within an off-eutectic bismuth-tin (BiSn) matrix. As depicted in Figure 2, the application of heat to a damaged specimen of this MMC initiates the NiTi's shape memory effect, thereby restoring the structural geometry and sealing any fractures. As the temperature rises further, the eutectic regions of the BiSn matrix undergo a softening and melting process, effectively soldering the fractures shut. Concurrently, the off-eutectic material continues to maintain the overall structural rigidity [7], [11], [35], [86], [95].

The exploration and understanding of SMA-reinforced metal-metal composites and the associated bonding dynamics are imperative for the advancement of self-healing material science. The findings of this research are expected to contribute to the development of robust and resilient self-healing metal-metal composites that can effectively respond to and repair in-service damage, offering immense potential to revolutionize various sectors, particularly aerospace.

Challenges

The investigation of self-healing materials and their potential for transformative impact across numerous industries requires an understanding of the unique challenges that underpin their creation and optimization. Within this sphere, a particular focus has been directed towards the exploration of composite materials that incorporate NiTi SMA which is gaining significant prominence due to its inherent mechanical properties [96]. However, the journey towards crafting an efficient and structurally robust self-healing composite involves the

strategic navigation of certain hurdles. The first challenge pertains to the interfacial bond between NiTi fibers and the matrix in the composite material, a critical determinant of the overall structural performance of the composite. The interfacial strength holds paramount significance in ensuring proper load transfer between the fibers and the matrix, enabling the composite to withstand external forces and maintain structural integrity [97]–[99].

One of the difficulties arising in the bonding process stems from the formation of a titanium oxide (TiO_2) layer on the NiTi surface upon exposure to oxygen. The inert nature of this TiO_2 layer hampers adhesion, thereby posing challenges to the formation of strong, reliable bonds [100]. Past solutions to counter this issue of debonding between NiTi fibers and the matrix have incorporated the use of mechanical anchors embedded within the composite structure. The NiTi fibers would then exert force on these anchors, creating a functional yet far from ideal composite structure. While this approach has exhibited self-healing abilities, it results in a less than optimal composite structure characterized by concentrated load paths through the anchors and disbonded fibers. In essence, the composite loses the advantage of evenly distributed load transfer, impacting its overall structural performance and healing efficiency [38]. Enhancing the interfacial strength and thus improving the load transfer between the NiTi fibers and the bismuth-tin (BiSn) matrix is therefore a critical research priority. Comprehensive knowledge of this interfacial strength is instrumental for the design and selection of suitable fiber diameters that can potentially enhance both the composite's strength and self-healing capabilities [97].

To date, several studies have demonstrated advanced self-healing properties of NiTi-SMA reinforced composites, characterized by impressive geometric restoration and near-total

strength recovery. However, these preliminary studies were mostly confined to testing the composite's self-healing abilities. They fell short of quantifying the critical properties that are indispensable for engineering design, modeling, and structural optimization.

Moreover, while recent research has pioneered processes to eliminate the TiO_2 layer, the strength of the interface between NiTi and BiSn remains largely unquantified [86], [101]. The absence of robust and reliable measurements of this interfacial strength represents a significant knowledge gap in the development and optimization of these self-healing composites. Consequently, the quantification of the interfacial strength between NiTi fibers and the BiSn matrix and the understanding of how it contributes to the overall composite's performance and healing ability are identified as significant focus areas for the continuation of this research. This will be instrumental in achieving the larger objective of creating structures that are not only lightweight and efficient but also imbued with remarkable reliability and durability.

Approach

This study's approach involves experimental quantification of the interface strength between Nickel-Titanium (NiTi) and Bismuth-Tin (BiSn), focusing on both cases: with the native, inert titanium oxide (TiO_2) layer intact and after its removal through chemical etching. To begin, single fiber specimens are prepared under these two distinct conditions. These specimens are then subjected to pull testing using a universal test machine. The test procedure involves attempting to pull out the fiber at a controlled rate and displacement while simultaneously measuring the forces. This methodology allows for an accurate determination of the interfacial strength between the NiTi fiber and the BiSn matrix under varying conditions.

Post-testing, a microscopic examination of the specimens is conducted to ascertain the failure mechanisms at the interface. The use of spectroscopy adds a further layer of analysis, providing insights into the materials present in the specimen and any potential transformations that occurred during testing.

An analytical method, developed previously, is employed to quantify the interfacial bonding strength between the NiTi wire and the BiSn matrix. Combined with microscopic studies performed to evaluate the matrix's surface condition, this enables a multi-faceted approach to understanding the behavior of the NiTi-BiSn interface under stress.

Lastly, a schematic representation of the interfacial failure phenomena is presented to provide a comprehensive visualization of the interface failure. This representation, grounded in both experimental data and analytical calculations, aims to capture a holistic view of the interfacial bonding dynamics in NiTi-SMA reinforced composites.

In essence, this approach represents a systematic and rigorous exploration of the NiTi-BiSn interface, leveraging both experimental procedures and analytical methods to produce a robust understanding of the composite's performance under stress. This understanding forms the foundation for addressing the challenges associated with self-healing composites and propels the progress towards the development of more resilient and reliable structures.

Major Tasks

For the purpose of this research, two distinct sets of test samples were meticulously synthesized. They were comprised of specimens embedded within a bismuth-tin (BiSn) matrix, thereby forming single fiber composite (SFC) samples. The methodical design and preparation of these samples formed the initial phase of the experimental study.

Following the fabrication phase, the prepared samples were put through rigorous testing protocols to evaluate their strength and structural integrity. Samples subjected to a series of single fiber pull tests, which are critical to understanding the resilience of the composite structures. All relevant data from these tests were carefully documented and retained for subsequent examination and interpretation.

Specimen Synthesis

In the course of this study, an array of specimens was meticulously fabricated. Each was composed of a single Nickel-Titanium (NiTi) wire embedded within a Bismuth-Tin (BiSn) block, with a portion of the wire protruding from the block to facilitate subsequent investigations. All NiTi wires were of the Flexinol 90 variety sourced from Dynalloy Inc. (Irvine, CA), each with a uniform diameter of precisely 0.508 mm to maintain consistency across the specimens. These wires were prepared by cutting them to a designated length and subsequently subjected to thermal cycling. This process triggered the reverse and forward transformations, conducted under an unloaded condition, facilitating the wires' return to their parent geometry.

Once this preparation stage was concluded, a specific subset of the prepared wires was set aside until the initiation of casting. This subset was intended to function as a control group of samples, offering a comparative benchmark throughout the ensuing stages of testing and analysis. This control group plays an integral role in providing an accurate assessment of experimental outcomes and in evaluating the developed composite material's performance. Two sets of specimens were created consisting of a single NiTi wire embedded in a block of BiSn:

1. A control set that was synthesized using NiTi wires with their native oxide intact and unetched, and
2. An experimental set of samples where the NiTi underwent treatments to remove the native TiO_2 layer.

TiO_2 Removal by Etching

The NiTi wires assigned to the experimental group were subjected to an etching process as outlined by Coughlin and his team [93], [94]. Initially, the wires were fully immersed in a solution comprising Hydrofluoric (HF) and Nitric acid (HNO_3) in a precise ratio (4.8% HF-10.5% HNO_3) for a 5-minute period. Subsequently, the wires were dipped in a Phosphoric acid-based flux (specifically, Indalloy Flux #2 provided by the Indium Corporation of America). This was followed by another dip into molten Bismuth-Tin (BiSn) for the application of a coating layer. Etching process is shown in the following Figure 23.

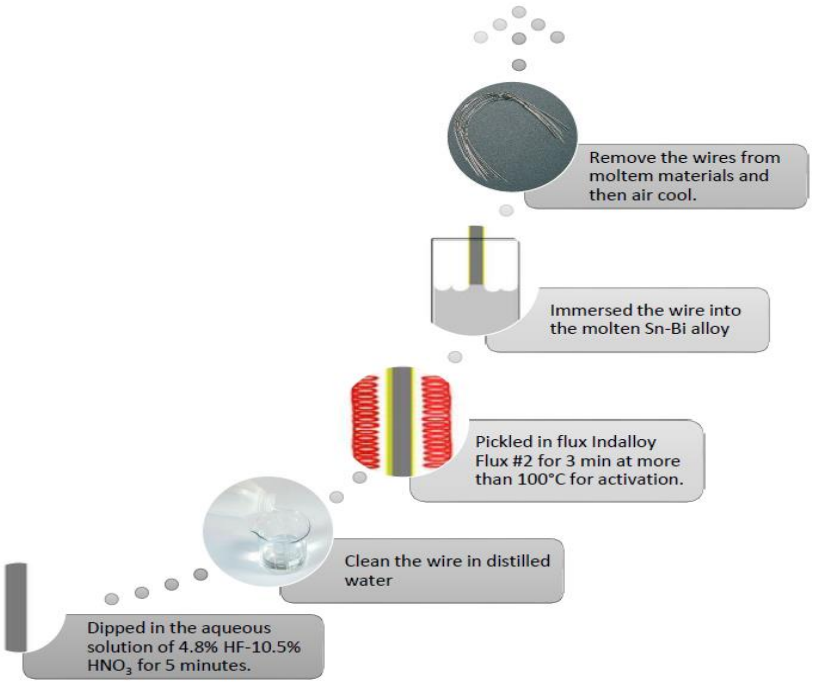

Figure 23: NiTi curing procedures adapted from Coughlin et al.

To circumvent the risk of re-oxidation, all of these steps were diligently carried out within an inert nitrogen environment. The final procedure involved the casting of these coated fibers into a BiSn matrix material, thereby forming the intended composite specimens. Coughlin et al. had previously conducted a comprehensive investigation into the etching process of NiTi and provided extensive analysis on the resultant material interfaces [93], [94]. In particular, their work focused on an in-depth exploration and analysis of interfacial reactions, a body of knowledge that has been instrumental in the present study. Their contributions offered valuable insights and detailed understanding of the underlying processes, which directly informed the approach adopted in this research for fabricating the composite material.

Single Fiber Composite (SFC) Synthesis

The development of the Sn-20% Bi matrix alloy involved the melting of tin and bismuth of 99.9% purity, generously provided by Kohler Company (Kohler, WI, USA). The melting process took place in a furnace, maintaining a stable temperature of 300°C. A composition of Sn-20% Bi was chosen due to its specific partial melting temperature range of 160-165°C. At this range, approximately 15 wt% of the alloy would exist in the liquid state, providing sufficient liquidity for the healing of the composite sample [9], [35], [86]. Subsequent to this, NiTi wires from the untreated control group and the etched experimental batch were affixed within a specially designed mold. This mold, crafted from steel and lined with a graphite coating, was specifically created to facilitate the construction of the single fiber metal matrix.

Molten BiSn was then carefully poured into the mold, effectively encasing the NiTi wires within the matrix. Upon solidification, Single Fiber Composite (SFC) test specimens were successfully created, as shown in Figure 24. Each SFC test specimen featured a rectangular

block of BiSn measuring 65 mm in length, 12 mm in width, and 6 mm in thickness. The NiTi wire, with a total length of 95 mm, traversed the full length of the BiSn block and protruded by 30 mm on one side. To ensure secure handling and to facilitate wire pulling during testing, a grip pad measuring 25.4 mm x 25.4 mm was affixed to the end of the NiTi wires. This systematic process laid the foundation for the creation of standardized, repeatable, and comparable samples for testing the interfacial strength and self-healing capabilities of the composite material.

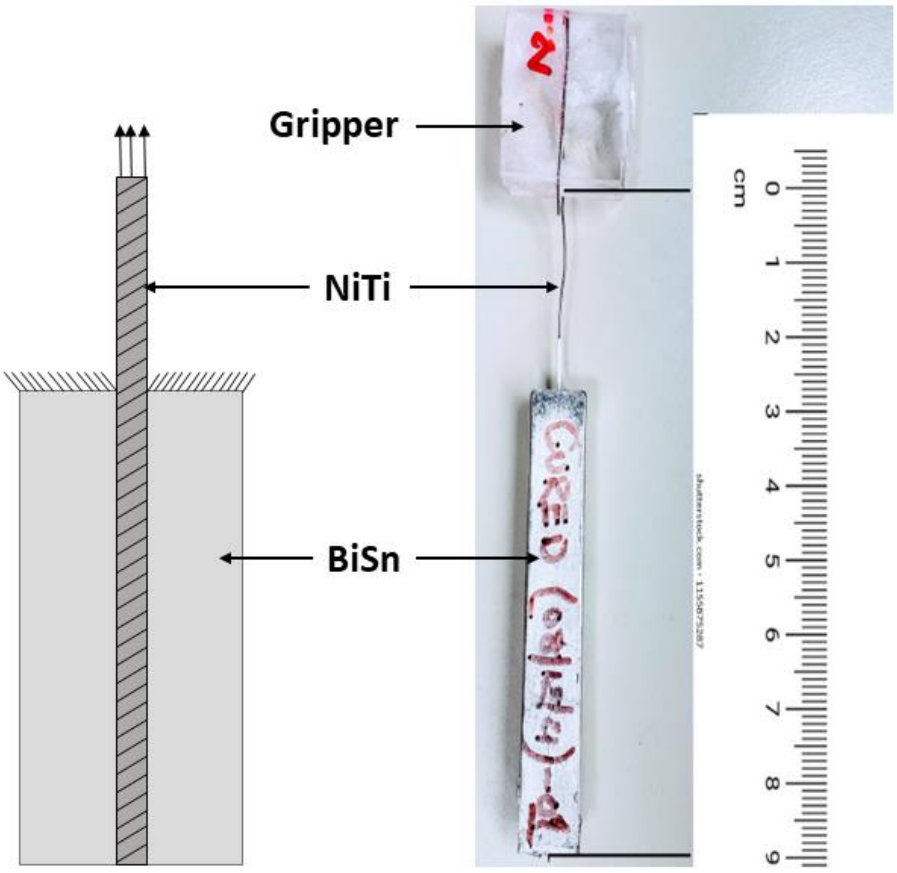

Figure 24: Depiction of pull test specimen and initial fabricated sample.

Experimental Testing

The synthesized Single Fiber Composite (SFC) specimens were prepared for pull testing by securing them into a universal test machine, as illustrated in Figure 25. This involved clamping the protruding NiTi wire to the moving head of the machine, while the BiSn block was held stationary in a custom jig. This setup ensured a controlled environment for the pulling of the embedded NiTi fiber from the BiSn matrix under a constant displacement rate of 0.5 mm/min. Testing continued until either the specimens experienced failure or the wires were entirely pulled out. Throughout this process, both the displacement and force applied were meticulously recorded, accompanied by comprehensive video documentation to facilitate an in-depth analysis of the pull-out phenomena.

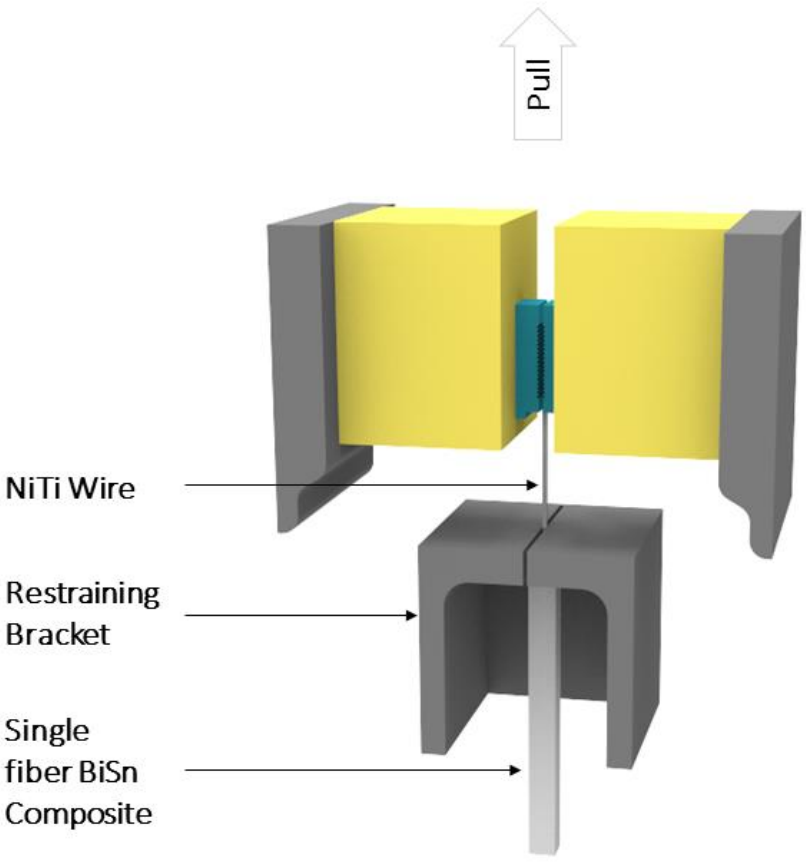

Figure 25: Test setup for single fiber pull test.

The experiment incorporated video recording technology, providing a high-resolution visual account of the wire extraction process, which was then correlated with the load-displacement data recorded. Subsequent to the testing, the samples were subjected to a grinding process to prepare for microscopic inspection. A confocal microscope was used to closely examine the resulting failure surface. This combination of rigorous testing and detailed observation allowed for a comprehensive understanding of the mechanics behind the NiTi-BiSn interface failure, and their correlation to the recorded force and displacement data.

Analytical Model to Quantify of interfacial strength

The fiber pull-out test holds a notable place in the pantheon of experimental methods for exploring the interaction between fibers and their encompassing matrix. This technique offers invaluable insights into the strength and quality of interfacial adhesion between the two components, as well as the mechanisms of elastic stress transfer during the fiber pull-out process [96], [102]–[104].

Traditional practices estimate the interfacial shear strength by dividing the maximum applied force by the lateral surface area of the embedded fiber. This approach assumes a uniform distribution of shear stress along the embedded length of the fiber, typically a small portion of the overall length. However, emerging research disrupts this assumption, illustrating a dependence of shear stress on the position along the embedded length [102]. Furthermore, it suggests that debonding between the fiber and matrix can manifest before the applied force reaches its maximum value.

Recognizing these complexities, Payandeh and colleagues introduced an innovative theory to calculate interfacial shear strength, particularly in longer shape memory wire

composites that experience martensitic transformations [91]. Their approach strays from the conventional formula ($F_{max}/2\pi rl$), which may not be suitable for such composites. Instead, the methodology developed by Payandeh et al. acknowledges the intricate behavior within the interface region, specifically between the Shape Memory Alloy (SMA) wire and its surrounding matrix. Their model paves the way for a more accurate estimation of the interfacial shear strength, thereby providing a more precise understanding of the fiber-matrix interaction in SMA composites.

After conducting the pull-out tests, an assessment of the interfacial shear strength between the Shape Memory Alloy (SMA) wire and its surrounding matrix becomes feasible. This evaluation hinges on the highest force experienced during the debonding process, and takes into account the mechanical attributes and geometrical properties of the SMA wire, the matrix, as well as the specimens subjected to the pull-out tests. This analytical approach represents a significant advancement in understanding the behavior of SMA wire-matrix interfaces. It extends beyond merely gauging the highest debonding force, incorporating a comprehensive perspective that involves the mechanical and geometrical characteristics of the constituent elements and the overall composite system. The equation of this analytical method unfolds as follows:

$$\tau_{max} = (\gamma \sinh(\gamma s)\,[M\,cosh(\gamma s) + N\,sinh(\gamma s)] + \frac{N\gamma}{2})\sigma_p \quad (1)$$

where

$$\gamma = \sqrt{\frac{1}{Q(1+\nu_m}}\left(\frac{S_f}{S_m} + \frac{E_m}{E_f}\right)$$

$$Q = -0 \cdot 25 + b^2\left[\frac{2b^2\,ln\left(\frac{b}{a}\right) - b^2 + a}{2(b^2 - a^2)}\right]$$

$$M = -\frac{S_f E_f}{S_F E_f + S_m E_m} \quad (2)$$

$$N = csc\,h(2\gamma s) - M\,tanh(\gamma s)$$

$$\sigma_p = \frac{F_{max}}{\pi a^2}$$

The two equations (equations (1) and (2)) outline the key variables that contribute to the computation of interfacial shear strength between the SMA wire and its surrounding matrix. Within this context, 'a' symbolizes the radius of the SMA wire, whereas 'b' signifies the radius of the matrix. The variables S_f and S_m, on the other hand, stand for the cross-sectional areas of the wire and matrix respectively. The Young's modulus of the wire and the matrix are denoted by E_f and E_m. Additionally, V_m is a representation of the Poisson's ratio of the BiSn matrix. The parameter '*s*' has been defined as $l/2a$, where 'l' stands for the length of the cylinders, and F_{max} is the maximum force exerted during the debonding process. This comprehensive list of parameters offers a thorough framework for assessing interfacial shear strength in these systems.

Table 1 provides a summary of the material properties of the SMA wire and BiSn matrix used in this study.

Table 8: Materials' properties utilized for the analytical model

SMA wire	Wire radius, *a*	0.254 mm
	Young's Modulus, E_f	33×10^3 MPa
	Cross sectional area, S_f	0.2027 mm^2
Metal Matrix	Matrix radius, *b*	3 mm
	Young's Modulus, E_M	26.11×10^3 MPa
	Cross sectional area, E_m	33000 mm^2
	Poison's ratio, v_m	0.33

Results and Discussion

The examination of NiTi-BiSn composites centers on a controlled pull of the Nickel-Titanium (NiTi) fiber from the Bismuth-Tin (BiSn) matrix. This pull out is carried out at a constant rate, facilitating a detailed study of the interfacial strength and failure mechanisms.

According to Hsueh's work on composite failure mechanisms [105], [106], the maximum shear stress is initially concentrated at the location where the NiTi fiber enters the BiSn matrix. This is due to the direct exposure of this part of the fiber to the applied load, making it the most probable site for failure initiation. As such, this area of the interface is critical to the overall performance of the composite, as it governs the initiation of failure under stress.

The axial load applied to the NiTi fiber needs to surpass the interfacial strength between the NiTi fiber and the BiSn matrix to trigger the onset of failure. Upon surpassing this threshold, relative movement between the NiTi fiber and BiSn matrix is enabled, leading to the initiation of interface failure. As the pull test progresses and the applied stress exceeds the interfacial frictional stress, further failure continues along the interface.

Ultimately, after complete interface failure, only frictional and sliding forces are at play along the remaining length of the NiTi fiber within the matrix. These forces represent the residual interaction between the NiTi fiber and BiSn matrix post-failure, which can provide important insights into the self-healing and residual strength capabilities of the composite. This process of progressive failure along the interface forms the basis for understanding the composite's performance and its potential for applications in various industries.

Analysis of Fiber Pull Test

In the context of the conducted experiment, the NiTi fiber, integrated within the BiSn matrix, was subjected to a controlled, steady pull. Early in the procedure, the highest shear stresses typically manifest at the contact point where the NiTi wire penetrates the BiSn matrix, making this the likely locus for failure initiation. This is a direct consequence of the inherent mechanics: for any kind of failure to commence, the axial stress applied on the NiTi fiber needs to supersede the interface strength that binds the fiber and the matrix. This excess stress propels relative movement between the two entities.

As the process continues, post the initial fracture, it's plausible for the phenomenon of failure to permeate throughout the length of the fiber during the pull test, particularly when the applied stress surpasses the frictional stress at the interface. This leads to an escalating sequence of failures that continue to affect the integrity of the interface. Upon culmination of the interface failure, the remaining fiber length within the matrix is subjected only to frictional and sliding forces. This stage marks a crucial shift in the interplay of forces acting on the fiber and matrix, as the dominating force transitions from the complex interfacial interactions to the more simple frictional forces. This progression from interfacial failure to purely frictional interactions is a critical part of understanding the mechanics at play during the pull out of the NiTi fiber from the BiSn matrix.

The force-displacement plots displayed in Figures 26 and Figure 27 reveal the characteristics of four SFC specimens that were subjected to the pull test. The horizontal axis, or abscissa, signifies the total linear distance that the fiber traverses while being extracted from the matrix. In the early stages of the experiment, an initial alignment of the fiber with the

imposed axial load was noted, appearing as the fiber straightening. Following this straightening phase, an initial tension begins to form in the free portion of the fiber, consequentially instigating the build-up of stresses. The relatively smaller diameter of this free portion, compared to the combined fiber and matrix cross-sectional area, culminates in a comparatively greater stress within this section.

As the experiment proceeds, the pathway of fiber pull out can be branched into two distinct scenarios, largely contingent on the resilience of the fiber-matrix interface. If the interfacial strength is on the weaker side, the fiber-matrix interface may yeild to failure before the NiTi enters the detwinning phase, thereby precluding the accumulation of recoverable strain and rendering the shape memory capabilities ineffective. Conversely, if the interface demonstrates robust strength, the NiTi SMA fibers could potentially accumulate recoverable strain due to the onset of detwinning upon loading in the free portion of the fiber, preceding any interface failure. However, when considering a NiTi fiber embedded in the matrix, potential elastic strain is anticipated due to the fiber's embedment in the matrix. Discrepancies in material properties between NiTi and BiSn, such as strain to failure, and their compatibility demand that the NiTi attached to the BiSn remains in its twinned state, subsequently disengaging from the BiSn as it undergoes detwinning. After this disengagement, the interface interactions diverted into frictional forces as the fiber continues its extraction from the matrix. This denotes a significant shift in the interfacial dynamics during the fiber extraction process.

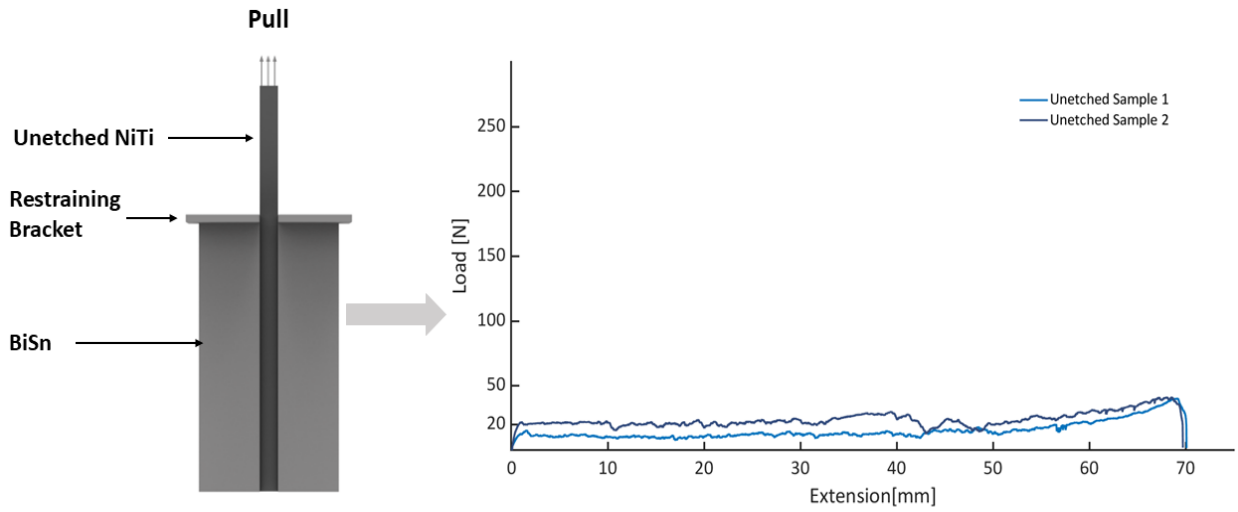

Figure 26: Load vs extension plot from pull test of the composites fabricated by etched NiTi wire and BiSn alloy.

Figures 26 and Figure 27 showcase the load-displacement relationship for different samples used in this study. The results presented in Figure 26 indicate a weak interfacial bond for the unetched specimens, signified by an initial failure force of merely 15 N. Previous research involving analogous NiTi wires, tested under ambient conditions, displayed that detwinning initiates when the exerted force reaches a threshold of 69 N, corresponding to an effective stress of 340 MPa. In light of these precedents, it can be inferred that the interface between the unetched NiTi wire and the BiSn matrix succumbed to failure prior to the onset of NiTi detwinning. This premature failure of the interface led to the NiTi fiber being readily dislodged from the matrix, even under minimal load, throughout the entire length of the pullout process. These findings illuminate the critical role of interfacial strength in dictating the pullout behavior of NiTi wires embedded within BiSn matrices, significantly impacting the material's mechanical performance.

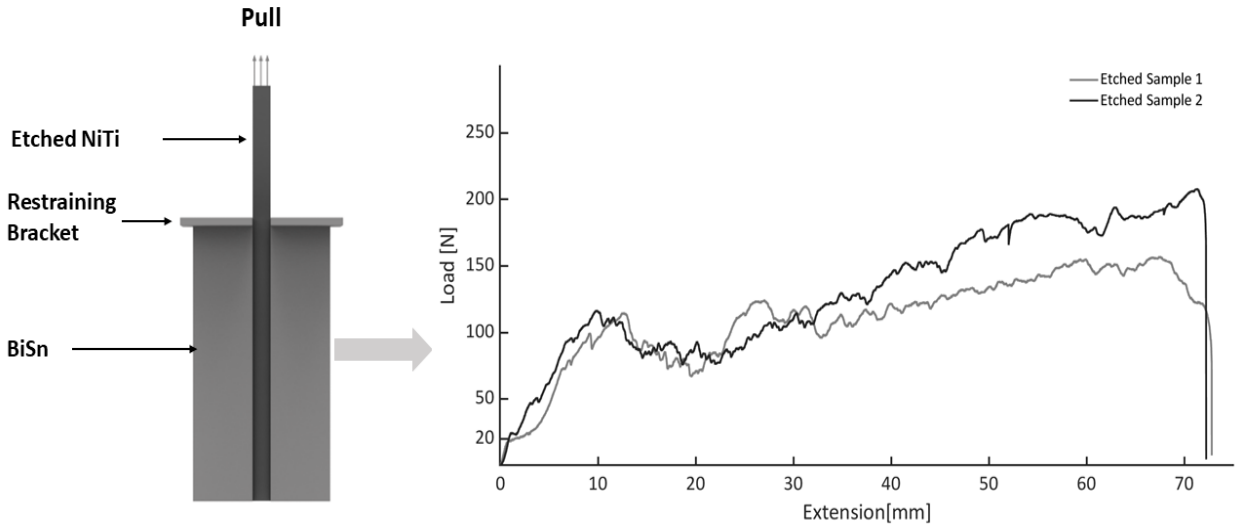

Figure 27: Load vs extension plot from pull test of the composites fabricated by etched NiTi wire and BiSn alloy.

Insightful outcomes can be drawn from the load-displacement plots depicted in Figure 27, which correspond to the etched samples. These curves demonstrate the requirement of a significantly increased force to debond the NiTi fiber from the BiSn matrix in comparison to their unetched counterparts. This behavior is suggestive of an enhanced interfacial strength between the NiTi fiber and the BiSn matrix after etching. Indeed, the initial load peak - a point before the curves settle into a plateau - is observed to be roughly five times higher than the loads encountered with unetched samples, as compared for both the samples in Figure 28. This increase in load culminates into elevated stresses, thereby instigating the detwinning process within the NiTi fibers. The transition in the material's behavior is evident in the distinct alteration in the slope near a load of 69 N. As the force escalates, rising stress levels prompt the initiation of interface failure, while concurrently perpetuating the detwinning process as the fiber detaches from the matrix.

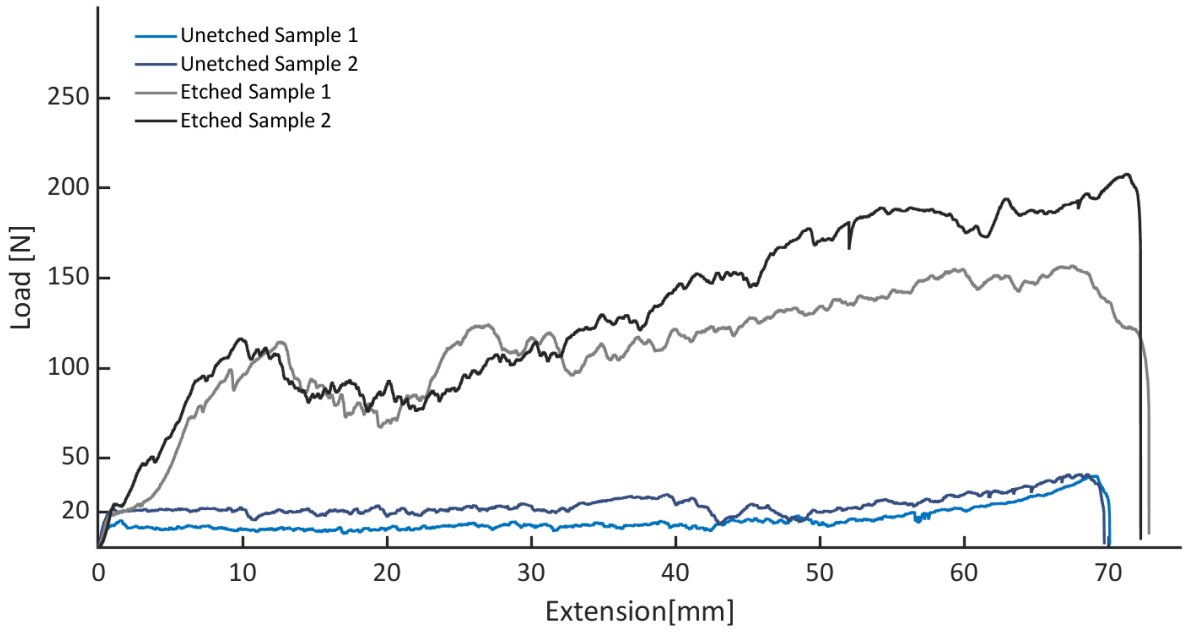

Figure 28: Comparison of load vs extension data obtained from pull test of the single fiber composites fabricated by both unetched and etched NiTi wire and BiSn alloy.

Post-experimental analyses, involving the measurement of lengths and heating of the NiTi fibers above the austenite finish temperature, substantiated these observations. Specifically, the unetched samples did not display any discernible change in length, indicating that they maintained their parent geometry and no detwinning occurred. Conversely, the etched samples were found to be elongated following mechanical testing and exhibited contraction upon heating, signifying the accumulation of recoverable strain as a result of detwinning during the tests. As can be seen in the Figure 27 and Figure 28, the force displacement curve for the etched samples leveled off at roughly 116.7 N with a corresponding stress of 575.77 MPa. Maximum interfacial shear stress was found to be 52.64 MPa in that location using the analytical model.

Another noteworthy observation pertains to the force experienced by the fiber as it continued to be pulled from the matrix beyond the point of presumed complete detachment.

The force was found to progressively increase, indicating the manifestation of a phenomenon beyond the realm of conventional Coulomb friction. This intriguing observation is currently the subject of ongoing investigation, promising further understanding of this complex fiber-matrix interaction.

Microscopic investigation of Fiber Matrix Interaction

The experimental results presented a curious observation. In every test, there was a consistent rise in force as the fiber was gradually extricated from the matrix, reaching its peak just before the final removal or definitive failure. This finding deviated from expectations, as it is intuitive to anticipate a decrease in force due to the reduction in contact length or area as the fiber pulls away from the matrix.

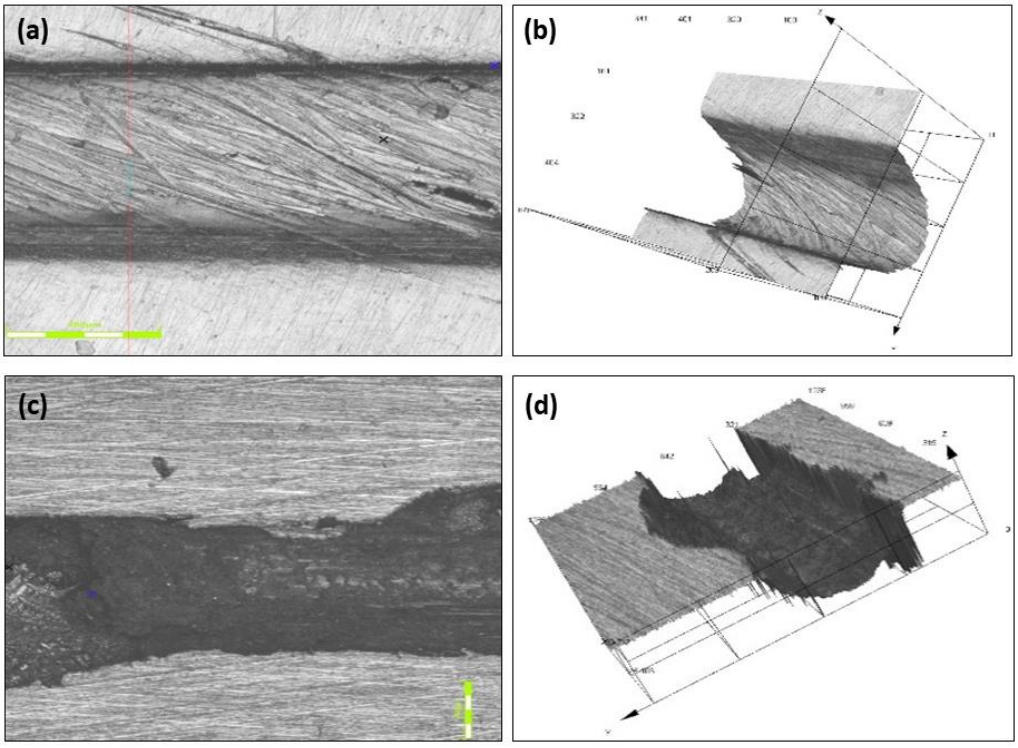

Figure 29: Microscopic images (using confocal microscope) to show the BiSn surface condition after the pull test. (a) and (b) for unetched sample and (c) and (d) are for etched samples.

A post-experimental inspection of the specimens was conducted to enhance a deeper understanding of the tensile test outcomes. The matrices were carefully sectioned and polished to expose the internal cavity left by the NiTi fiber. The subsequent investigation employed both optical and confocal microscopy techniques, with the findings illustrated in Figure 29. In this figure, the left-side images (a & c) were captured using an optical microscope, while the right-side images (b & d) utilized a confocal microscope, chosen deliberately to highlight the contrasts.

The top images in Figure 29 (a & b) are derived from a control sample produced with unetched NiTi. Remarkably, the interior surface of the cavity exhibits a rather uniform texture, mirroring the geometry of the NiTi wire. A subtle spiraling scratch pattern graces this even surface. This feature is consistent with expected results of failure at a weak surface bond against inert TiO2. The scratching could possibly be linked to the wire's sliding motion during testing, but the origin of the spiraling pattern remains uncertain, especially given the absence of any detectable macroscopic wire rotation relative to the matrix.

Conversely, the lower images of Figure 29 (c & d) reveal an experimental sample created with etched NiTi. The interior cavity herein exhibits noticeable differences from the control sample. Observable is the extensive gouging of the BiSn beyond the NiTi wire's diameter and small-scale pitting on the surface. This significant departure suggests an entirely different failure mechanism, potentially hinting at a failure within the BiSn matrix near the interface rather than at the interface itself.

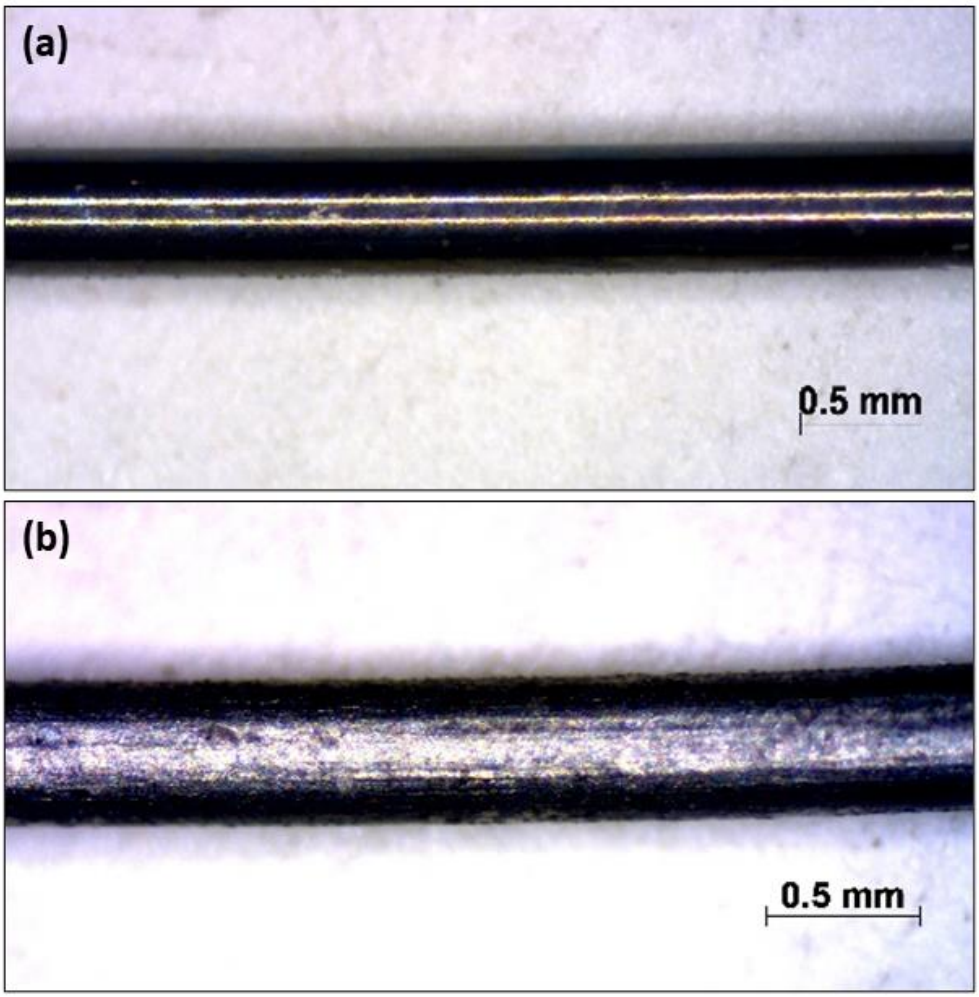

Figure 30: Optical Microscopic images (using optical microscope) to show the NiTi surface condition after the pull test. (a) for unetched sample and (b) for etched samples.

Figure 30 provides an insightful observation of the NiTi fiber's surface state following the pull test, shedding light on the interfacial failure mode. The individual images taken by using optical microscope represent different surface conditions, with Figure 30 (a) portraying the surface of a pulled-out unetched NiTi fiber, and Figure 30 (b) depicting the condition of an etched NiTi fiber post-extraction. A clear observation can be made from the surface of the unetched NiTi wire, as shown in Figure 30 (a). The notably smooth texture of the wire's surface suggests an absence of matrix adhesion, supporting the notion of a weak bond between the

unetched NiTi fiber and the BiSn matrix. In contrast, the surface condition of the etched NiTi fiber presented in Figure 30 (b) tells a different story. The image reveals a predominantly rough texture, indicative of substantial interaction between the fiber and the matrix. This roughness is possibly attributable to matrix pitting or gouging, providing compelling evidence of matrix particle adhesion to the NiTi fiber. This suggests that the etching process enhances the fiber-matrix interfacial bond strength, leading to a different failure mechanism than that observed for unetched NiTi fibers. These observations underscore the significant impact of the surface condition of the NiTi wire on the fiber-matrix interface behavior during the pull-out test.

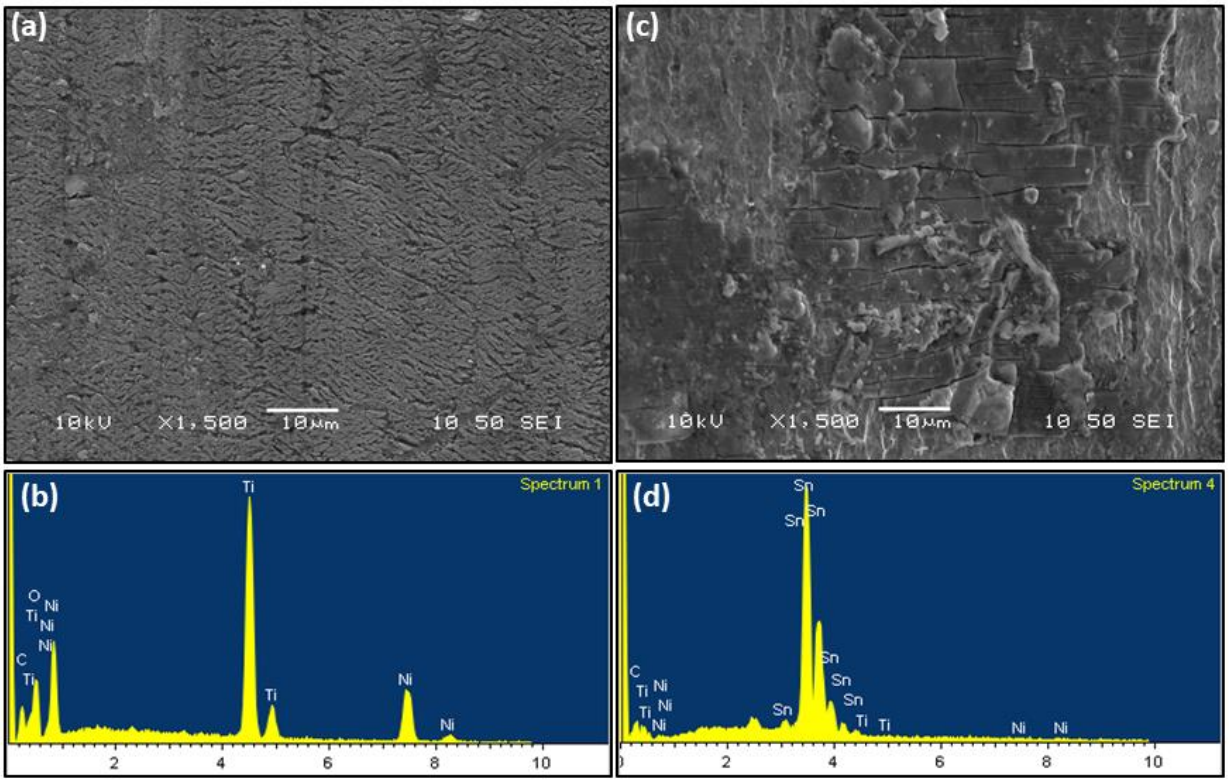

Figure 31: Scanning electron microscopy-energy dispersive spectrum (SEM-EDS) analysis of the surfaces of (a & b) unetched and (c & d) etched NiTi wires after pull out.

Optical microscopic analyses of both unetched and etched NiTi sample surfaces post-pullout led to a notable observation. Surface roughness in the etched NiTi samples was linked to matrix pitting and gouging, attributed to the adhesion of the metal matrix particles on the

NiTi surface. To gain a deeper understanding, Scanning Electron Microscopy (SEM) coupled with Energy Dispersive Spectroscopy (EDS) was employed to ascertain the composition of the materials adhering to the NiTi surface, as shown in the Figure 31. This analysis was conducted for both unetched and etched samples. The SEM images unmistakably exhibited a rougher surface for the etched samples compared to their unetched counterparts. Concurrently, EDS results revealed a substantial amount of Sn adhering to the etched NiTi surface, while the unetched NiTi surface predominantly consisted of Ni and Ti. The combined SEM-EDS evaluation thus substantiated the occurrence of matrix adhesion on the NiTi surface during pullout, leading to pitting and gouging. This, in turn, enhanced the interfacial strength, supporting the observed phenomena.

Interfacial Debonding and Pullout Phenomena

The process of pulling a wire out of a metal matrix is a complex one, governed by the interplay of several mechanical and material properties. The wire pull-out mechanism is influenced significantly by the interfacial characteristics between the wire and the metal matrix, specifically the presence of mechanical interlocking.

The exploration of the mechanical interactions occurring during the pull-out test of NiTi fibers from the BiSn matrix unveils various complexities, largely determined by the interfacial strength. Initial observations confirm that strong interfacial bonding prompts the NiTi fiber to straighten under the influence of an applied axial load. This then triggers the accumulation of initial stresses in the free fiber portion, due to tension. Considering the disparity in diameters between the free fiber portion and the matrix's cross-sectional area, this tension exerts a comparatively higher stress on the combined embedded fiber and matrix region. In instances

where interfacial strength is substantial, NiTi Shape Memory Alloy (SMA) fibers manifest recoverable strain from detwinning during the loading in the free fiber portion prior to interface failure.

When the NiTi fiber is integrated into the matrix, potential elastic strain emerges as a result of the inherent material property mismatch between NiTi and BiSn. This mismatch stipulates that the NiTi should maintain its twinned state and decouple from the bulk BiSn as it detwins. Despite this, the free length of the NiTi continues to detwin, accruing substantial interfacial stress at the juncture of the wire and matrix. Once the interfacial shear strength surpasses the strength of the interface, debonding initiates and continues until the NiTi wire is completely detwinned. Subsequent to this phase of interface failure, one would typically anticipate the occurrence of conventional Coulomb friction. However, what was observed was a persistent escalation in force as the fiber was pulled out of the matrix, even after the point where compatibility would necessitate the fiber's complete disengagement. This divergence from expectation points to the existence of a phenomenon distinct from traditional Coulomb friction.

Microscopic analysis of the surfaces of the matrix and NiTi revealed notable differences when compared to the control sample. Significant gouging of the BiSn, extending beyond the NiTi wire's diameter, along with minor pitting on the surface, was observed. Additionally, the NiTi surfaces displayed roughness, with tiny matrix fragments adhering to them. Thus, during NiTi wire pull-out, the irregular matrix surface characterized by gouging and pitting, along with the rough NiTi surface with adhered matrix fragments, activate a stress-peaking mechanism suggestive of mechanical interlocking (see Figure 32).

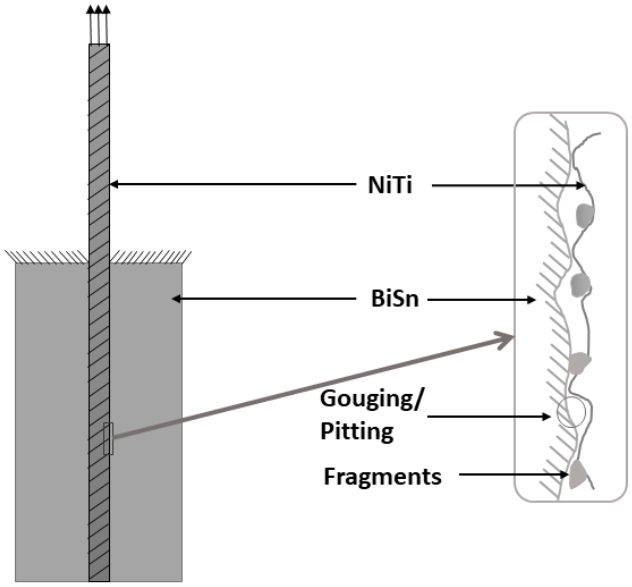

Figure 32: A representation of surface condition of NiTi with matrix fragment adhered and surface condition of BiSn with irregular gouging and pitting.

Although the mean stress was peaking, a fluctuation of stress over the length was evident, suggesting the occurrence of local stick-slip phenomena while the matrix chunk was forced to traverse over the pits in the matrix interfaces. These observations hint at a unique failure mechanism, likely involving the failure within the BiSn matrix near the interface, rather than the interface itself. The stress-peaking phenomenon identified here mirrors failure mechanisms seen in concrete, where friction from concrete surface shearing or mechanical interlocking with rods contributes to an increased stress during wire pull-out.

Mechanical interlocking can be conceptualized as a series of miniature hooks or projections on the wire surface engaging with corresponding features inside the matrix, creating a network of physical bonds. This network of physical bonds strongly influences the interaction between the wire and the metal matrix, enhancing the bond strength and causing the wire to resist removal from the matrix. Upon axial load application to withdraw the wire, the interlocking features oppose this motion. This resistance causes an initial 'stick' phase,

during which the wire stays embedded within the matrix. Shear stress accumulation happens during this phase at the wire-matrix interface. This stress concentration is particularly pronounced at the point where the wire enters the matrix, an area where mechanical interlocking is most effective.

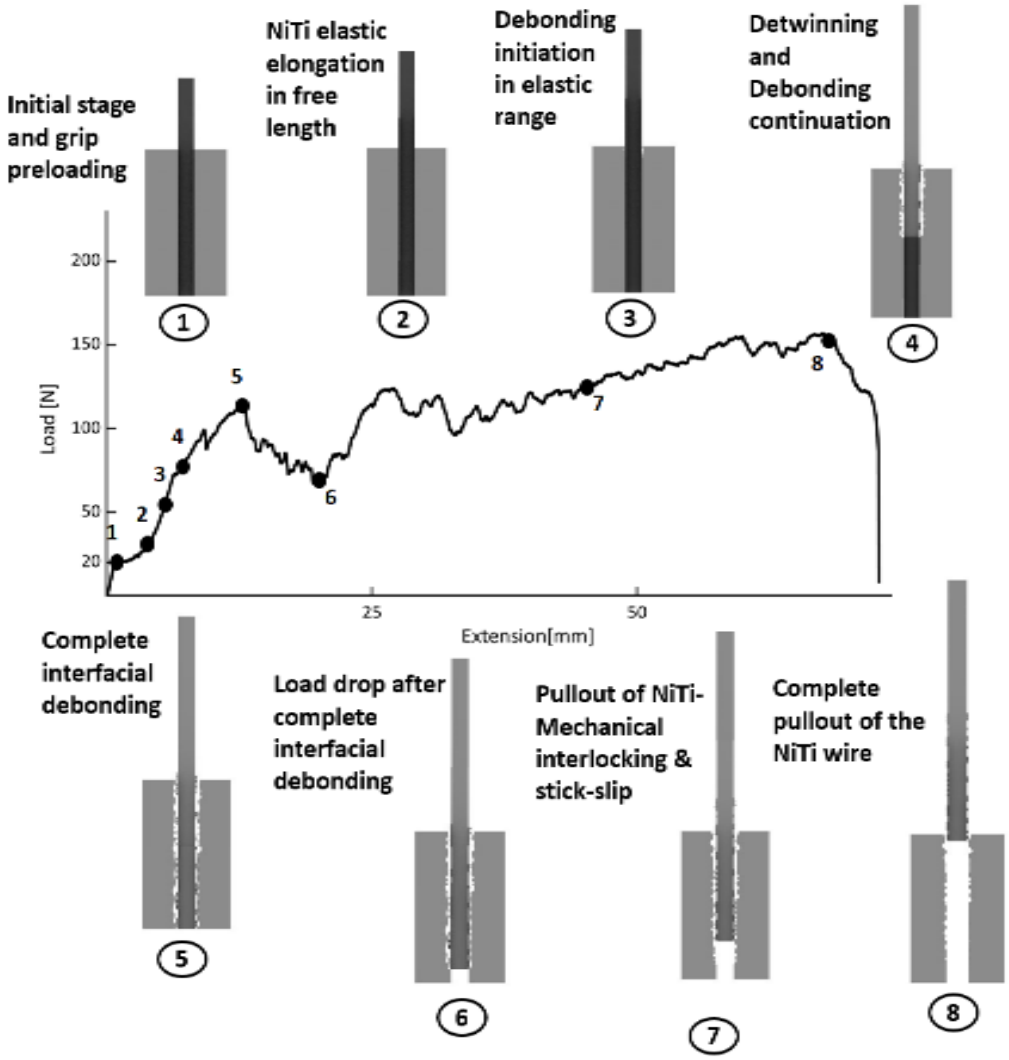

Figure 33: Detailed force-extension pull test curve with schematic representation of entire pull-out phenomena.

Once this ‘stick’ phase is surpassed, the 'slip' phase begins. The mechanical interlocks start to disengage as the wire begins to slide out of the matrix, resulting more pullout and stress build up. The interface failure is typically uneven and irregular due to the mechanical

interlocking. This uneven disengagement results in a pitting or gouging pattern on the matrix surface, indicative of the points where the mechanical interlocks were strongest. Simultaneously, as the wire is pulled out, the matrix particles adhered to the wire due to the mechanical interlocking create additional frictional resistance. This resistance generates a continually increasing force profile, even as the wire is being pulled free from the matrix. Figure 33 encapsulates the complex nature of the NiTi fiber pull-out process from a BiSn matrix, providing a step-by-step illustration of the event.

Upon the onset of displacement, the NiTi wire seemingly aligns and straightens in tension with the applied load, as represented at point 1 in Figure 33. This preliminary phase, driven by escalating tension, necessitates minimal force. As displacement progresses towards point 2, the specimen's internal tension surges, leading to some elastic strain. At point 3, the pull force intensifies the stress, initiating debonding within the elastic zone. Owing to the disparity in cross-sectional areas of the wire and wire/matrix structure, the NiTi wire encounters considerably elevated stresses, surpassing those required for NiTi detwinning, signified by a marked slope alteration near point 4. Continued extension culminates in total NiTi wire debonding from the matrix, as illustrated at point 5. This juncture indicates the NiTi fiber's full detachment from the BiSn matrix. A rapid load reduction from point 5 to point 6 infers the initial NiTi wire pull-out from the BiSn matrix subsequent to debonding.

Upon reaching extensions that necessitate complete wire debonding from the BiSn and observing the force decline, the force required for further pull-out was observed to progressively increase, as shown around point 7. This pattern suggests the simultaneous occurrence of a mechanical interlocking phenomenon and stick-slip dynamics, reminiscent of

failure mechanisms seen in concrete structures. Upon attaining its peak after the onset of mechanical interlocking and stick-slip, the pull-out process concludes past point 8, where the fully embedded NiTi wire is extracted from the BiSn matrix. The multifaceted nature of these interactions underlines the pull-out phenomenon's complexities in NiTi fiber-reinforced BiSn matrix composites, further enriching our understanding of self-healing metallic materials and their potential applications.

Summary

The current research intricately explores the pull-out behavior of NiTi Shape Memory Alloy (SMA) fibers embedded in a BiSn matrix, constituting a self-healing metal-metal composite. The study lays emphasis on understanding the interfacial strength and the associated failure mechanisms at the juncture of the wire and matrix. Through pull tests conducted on two types of specimens - etched and unetched, the force-displacement curves offered insightful revelations into the role of fiber-matrix interface strength on the pull-out process.

From the observations, it was apparent that unetched specimens, characterized by weak interfacial strength, succumbed to premature interface failure. This early failure thwarted the NiTi detwinning process, thereby leading to the suppression of the SMA's inherent shape memory functionality. Conversely, the etched specimens demonstrated stronger interfacial bonds, requiring substantially greater forces for the pull-out of the fiber, thus allowing for the NiTi wire to undergo detwinning, a prerequisite for harnessing the shape memory effect.

A peculiar yet consistent increase in force was detected during the pull-out process, which ran contrary to the anticipated decrease given the corresponding reduction in potential

contact length or area as the fiber progressively detached from the matrix. The scrutiny of this behavior through microscopic examination revealed significant gouging of the BiSn matrix along with small-scale pitting on its surface. These features hinted at an alternative failure mechanism, suggesting an internal failure within the BiSn matrix in close proximity to the interface.

This intriguing stress-peaking phenomenon shares characteristics with failure mechanisms observed in rock or concrete. In these materials, mechanical interlocking generates friction, which in turn amplifies the stress experienced during wire pull-out, much like the behavior observed in our study. The microscopic exploration further revealed roughened NiTi wire surfaces adorned with adhered matrix fragments. Along with the irregularities in the matrix interface, characterized by gouging and pitting, these observations suggested the onset of a mechanical interlocking mechanism.

Interestingly, despite a peaking mean stress, the presence of stress fluctuation over the fiber length indicated a stick-slip phenomenon. This occurrence becomes evident when the adhered matrix chunk is forced to traverse over the pitted matrix interface during fiber pull-out, thus demonstrating an intricate self-healing mechanism in the metal matrix composite.

In summary, this research offers a comprehensive understanding of the pull-out phenomenon in NiTi fiber reinforced BiSn matrix composites, revealing complex mechanics and interactions that dictate the pull-out behavior. These insights hold significant potential to inform future design strategies and enhance manufacturing processes for self-healing metal-metal composites.

Conclusion

This investigation is primarily concentrated on the transformative potential of self-healing materials, with particular emphasis on metal-metal composites. These materials possess the remarkable capacity to redefine the conventional paradigms of engineering design by offering enhanced efficiency, lower maintenance requirements, reduced weight, and a transformative concept of failure. Among self-healing materials, Nickel Titanium (NiTi) Shape Memory Alloy (SMA) fibers encased in a Bismuth Tin (BiSn) matrix composite stand out due to their exceptional attributes. They exhibit structural healing properties that are independent of consumable healing agents, thereby setting a pioneering standard in the realm of materials engineering.

A comprehensive exploration of the post constrained recovery residual stress (PCRRS) observed in NiTi SMAs constitutes a significant part of this research. A series of rigorous experiments have demonstrated a fascinating phenomenon in which the material consistently exhibits a reduction in stress after each loading cycle, demonstrating a pattern akin to cyclic softening. Notably, the original magnitude of the PCRRS could be reinstated by reapplying the thermo-mechanical cycle, suggesting a stable, reproducible, and reversible event, contrary to a scenario of actual material degradation. The results of these studies thus open up new pathways in the design of advanced engineering applications, potentially enabling the creation of materials that demonstrate self-healing and fatigue-resistant characteristics.

The research has also delved into a thorough examination of interfacial bonding of NiTi SMA reinforced the BiSn matrix, a fundamental aspect of the self-healing metal-metal composite under scrutiny. Detailed analyses have been conducted to understand the interfacial

strength and the failure mechanisms that occur at the juncture of the wire and the matrix. The experimental process highlighted that unetched specimens, characterized by weaker interfacial strength, are susceptible to premature interface failure. This early failure restrains the detwinning process in NiTi, suppressing the inherent shape memory functionality of the SMA. In contrast, etched specimens exhibiting stronger interfacial bonds demand considerably larger forces for fiber pull-out, allowing the NiTi wire to undergo detwinning.

A crucial discovery during these investigations was an unexpected increase in force during the pull-out process. This observation contradicts the anticipated decrease associated with the reduction in potential contact length or area as the fiber progressively detached from the matrix. Microscopic examination and analysis of this behavior revealed significant gouging of the BiSn matrix along with small-scale pitting on its surface, suggesting an alternative failure mechanism: an internal failure within the BiSn matrix in proximity to the interface. This intriguing phenomenon shares similarities with failure mechanisms observed in materials such as rock or concrete, where mechanical interlocking results in amplified stress during wire pull-out.

This comprehensive study presents significant progress in understanding the complex mechanics and interactions within NiTi fiber reinforced BiSn matrix composites. By clarifying the interfacial strength and failure mechanisms between the fiber and the matrix, this research provides critical knowledge that paves the way for optimizing parameters such as wire diameter, thereby propelling the sophistication of self-healing metal-metal composites. Furthermore, the results underscore the feasibility of these composites for energy-efficient actuation methodologies, eliminating the need for constant energy input, thereby expanding

the horizons of smart materials design. The findings from this research not only improve the understanding of the mechanics of these materials but also represent a substantial step towards the realization of a revolutionary vision: the fabrication of fully autonomous, advanced monitoring and efficient healing structures. These systems would seamlessly integrate structural health monitoring techniques into self-healing materials, giving birth to what termed as "Structural Health Monitoring 2.0" (*SHM*^{2}).

Inspired by biological systems, the SHM^2 concept envisages a materials system that autonomously detects and locates damage as it happens. It would then trigger an appropriate healing response while concurrently inspecting and monitoring the material for the emergence of further damage during service. Such a system would thereby mitigate the extent of damage, prevent its propagation, and enhance the longevity and reliability of the material. Thus, the current research work paves the way towards such a transformative leap in smart materials technology.

References

[1] B. Aïssa, D. Therriault, E. Haddad, and W. Jamroz, “Self-Healing Materials Systems: Overview of Major Approaches and Recent Developed Technologies,” Advances in Materials Science and Engineering, p. e854203, Feb. 2012, doi: 10.1155/2012/854203.

[2] Z. G. Wei, R. Sandstroröm, and S. Miyazaki, “Shape-memory materials and hybrid composites for smart systems: Part I Shape-memory materials,” Journal of Materials Science, vol. 33, no. 15, pp. 3743–3762, Aug. 1998, doi: 10.1023/A:1004692329247.

[3] S. A. Hayes, F. R. Jones, K. Marshiya, and W. Zhang, “A self-healing thermosetting composite material,” Composites Part A: Applied Science and Manufacturing, vol. 38, no. 4, pp. 1116–1120, Apr. 2007, doi: 10.1016/j.compositesa.2006.06.008.

[4] S. R. White et al., “Autonomic healing of polymer composites,” Nature, vol. 409, no. 6822, pp. 794–797, Feb. 2001, doi: 10.1038/35057232.

[5] R. S. Trask, H. R. Williams, and I. P. Bond, “Self-healing polymer composites: mimicking nature to enhance performance,” Bioinspir. Biomim., vol. 2, no. 1, pp. P1–P9, Jan. 2007, doi: 10.1088/1748-3182/2/1/P01.

[6] R. Das, C. Melchior, and K. M. Karumbaiah, “Self-healing composites for aerospace applications,” in Advanced Composite Materials for Aerospace Engineering, Elsevier, 2016, pp. 333–364. doi: 10.1016/B978-0-08-100037-3.00011-0.

[7] J. B. Ferguson, B. F. Schultz, and P. K. Rohatgi, “Self-Healing Metals and Metal Matrix Composites,” JOM, vol. 66, no. 6, pp. 866–871, Jun. 2014, doi: 10.1007/s11837-014-0912-4.

[8] V. Kilicli, X. Yan, N. Salowitz, and P. K. Rohatgi, “Recent Advancements in Self-Healing Metallic Materials and Self-Healing Metal Matrix Composites,” JOM, vol. 70, no. 6, pp. 846–854, Jun. 2018, doi: 10.1007/s11837-018-2835-y.

[9] M. V. Manuel and G. B. Olson, “Biomimetic Self-Healing Metals,” in Proceedings of the 1st International Conference on Self-Healing Materials, Noordwijk aan Zee, Netherlands, 2007.

[10] A. C. Ruzek, “Synthesis and characterization of metallic systems with potential for self-healing,” MSc, University of Wisconsin-Milwaukee, 2009.

[11] S. Misra, “Shape Memory Alloy Reinforced Self-healing Metal Matrix Composites,” MSc, University of Wisconsin-Milwaukee, 2013.

[12] M. R. Hassan, M. Mehrpouya, S. Emamian, and M. N. Sheikholeslam, “Review of Self-Healing Effect on Shape Memory Alloy (SMA) Structures,” Advanced Materials Research, vol. 701, pp. 87–92, 2013, doi: 10.4028/www.scientific.net/AMR.701.87.

[13] P. K. Rohatgi, “Al-shape memory alloy self-healing metal matrix composite,” Materials Science and Engineering: A, vol. 619, pp. 73–76, Dec. 2014, doi: 10.1016/j.msea.2014.09.050.

[14] J. B. Ferguson, B. F. Schultz, and P. K. Rohatgi, “Zinc alloy ZA-8/shape memory alloy self-healing metal matrix composite,” Materials Science and Engineering: A, vol. 620, pp. 85–88, Jan. 2015, doi: 10.1016/j.msea.2014.10.002.

[15] M. Nosonovsky and P. K. Rohatgi, “Development of Metallic and Metal Matrix Composite Self-Healing Materials,” in Biomimetics in Materials Science: Self-Healing, Self-Lubricating, and Self-Cleaning Materials, M. Nosonovsky and P. K. Rohatgi, Eds., in Springer Series in Materials Science. New York, NY: Springer, 2012, pp. 87–122. doi: 10.1007/978-1-4614-0926-7_5.

[16] J. Martínez Lucci, R. S. Amano, and P. K. Rohatgi, “Heat transfer and fluid flow analysis of self-healing in metallic materials,” Heat Mass Transfer, vol. 53, no. 3, pp. 825–848, Mar. 2017, doi: 10.1007/s00231-016-1837-y.

[17] J. Li, H. Shi, F. Liu, and E.-H. Han, “Self-healing epoxy coating based on tung oil-containing microcapsules for corrosion protection,” Progress in Organic Coatings, vol. 156, p. 106236, Jul. 2021, doi: 10.1016/j.porgcoat.2021.106236.

[18] X. G. Zheng, Y.-N. Shi, and K. Lu, “Electro-healing cracks in nickel,” Materials Science and Engineering: A, vol. 561, pp. 52–59, Jan. 2013, doi: 10.1016/j.msea.2012.10.080.

[19] S. van der Zwaag, Ed., Self Healing Materials: An Alternative Approach to 20 Centuries of Materials Science. in Springer Series in Materials Science. Springer Netherlands, 2007. doi: 10.1007/978-1-4020-6250-6.

[20] S. Hautakangas, H. Schut, N. H. van Dijk, P. E. J. Rivera Díaz del Castillo, and S. van der Zwaag, “Self-healing of deformation damage in underaged Al–Cu–Mg alloys,” Scripta Materialia, vol. 58, no. 9, pp. 719–722, May 2008, doi: 10.1016/j.scriptamat.2007.11.039.

[21] S. van der Zwaag, N. H. van Dijk, H. M. Jonkers, S. D. Mookhoek, and W. G. Sloof, “Self-healing behaviour in man-made engineering materials: bioinspired but taking into account their intrinsic character,” Philosophical Transactions of the Royal Society A: Mathematical, Physical and Engineering Sciences, vol. 367, no. 1894, pp. 1689–1704, May 2009, doi: 10.1098/rsta.2009.0020.

[22] S. van der Zwaag, “Routes and mechanisms towards self healing behaviour in engineering materials,” Bulletin of the Polish Academy of Sciences: Technical Sciences, vol. 58, no. 2, Jan. 2010, doi: 10.2478/v10175-010-0022-6.

[23] K. K. Alaneme and O. I. Omosule, “Experimental Studies of Self Healing Behaviour of Under-Aged Al-Mg-Si Alloys and 60Sn-40Pb Alloy Reinforced Aluminium Metal-Metal

Composites," Journal of Minerals and Materials Characterization and Engineering, vol. 3, no. 1, Art. no. 1, Dec. 2014, doi: 10.4236/jmmce.2015.31001.

[24] G. Q. Xu and M. J. Demkowicz, "Healing of Nanocracks by Disclinations," Phys. Rev. Lett., vol. 111, no. 14, p. 145501, Oct. 2013, doi: 10.1103/PhysRevLett.111.145501.

[25] B. Grabowski and C. C. Tasan, "Self-Healing Metals," in Self-healing Materials, M. D. Hager, S. van der Zwaag, and U. S. Schubert, Eds., in Advances in Polymer Science. Cham: Springer International Publishing, 2016, pp. 387–407. doi: 10.1007/12_2015_337.

[26] N. Shinya and J. Kyono, "Effect of Boron Nitride Precipitation at Cavity Surface on Rupture Properties," Materials Transactions, vol. 47, no. 9, pp. 2302–2307, 2006, doi: 10.2320/matertrans.47.2302.

[27] R. Lumley, "Self Healing in Aluminium Alloys," in Self Healing Materials: An Alternative Approach to 20 Centuries of Materials Science, S. van der Zwaag, Ed., in Springer Series in Materials Science. Dordrecht: Springer Netherlands, 2007, pp. 219–254. doi: 10.1007/978-1-4020-6250-6_11.

[28] R. N. Lumley, A. J. Morton, and I. J. Polmear, "Enhanced creep performance in an Al–Cu–Mg–Ag alloy through underageing," Acta Materialia, vol. 50, no. 14, pp. 3597–3608, Aug. 2002, doi: 10.1016/S1359-6454(02)00164-7.

[29] D. G. Bekas, K. Tsirka, D. Baltzis, and A. S. Paipetis, "Self-healing materials: A review of advances in materials, evaluation, characterization and monitoring techniques," Composites Part B: Engineering, vol. 87, pp. 92–119, Feb. 2016, doi: 10.1016/j.compositesb.2015.09.057.

[30] J. Martinez Lucci, R. S. Amano, P. Rohatgi, and B. Schultz, "Self-Healing in an Aluminum Alloy Reinforces With Microtubes," presented at the ASME 2008 3rd Energy Nanotechnology International Conference collocated with the Heat Transfer, Fluids Engineering, and Energy Sustainability Conferences, American Society of Mechanical Engineers Digital Collection, Jun. 2009, pp. 79–88. doi: 10.1115/ENIC2008-53011.

[31] R. Amano, P. Rohatgi, J. Martínez Lucci, B. Schultz, and A. Ruzek, "Design and Demonstration of Self-Healing Behavior in a Lead-Free Solder Alloy," in 7th International Energy Conversion Engineering Conference, in International Energy Conversion Engineering Conference (IECEC). American Institute of Aeronautics and Astronautics, 2009. doi: 10.2514/6.2009-4514.

[32] K. K. Alaneme and M. O. Bodunrin, "Self-healing using metallic material systems – A review," Applied Materials Today, vol. 6, pp. 9–15, Mar. 2017, doi: 10.1016/j.apmt.2016.11.002.

[33] P. E. Leser et al., “Mitigation of Crack Damage in Metallic Materials,” NF1676L-18936, May 2014. Accessed: May 02, 2023. [Online]. Available: https://ntrs.nasa.gov/citations/20140006911

[34] J. Van Humbeeck, “Non-medical applications of shape memory alloys,” Materials Science and Engineering: A, vol. 273–275, pp. 134–148, Dec. 1999, doi: 10.1016/S0921-5093(99)00293-2.

[35] M. V. Manuel, “Design of a biomimetic self -healing alloy composite,” Ph.D., Northwestern University, Illinois, United States, 2007.

[36] M. C. Wright, M. V. Manuel, and T. Wallace, “Fatigue Resistance of Liquid-Assisted Self-Repairing Aluminum Alloys Reinforced with Shape Memory Alloys.” NASA, Sep. 2013. [Online]. Available: https://ntrs.nasa.gov/api/citations/20140013299/downloads/20140013299.pdf

[37] M. C. Wright, M. Manuel, T. Wallace, A. Newman, and K. Brinson, “Self-Repairing Fatigue Damage in Metallic Structures for Aerospace Vehicles Using Shape Memory Alloy Self-healing (SMASH) Technology,” presented at the ARMD NARI Seedling Phase II Webinar, Virtual, Mar. 2015. Accessed: May 12, 2023. [Online]. Available: https://ntrs.nasa.gov/citations/20150005789

[38] N. Salowitz, A. Correa, T. Santebennur, A. Dorri Moghadam, X. Yan, and P. Rohatgi, “Mechanics of nickel–titanium shape memory alloys undergoing partially constrained recovery for self-healing materials,” Journal of Intelligent Material Systems and Structures, vol. 29, no. 15, pp. 3025–3036, Sep. 2018, doi: 10.1177/1045389X18781260.

[39] N. Salowitz, A. Correa, and A. Moghadam, “Mechanics of NiTi Reinforced Self-Healing Materials Producing Crack Closing Loads,” presented at the ASME 2017 Conference on Smart Materials, Adaptive Structures and Intelligent Systems, American Society of Mechanical Engineers Digital Collection, Nov. 2017. doi: 10.1115/SMASIS2017-3939.

[40] D. J. Leo, “Shape Memory Alloys,” in Engineering Analysis of Smart Material Systems, John Wiley & Sons, Ltd, 2007, pp. 298–345. doi: 10.1002/9780470209721.ch6.

[41] T. W. Duerig, K. N. Melton, D. Stöckel, and C. M. Wayman, Engineering Aspects of Shape Memory Alloys. Elsevier, 1990. doi: 10.1016/C2013-0-04566-5.

[42] J. Mohd Jani, M. Leary, A. Subic, and M. A. Gibson, “A review of shape memory alloy research, applications and opportunities,” Materials & Design (1980-2015), vol. 56, pp. 1078–1113, Apr. 2014, doi: 10.1016/j.matdes.2013.11.084.

[43] K. Otsuka and C. M. Wayman, Shape Memory Materials. Cambridge University Press, 1999.

[44] D. C. Lagoudas, Ed., Shape Memory Alloys: Modeling and Engineering Applications. Springer US, 2008. doi: 10.1007/978-0-387-47685-8.

[45] J. A. Shaw and S. Kyriakides, “Thermomechanical aspects of NiTi,” Journal of the Mechanics and Physics of Solids, vol. 43, no. 8, pp. 1243–1281, Aug. 1995, doi: 10.1016/0022-5096(95)00024-D.

[46] G. Scalet, F. Niccoli, C. Garion, P. Chiggiato, C. Maletta, and F. Auricchio, “A three-dimensional phenomenological model for shape memory alloys including two-way shape memory effect and plasticity,” Mechanics of Materials, vol. 136, p. 103085, Sep. 2019, doi: 10.1016/j.mechmat.2019.103085.

[47] R. Sewak and C. C. Dey, “Martensitic phase transformation in TiNi,” Sci Rep, vol. 9, no. 1, Art. no. 1, Sep. 2019, doi: 10.1038/s41598-019-49605-z.

[48] B. Li, Y. Shen, and Q. An, “Structural origin of reversible martensitic transformation and reversible twinning in NiTi shape memory alloy,” Acta Materialia, vol. 199, pp. 240–252, Oct. 2020, doi: 10.1016/j.actamat.2020.08.039.

[49] J. Wang and H. Sehitoglu, “Martensite modulus dilemma in monoclinic NiTi-theory and experiments,” International Journal of Plasticity, vol. 61, pp. 17–31, Oct. 2014, doi: 10.1016/j.ijplas.2014.05.005.

[50] Y. Liu, A. Mahmud, F. Kursawe, and T.-H. Nam, “Effect of pseudoelastic cycling on the Clausius–Clapeyron relation for stress-induced martensitic transformation in NiTi,” Journal of Alloys and Compounds, vol. 449, no. 1, pp. 82–87, Jan. 2008, doi: 10.1016/j.jallcom.2006.02.080.

[51] R. Srivastava, S. H. Alsamhi, N. Murray, and D. Devine, “Shape Memory Alloy-Based Wearables: A Review, and Conceptual Frameworks on HCI and HRI in Industry 4.0,” Sensors, vol. 22, no. 18, Art. no. 18, Jan. 2022, doi: 10.3390/s22186802.

[52] N. B. Morgan, “Medical shape memory alloy applications—the market and its products,” Materials Science and Engineering: A, vol. 378, no. 1, pp. 16–23, Jul. 2004, doi: 10.1016/j.msea.2003.10.326.

[53] H. Funakubo, J. B. Kennedy, and Gordon & Breach, Shape memory alloys. New York: Gordon and Breach Science Publishers, 1987.

[54] A. Amini, C. Cheng, Q. Kan, M. Naebe, and H. Song, “Phase Transformation Evolution in NiTi Shape Memory Alloy under Cyclic Nanoindentation Loadings at Dissimilar Rates,” Sci Rep, vol. 3, no. 1, Art. no. 1, Dec. 2013, doi: 10.1038/srep03412.

[55] H. Prahlad and I. Chopra, “Comparative Evaluation of Shape Memory Alloy Constitutive Models with Experimental Data,” Journal of Intelligent Material Systems and Structures, vol. 12, no. 6, pp. 383–395, Jun. 2001, doi: 10.1106/104538902022599.

[56] J.-H. Roh and J.-S. Bae, “Thermomechanical behaviors of Ni–Ti shape memory alloy ribbons and their numerical modeling,” Mechanics of Materials, vol. 42, no. 8, pp. 757–773, Aug. 2010, doi: 10.1016/j.mechmat.2010.06.005.

[57] J. Schrooten, K. A. Tsoi, R. Stalmans, Y. Zheng, and P. Sittner, “Comparison between generation of recovery stresses in shape memory wires and composites: theory and reality,” in Smart Materials, SPIE, Apr. 2001, pp. 114–124. doi: 10.1117/12.424397.

[58] S. M. Russell, “Design Considerations for Nitinol Bone Staples,” J. of Materi Eng and Perform, vol. 18, no. 5, pp. 831–835, Aug. 2009, doi: 10.1007/s11665-009-9402-1.

[59] O. Benafan et al., “Temperature dependent deformation of the B2 austenite phase of a NiTi shape memory alloy,” International Journal of Plasticity, vol. 51, pp. 103–121, Dec. 2013, doi: 10.1016/j.ijplas.2013.06.003.

[60] P. Šittner, D. Vokoun, G. N. Dayananda, and R. Stalmans, “Recovery stress generation in shape memory Ti50Ni45Cu5 thin wires,” Materials Science and Engineering: A, vol. 286, no. 2, pp. 298–311, Jul. 2000, doi: 10.1016/S0921-5093(00)00816-9.

[61] Y. Li, H. B. Xu, L. S. Cui, and D. Z. Yang, “Constrained phase-transformation of a TiNi shape-memory alloy,” Metall Mater Trans A, vol. 34, no. 2, pp. 219–223, Feb. 2003, doi: 10.1007/s11661-003-0324-5.

[62] D. Vokoun, V. Kafka, and C. T. Hu, “Recovery stresses generated by NiTi shape memory wires under different constraint conditions,” Smart Mater. Struct., vol. 12, no. 5, pp. 680–685, Aug. 2003, doi: 10.1088/0964-1726/12/5/303.

[63] K. Tanaka, “A Thermomechanical Sketch of Shape Memory Effect: One-Dimensional Tensile Behavior,” Res Mechanica, vol. 2, no. 3, pp. 59–72, 1986.

[64] C. Liang and C. A. Rogers, “One-Dimensional Thermomechanical Constitutive Relations for Shape Memory Materials,” Journal of Intelligent Material Systems and Structures, vol. 1, no. 2, pp. 207–234, Apr. 1990, doi: 10.1177/1045389X9000100205.

[65] L. C. Brinson, “One-Dimensional Constitutive Behavior of Shape Memory Alloys: Thermomechanical Derivation with Non-Constant Material Functions and Redefined Martensite Internal Variable,” Journal of Intelligent Material Systems and Structures, vol. 4, no. 2, pp. 229–242, Apr. 1993, doi: 10.1177/1045389X9300400213.

[66] H. Kato, N. Inagaki, and K. Sasaki, “A one-dimensional modelling of constrained shape memory effect,” Acta Materialia, vol. 52, no. 11, pp. 3375–3382, Jun. 2004, doi: 10.1016/j.actamat.2004.03.036.

[67] J. Lubliner and F. Auricchio, “Generalized plasticity and shape-memory alloys,” International Journal of Solids and Structures, vol. 33, no. 7, pp. 991–1003, Mar. 1996, doi: 10.1016/0020-7683(95)00082-8.

[68] F. Auricchio and J. Lubliner, “A uniaxial model for shape-memory alloys,” International Journal of Solids and Structures, vol. 34, no. 27, pp. 3601–3618, Sep. 1997, doi: 10.1016/S0020-7683(96)00232-6.

[69] T. Videnic, F. Kosel, V. Sajn, and M. Brojan, “Biaxial Constrained Recovery in Shape Memory Alloy Rings,” Journal of Intelligent Material Systems and Structures, vol. 19, no. 8, pp. 861–874, Aug. 2008, doi: 10.1177/1045389X07082378.

[70] T. Videnic, M. Brojan, and F. Kosel, “One-Dimensional Model of Constrained Recovery in SMA with Non-Constant Young’s Modulus,” in International Conference on Martensitic Transformations (ICOMAT), John Wiley & Sons, Ltd, 2010, pp. 239–244. doi: 10.1002/9781118803592.ch33.

[71] T. Videnic, M. Brojan, J. Kunavar, and F. Kosel, “A Simple One-Dimensional Model of Constrained Recovery in Shape Memory Alloys,” Mechanics of Advanced Materials and Structures, vol. 21, no. 5, pp. 376–383, May 2014, doi: 10.1080/15376494.2012.697599.

[72] M. I. Haider, M. Rezaee, A. Yazdi, and N. Salowitz, “Investigation into post constrained recovery properties of nickel titanium shape memory alloys,” Smart Mater. Struct., vol. 28, no. 10, p. 105044, Sep. 2019, doi: 10.1088/1361-665X/ab3ad4.

[73] M. I. Haider, A. Yazdi, M. Rezaee, L. C. Tsai, and N. Salowitz, “Mechanics of Post Constrained Recovery Residual Stress Produced by NiTi,” in Proceedings of the ASME 2019 Conference on Smart Materials, Adaptive Structures and Intelligent Systems, Dec. 2019. doi: 10.1115/SMASIS2019-5619.

[74] M. I. Haider, A. Correa, A. Moghadam, X. Yan, and N. Salowitz, “Experimental Exploration of Post Constrained Recovery Mechanics of NiTi,” in Proceedings of the ASME 2018 Conference on Smart Materials, Adaptive Structures and Intelligent Systems, Nov. 2018. doi: 10.1115/SMASIS2018-8168.

[75] M. I. Haider and N. Salowitz, “Phenomenological Assessment of Post Constrained Recovery Residual Stress of Shape Memory Alloys,” presented at the ASME 2021 Conference on Smart Materials, Adaptive Structures and Intelligent Systems, American Society of Mechanical Engineers Digital Collection, Oct. 2021. doi: 10.1115/SMASIS2021-68111.

[76] F. Daghia, E. Viola, T. M. Seigler, and D. J. Inman, “Constitutive Modeling of SMA in Constrained Recovery Mode,” presented at the ASME 2006 International Mechanical Engineering Congress and Exposition, American Society of Mechanical Engineers Digital Collection, Dec. 2007, pp. 395–401. doi: 10.1115/IMECE2006-15616.

[77] H. Tran, X. Balandraud, and J.-F. Destrebecq, “Recovery stresses in SMA wires for civil engineering applications: experimental analysis and thermomechanical modelling,”

Materialwissenschaft und Werkstofftechnik, vol. 45, no. 5, pp. 435–443, 2011, doi: 10.1002/mawe.201100805.

[78] W. J. Lee, B. Weber, G. Feltrin, C. Czaderski, M. Motavalli, and C. Leinenbach, “Stress recovery behaviour of an Fe–Mn–Si–Cr–Ni–VC shape memory alloy used for prestressing,” Smart Mater. Struct., vol. 22, no. 12, p. 125037, Nov. 2013, doi: 10.1088/0964-1726/22/12/125037.

[79] W. J. Lee, B. Weber, and C. Leinenbach, “Recovery stress formation in a restrained Fe–Mn–Si-based shape memory alloy used for prestressing or mechanical joining,” Construction and Building Materials, vol. 95, pp. 600–610, Oct. 2015, doi: 10.1016/j.conbuildmat.2015.07.098.

[80] M. Shahverdi, J. Michels, C. Czaderski, and M. Motavalli, “Iron-based shape memory alloy strips for strengthening RC members: Material behavior and characterization,” Construction and Building Materials, vol. 173, pp. 586–599, Jun. 2018, doi: 10.1016/j.conbuildmat.2018.04.057.

[81] X.-L. Gu, Z.-Y. Chen, Q.-Q. Yu, and E. Ghafoori, “Stress recovery behavior of an Fe-Mn-Si shape memory alloy,” Engineering Structures, vol. 243, p. 112710, Sep. 2021, doi: 10.1016/j.engstruct.2021.112710.

[82] S. Kajiwara, “Characteristic features of shape memory effect and related transformation behavior in Fe-based alloys,” Materials Science and Engineering: A, vol. 273–275, pp. 67–88, Dec. 1999, doi: 10.1016/S0921-5093(99)00290-7.

[83] E. Choi, S.-C. Cho, J. W. Hu, T. Park, and Y.-S. Chung, “Recovery and residual stress of SMA wires and applications for concrete structures,” Smart Mater. Struct., vol. 19, no. 9, p. 094013, Aug. 2010, doi: 10.1088/0964-1726/19/9/094013.

[84] E. Choi, T. Nam, Y.-S. Chung, Y.-W. Kim, and S. Lee, “Behavior of NiTiNb SMA wires under recovery stress or prestressing,” Nanoscale Research Letters, vol. 7, no. 1, p. 66, Jan. 2012, doi: 10.1186/1556-276X-7-66.

[85] Y. Liu and D. Favier, “Stabilisation of martensite due to shear deformation via variant reorientation in polycrystalline NiTi,” Acta Materialia, vol. 48, no. 13, pp. 3489–3499, Aug. 2000, doi: 10.1016/S1359-6454(00)00129-4.

[86] N. Salowitz, S. Misra, M. I. Haider, M. Povolo, and P. Rohatgi, “Investigation into the Performance of NiTi Shape Memory Alloy Wire Reinforced Sn-Bi Self-Healing Metal Matrix Composite,” Materials, vol. 15, no. 9, Art. no. 9, Jan. 2022, doi: 10.3390/ma15092970.

[87] C. Poon, L. Zhou, W. Jin, and S. Shi, “Interfacial debond of shape memory alloy composites,” Smart Mater. Struct., vol. 14, no. 4, pp. N29–N37, Jul. 2005, doi: 10.1088/0964-1726/14/4/N05.

[88] Y. Wang, L. Zhou, Z. Wang, H. Huang, and L. Ye, “Analysis of internal stresses induced by strain recovery in a single SMA fiber–matrix composite,” Composites Part B: Engineering, vol. 42, no. 5, pp. 1135–1143, Jul. 2011, doi: 10.1016/j.compositesb.2011.03.017.

[89] Y. Jia, W. Yan, and H.-Y. Liu, “Numerical Study on Carbon Fibre Pullout using a Cohesive Zone Model,” in Proceeding of 18th International Conference on composite materials, Jeju Island, Korea, Aug. 2011.

[90] Y. Wang, L. Zhou, Z. Wang, H. Huang, and L. Ye, “Stress distributions in single shape memory alloy fiber composites,” Materials & Design, vol. 32, no. 7, pp. 3783–3789, Aug. 2011, doi: 10.1016/j.matdes.2011.03.039.

[91] Y. Payandeh, F. Meraghni, E. Patoor, and A. Eberhardt, “Debonding initiation in a NiTi shape memory wire–epoxy matrix composite. Influence of martensitic transformation,” Materials & Design, vol. 31, no. 3, pp. 1077–1084, Mar. 2010, doi: 10.1016/j.matdes.2009.09.048.

[92] F. Barrie, D. B. Futch, D. H. D. Hsu, and M. V. Manuel, “Effect of phase on debond strength in shape memory alloy reinforced composites,” Materials & Design, vol. 57, pp. 98–102, May 2014, doi: 10.1016/j.matdes.2013.11.062.

[93] J. P. Coughlin, J. J. Williams, and N. Chawla, “Mechanical behavior of NiTi shape memory alloy fiber reinforced Sn matrix ‘smart’ composites,” J Mater Sci, vol. 44, no. 3, pp. 700–707, Feb. 2009, doi: 10.1007/s10853-008-3188-7.

[94] J. P. Coughlin, J. J. Williams, G. A. Crawford, and N. Chawla, “Interfacial Reactions in Model NiTi Shape Memory Alloy Fiber-Reinforced Sn Matrix ‘Smart’ Composites,” Metall Mater Trans A, vol. 40, no. 1, pp. 176–184, Jan. 2009, doi: 10.1007/s11661-008-9676-1.

[95] M. I. Haider, M. Rezaee, and N. Salowitz, “Explorations of Post Constrained Recovery Residual Stress of Shape Memory Alloys in Self-healing Applications,” in Proceedings of the Wisconsin Space Conference, Milwaukee, Wisconsin, 2021. doi: 10.17307/wsc.v1i1.341.

[96] C. Y. Yue, H. C. Looi, and M. Y. Quek, “Assessment of fibre-matrix adhesion and interfacial properties using the pull-out test,” International Journal of Adhesion and Adhesives, vol. 15, no. 2, pp. 73–80, Apr. 1995, doi: 10.1016/0143-7496(95)98740-D.

[97] J.-K. Kim and Y.-W. Mai, Eds., Engineered Interfaces in Fiber Reinforced Composites, 1st ed. Elsevier Science Ltd, 1998. Accessed: Dec. 14, 2021. [Online]. Available: https://www.sciencedirect.com/book/9780080426952/engineered-interfaces-in-fiber-reinforced-composites

[98] Y. Liu, B. Al-Matar, and G. Newaz, “An Investigation on the Interface in a NiTi Short-Fiber-Reinforced 6061 Aluminum Composite by Transmission Electron Microscope,” Metall

Mater Trans A, vol. 39, no. 11, pp. 2749–2759, Nov. 2008, doi: 10.1007/s11661-008-9627-x.

[99] D. R. Ni and Z. Y. Ma, “Shape Memory Alloy-Reinforced Metal-Matrix Composites: A Review,” Acta Metall. Sin. (Engl. Lett.), vol. 27, no. 5, pp. 739–761, Oct. 2014, doi: 10.1007/s40195-014-0164-x.

[100] C. w. Ng, A. s. Mahmud, M. n. Ahmad, M. f. Razali, and Y. Liu, “Estimation of titanium oxide layer thickness on thermally oxidized NiTi alloy based on color variations,” Materialwissenschaft und Werkstofftechnik, vol. 53, no. 1, pp. 47–55, 2022, doi: 10.1002/mawe.202100084.

[101] M. I. Haider, B. Church, P. Rohatgi, and N. Salowitz, “Investigation Into Etching Effects on the Interface Strength Between Nickel Titanium and Bismuth Tin for the Creation of Metal Matrix Self Healing Composites,” presented at the ASME 2022 Conference on Smart Materials, Adaptive Structures and Intelligent Systems, Dearborn, MI: ASME 2022 Conference on Smart Materials, Adaptive Structures and Intelligent Systems, Nov. 2022. doi: 10.1115/SMASIS2022-90256.

[102] S.-Y. Fu, C.-Y. Yue, X. Hu, and Y.-W. Mai, “Analyses of the micromechanics of stress transfer in single- and multi-fiber pull-out tests,” Composites Science and Technology, vol. 60, no. 4, pp. 569–579, Mar. 2000, doi: 10.1016/S0266-3538(99)00157-8.

[103] Y. C. Gao and L. M. Zhou, “Energy release rate for interface debonding with prestress and friction,” Theoretical and Applied Fracture Mechanics, vol. 32, no. 3, pp. 203–207, Nov. 1999, doi: 10.1016/S0167-8442(99)00040-3.

[104] E. Pisanova, S. Zhandarov, E. Mäder, I. Ahmad, and R. J. Young, “Three techniques of interfacial bond strength estimation from direct observation of crack initiation and propagation in polymer–fibre systems,” Composites Part A: Applied Science and Manufacturing, vol. 32, no. 3, pp. 435–443, Mar. 2001, doi: 10.1016/S1359-835X(00)00054-3.

[105] C.-H. Hsueh, “Analytical analyses of stress transfer in fibre-reinforced composites with bonded and debonded fibre ends,” J Mater Sci, vol. 24, no. 12, pp. 4475–4482, Dec. 1989, doi: 10.1007/BF00544532.

[106] C.-H. Hsueh, “Interfacial debonding and fiber pull-out stresses of fiber-reinforced composites,” Materials Science and Engineering: A, vol. 123, no. 1, pp. 1–11, Jan. 1990, doi: 10.1016/0921-5093(90)90203-F.